Super-omics and PCAS reveal rheumatoid arthritis as a tumor-like disease

Lanlan Xiao[1#], Nadire Aishan[2#], Siwei Ju[2#], Fengchao Zhao[3#], Xiaoxi Ouyang[4#], Dazhi Chen[5], Weiqian Chen[1], Jie Xie[3], Danhua Zhu[4], Junchi Zhang[2], Lingyun Sun[6], Yimin Li[1], Dan Zhou[7], Qingqing Hu[4], Jinzhi Wu[1], Qingna Meng[8], Jichun Zhou[2], Danyi Xu[1], Jingyi Yu[2], Junyu Liang[1], Yangjun Cai[9], Minmin Zhang[10], Yanlin He[1], Zeyu Sun[4*], Linbo Wang[2*], Jin Lin[1*], Feiyang Ji[2,4*]

Affiliation

1 Department of Rheumatology, the First Affiliated Hospital, Zhejiang University School of Medicine, Hangzhou 310003, China

2 Department of Surgical Oncology, Sir Run Run Shaw Hospital, Zhejiang University College of Medicine, Hangzhou 310000, China

3 Department of Orthopedics, the First Affiliated Hospital, Zhejiang University School of Medicine, Hangzhou 310003, China

4 State Key Laboratory for the Diagnosis and Treatment of Infectious Diseases, National Clinical Research Center for Infectious Diseases, Collaborative Innovation Center for Diagnosis and Treatment of Infectious Diseases, National Medical Center for Infectious Diseases, The First Affiliated Hospital, Zhejiang University School of Medicine, Hangzhou 310003, China

5 School of Clinical Medicine, The First People's Hospital of Lin'an District, Hangzhou, Lin'an People's Hospital Affiliated to Hangzhou Medical College, Hangzhou Medical College, Hangzhou 311300, China

6 School of Public Health and the Second Affiliated Hospital, Zhejiang University School of Medicine, 388 Yuhangtang Road, Hangzhou, 310058, China

7 The Second Affiliated Hospital, School of Public Health, Zhejiang University School of Medicine, Hangzhou, China

8 School of Basic Medical Sciences and Forensic Medicine, Hangzhou Medical College, Hangzhou, Zhejiang, China

9 Department of Thyroid and Breast Surgery, Taizhou Hospital of Zhejiang

Province Affiliated to Wenzhou Medical University

10 Jinan Microecological Biomedicine Shandong Laboratory, Jinan, Shandong, China

# These authors contributed equally to this work

Correspndence

feiyangji@zju.edu.cn (F. J.); linjinzju@zju.edu.cn (J.L.); 3198012@zju.edu.cn (L.W.); zeyusun@zju.edu.cn (Z.S.)

SUMMARY

Rheumatoid arthritis (RA) is a debilitating systemic autoimmune disorder that significantly impairs quality of life. To elucidate the molecular alterations in RA progression, we performed comprehensive super-omics analyses on synovial tissues from patients with joint trauma, arthritis, and RA. These analyses included transcriptomics, proteomics, metabolomics, microbiomics, and fourteen PTMs (phosphorylation, acetylation, lactylation, O-GlcNAc glycosylation, arginine monomethylation, lysine monomethylation, lysine dimethylation, lysine trimethylation, succinylation, malonylation, glutarylation, tyrosine nitration, N-glycosylation, and O-glycosylation). Additionally, we developed a protein-centered association study (PCAS) method to integrate these complex datasets. Using this approach, we identified key proteins, such as STK17B, and its interactors, which may be crucial in RA pathogenesis. Tumor-like features, including aberrant angiogenesis and epithelial-mesenchymal transition, were observed in RA, alongside the potential involvement of oncogenes and tumor suppressor genes. Finally, we constructed a molecular interaction blueprint of RA, providing a comprehensive framework for advancing RA pathogenesis, diagnosis, and therapy.

INTRODUCTION

Rheumatoid arthritis (RA) is one of the most prevalent systemic autoimmune diseases, affecting approximately 0.5% to 1% of the global population(Smolen et al., 2018). RA is characterized by immune-mediated persistent synovial inflammation, manifesting as symmetric polyarthritis with pain and swelling, typically involving small joints of the hands and feet, and frequently affecting critical organs such as the heart, lungs, and kidneys(Tobón et al., 2010). The

loss of tissue-protective macrophage populations, the emergence of tissue-invasive T effector cells, and the formation of an aggressive fibroblast-like synoviocyte (FLS) phenotype contribute to joint damage(Weyand and Goronzy, 2021). Another hallmark of RA is the production of autoantibodies, particularly anti-citrullinated protein antibodies (ACPA), which are generated through the activation of antigen-presenting cells (APCs) that present citrullinated proteins, further activating specific T and B cells(McInnes and Schett, 2011). This leads to the initiation of a series of immune responses that contribute to the autoimmune inflammatory process characteristic of RA. Consequently, RA is widely considered to be an immune and inflammatory disorder. The continuous development and application of biologic and targeted synthetic disease-modifying antirheumatic drugs (b/tsDMARDs) have significantly improved treatment outcomes. However, some patients remain refractory to therapy due to drug resistance, side effects, or other factors, leading to severe impacts on their quality of life. This highlights the need for a more comprehensive understanding of RA.

Advancements in biotechnology, coupled with the development of various omics technologies, have enabled a deeper understanding of the disease. Post-translational modification (PTM) refers to the chemical modification of protein amino acid residues after translation through the addition or removal of specific groups, thereby regulating protein activity, localization, folding, and interactions with other biomolecules. PTMs play a crucial role in various biological processes and disease pathogenesis(Wu et al., 2023). Phosphorylation is one of the most common and important PTMs, widely involved in regulating immune cell behavior. Tyrosine nitration is closely associated with cellular oxidative stress(Chen et al., 2024), while malonylation is involved in energy metabolism, macrophage inflammatory signaling, and cartilage cell metabolic regulation. Glutarylation has been reported to participate in transcriptional regulation, immune inflammation, and amino acid metabolism (Fu et al., 2022). Lysine and arginine methylation play significant roles in transcriptional regulation and signal transduction(Demicco et al., 2024; Yan et al., 2024). Lactylation can affect the function of key immune regulatory molecules, such as NLRP3 and TCR, altering immune cell activity and the intensity of autoimmune responses(Souto-Carneiro et al., 2020). Previous studies have shown that succinylation of the mitochondrial transcription factor BRD2 promotes the abnormal differentiation of tissue-resident memory T cells (Trm cells) in RA patients(Wu et al., 2024), and acetylation of the T cell

microtubule system facilitates T cell migration(Wu et al., 2020). In RA patients, the immune response to post-translationally modified proteins is abnormally active(Scherer et al., 2022), yet proteomic studies on PTMs other than citrullination in RA remain rare.

Existing multi-omics studies have provided valuable insights into the cellular composition and functions of synovial tissues in RA, identifying key factors driving FLS heterogeneity(Floudas et al., 2022; Zhang et al., 2019), the significance of immune regulation in RA(Consortium, 2007; Weyand and Goronzy, 2021), and characteristics of the gut microbiome and serum metabolic profiles in RA patients(Cheng et al., 2022). However, current multi-omics studies are limited in both the types of omics and the depth of analysis, resulting in incomplete molecular portraits and a lack of specialized data analysis methods for multi-omics data. The analysis of multi-omics data faces significant challenges due to the increasing complexity and diversity of data types. To address these issues, we propose a more advanced multi-omics approach, super-omics, which integrates a comprehensive analysis of key functional molecules in biological activities. Based on this, we have developed a protein-centered association study (PCAS), leveraging known interactions among biomolecules. This new super-omics data analysis pipeline—comprising data preprocessing, differential analysis, PCAS analysis, and network/enrichment analysis—aims to handle the increased omics layers and data diversity, addressing the complexities that arise from traditional analytical methods and identifying key molecular changes.

RESULTS

Super-omics and PCAS analysis

Traditional multi-omics studies typically combine multiple omic layers, but without strict requirements for the specific levels of omic analysis (such as DNA, DNA modifications, RNA, RNA modifications, proteins, protein modifications, metabolites, etc.). Additionally, these studies often lack sufficient diversity in the area of protein post-translational modifications (PTMs). As a result, both single-omic and multi-omic approaches can be limited by the depth of omic layers and the number of omics types included, leading to outcomes that are often narrowly focused. In these cases, researchers may be so focused on a small number of omics that they can’t see the forest for the trees, failing to provide a comprehensive reflection of the entire biological system and introducing the potential for biased or even inaccurate results. In contrast,

super-omics study requires the incorporation of at least ten omic types, spanning at least three omic layers, with a strong emphasis on proteins and PTMs, which are directly involved in the regulation of biological functions. Super-omics offers a significant advancement over traditional multi-omics by broadening both the number and depth of omic layers, thus offering a more holistic perspective. Furthermore, with advances in mass spectrometry, the detection depth of PTMs has been greatly enhanced, enabling the identification of an expanding array of modifications. This progress improves our ability to map the molecular landscape more comprehensively. The Protein-Centered Association Study (PCAS) integrates differential omic data from various layers, based on known molecular interactions and upstream-downstream regulatory pathways, enabling a more nuanced understanding of molecular changes. This approach significantly reduces the risk of error and false discovery rates, ensuring that key alterations are identified (Figure 1).

Comprehensive super-omics analysis of synovial tissue

Between December 2023 and May 2024, we recruited 6 patients with rheumatoid arthritis (RA), 6 with osteoarthritis (OA), and 6 with meniscus injuries (normal controls, NC) (Supplemental Table 1). Synovial tissue samples were collected through Knee Arthroplasty and arthroscopic surgery. We performed a super-omics analysis on these samples, encompassing 18 distinct omic layers: transcriptomics (mRNA), proteomics (WCP), metabolomics (Meta), microbiomics, and 14 types of PTMs, including phosphorylation (P), acetylation (Ac), lactylation (Lac), O-GlcNAc glycosylation (Oglc), arginine monomethylation (Rmme), lysine monomethylation (Pmm), lysine dimethylation (Pmd), lysine trimethylation (Pmt), succinylation (Succ), malonylation (Mal), glutarylation (Glut), tyrosine nitration (Ynit), N-glycosylation (Ng), and O-glycosylation (Og). Our analysis identified 27,459 genes in transcriptomics, 3,424 metabolites in metabolomics, 2,271 amplicon sequence variants (ASV) in microbiomics, and 6,540 proteins in proteomics. PTMs were extensively characterized, with 18,838 phosphorylation sites, 3,420 acetylation sites, 11,684 succinylation sites, 300 lactylation sites, 158 malonylation sites, 74 O-GlcNAc glycosylation sites, 55 lysine monomethylation sites, 69 lysine dimethylation sites, 1,142 lysine trimethylation sites, 70 glutarylation sites, 136 arginine monomethylation sites, 105 tyrosine nitration sites, 566 N-glycosylation sites, and 377 O-glycosylation sites (Figure 2A, Supplementary materials 1). Notably, many proteins displayed multiple PTMs.

For example, 440 proteins exhibited both phosphorylation and succinylation, and 144 proteins were modified by acetylation, succinylation, and trimethylation. Among these, alpha-1-antitrypsin (SERPINA1) displayed 10 PTMs, and Mimecan (OGN) displayed 9 PTMs (Figure 2B). The predominant modifications observed were phosphorylation, succinylation, and acetylation (Figure 2C). The correlation analysis of the quantitative results across various omics showed that the within-group correlation in the RA, OA, and NC groups was higher than the between-group correlation, and the within-group correlation among the samples in the RA group was lower than that in the other two groups (Figure S1A). When proteins underwent multiple modifications, the proportion of phosphorylation decreased, while succinylation and acetylation increased, with succinylation emerging as the dominant modification (Figure S1B). The results of the principal component analysis show that in most omics, the RA group is well-distinguished from the OA and NC groups, while the OA and NC groups are closer to each other. At the same time, the samples within the RA group are farther apart, which is consistent with the results of the correlation analysis (Figure S2A). The quantitative results for proteins and PTMs are detailed in Figure S2B (Supplementary materials 2). Among the detected PTMs, O-GlcNAc glycosylation exhibited the highest intensity, followed by phosphorylation, with tyrosine nitration showing the lowest intensity (Figure S2C). N-glycosylation and O-glycosylation were most strongly correlated with protein expression levels (Figure 2D), likely due to their prevalence in secretory proteins. In contrast, arginine monomethylation and lysine monomethylation displayed the weakest correlation with protein expression, potentially because these modifications predominantly occur in nuclear proteins. The relatively low correlation between mRNA and protein levels suggests that protein expression is primarily regulated at post-transcriptional and post-translational levels (Figure 2D).

Subcellular localization analysis of omic data revealed that N-glycosylation and O-glycosylation were primarily localized in the endoplasmic reticulum and secretory proteins, indicating their involvement in humoral immunity and inflammatory responses(Rudd et al., 1998). O-GlcNAc glycosylation was concentrated in the nucleus and cytoplasm, suggesting its role in signal transduction, in line with existing literature(Rudd et al., 1998). Glutarylation was more prevalent in membrane proteins, implying a role in substance transport, signal transduction, and cell-cell recognition. Acetylation and lysine trimethylation were found primarily in mitochondria, pointing to their

involvement in cellular metabolism (Figure 2E). There are differences in the overall level of certain omics modifications among the three groups. For instance, the levels of acetylation, malonylation, lysine dimethylation, and lysine trimethylation are higher in the RA compared to the OA, while the N-glycosylation level is lower in the RA group compared to the OA group. Additionally, the lysine trimethylation was higher in the RA group compared to the NC group (Figure 2F).

Metabolomics identified 9 major classes of metabolites, with carboxylic acids and derivatives (15.74%) and fatty acyls (13.76%) being the most abundant (Figure S2D). Microbiome analysis revealed that the most abundant bacterial families in the synovial tissue were *Muribaculaceae*, *Prevotellaceae*, and *Lachnospiraceae* (Figure S2E).

Differential analysis of RA synovial tissue

Comparison of RA with NC revealed significant differences in mRNA, proteins, and PTM sites. Specifically, 1,250 mRNA, 169 proteins, and multiple PTM sites (including 665 phosphorylation sites, 67 acetylation sites, 232 succinylation sites, 12 lactylation sites, 7 malonylation sites, and others) were upregulated in RA, while 1,324 mRNA, 302 proteins, and several PTM sites (including 617 phosphorylation sites and 118 acetylation sites) were downregulated (Figure 3A, Figure S3, Supplementary materials 3). When compared to OA, RA showed upregulation of 381 mRNA, 8 proteins, and several PTM sites, while 1 protein and several PTM sites were downregulated. In entries of the PTMs analyzed in this study, the overall number of upregulated and downregulated PTMs between RA and NC were relatively similar (up: 1133; down: 1204). However, a closer examination of specific PTMs revealed that, compared to NC, the overall levels of acetylation (up: 67; down: 118) and succinylation (up: 232; down: 288) in RA were reduced. When compared to OA, RA exhibited significantly increased levels of phosphorylation and acetylation (Figure S3). Further analysis of the overall differences across various omics showed that the proteomics and phosphorylation differences between the comparison groups were relatively small. Notably, the greatest differences were observed between RA and NC in entries of N-glycosylation, and O-glycosylation, while the overall differences in malonylation were most pronounced between RA and OA, as well as between OA and NC (Figure 3B, Figure S4A). After summarizing the differential entries between the RA and NC comparison groups across all omics, we found that the intensity variation among the differential entries in the RA group is larger, which may indicate greater

synovial heterogeneity in RA patients (Figure 3C). Notably, SYK, and BTK(Ding et al., 2023), and protein expression of SUCLG2(Wu et al., 2020) were consistent with previous findings in RA research (Figure 3D). In general, greater intensity in PTMs was associated with fewer differential genes, suggesting that housekeeping proteins are more stable and less prone to regulation. However, genes such as ALB, which are typically stable, exhibited significant changes, highlighting their potential role in the pathogenesis of RA. Of course, this could also be due to contamination, as we deliberately retained contaminant proteins when searching the database (Figure 3E, Figure S4B). To screen candidate clinical diagnostic markers, we selected the top five entries with the largest differential changes in each omics from the comparison groups. After summarizing all omics, the top 10 entries with the highest intensity were chosen. These entries are easier to detect due to their high intensity, and they exhibit better specificity for detection because of the large differences between the comparison groups. For example, serine phosphorylation at position 241 of SPP1 and threonine O-glycosylation at position 519 of HCFC1 can serve as candidate diagnostic markers for differentiating RA and NC (Figure 3F).

In our investigation of differential genes between RA and NC, we identified 24 genes exhibiting concurrent alterations in both phosphorylation and succinylation. Additionally, 13 genes showed changes in succinylation as well as transcriptomic and proteomic alterations, while 4 genes displayed significant differences in succinylation, acetylation, and lysine trimethylation. Mimecan (OGN) was found to be downregulated across eight PTMs, including succinylation, lactylation, malonylation, O-GlcNAc glycosylation, lysine dimethylation), tyrosine nitration, N-glycosylation, and O-glycosylation. Lumican showed decreased protein levels, accompanied by downregulation in acetylation, succinylation, lactylation, lysine trimethylation, tyrosine nitration, N-glycosylation, and O-glycosylation, indicating that some of these changes may stem from alterations at the protein expression level (Figure 3G, Figure S4C).

The top 10 genes with the highest number of differential PTMs sites between RA and NC were identified, including AHNAK, IGHG1, ASPN, LAMCA1, LUM, SPTAN1, OGN, ANXA2, TNS1, and IGHM (Figure S4D). Furthermore, genes with a large proportion of differential PTMs sites were also examined (Figure S4E). Genes such as AHNAK, IGHG1, ASPN, ATP5PO, PLIN1, and SPP1 exhibited numerous differential PTMs sites with a high proportion relative to

protein expression, suggesting that these genes may serve as potential clinical biomarkers of RA (Figure 3H). A joint analysis of transcriptomic and proteomic data revealed 97 genes exhibiting consistent changes in both transcript and protein levels between RA and NC. Among these, SAA1(Chambers et al., 1983) and GBP5(Li et al., 2023) were notably upregulated at both the transcript and protein levels (Figure S5A), corroborating previous studies that suggest these genes as potential contributors to RA pathogenesis. In contrast, the transcriptional and protein levels of FABP4 and PLIN1 were significantly lower in comparison to NC, with further reductions observed in the phosphorylation and succinylation of PLIN1, and succinylation, acetylation, malonylation and lysine trimethylation of FABP4. Although no changes were detected in the protein levels of Serotransferrin, PEA15, and SERPINA3, substantial increases were found in the lysine trimethylation and glutarylation of Serotransferrin, and acetylation in the latter two proteins showed marked alterations. OGN exhibited reduced protein expression, with concurrent downregulation in lysine dimethylation and lactylation (Figure S5B).

Metabolic alterations, which are critical for cellular energy homeostasis, were found to be significantly more active in RA compared to both OA and NC, as evidenced by a higher number of upregulated differential metabolites (Figure S5C). Specifically, RA exhibited elevated levels of L-Glutamic acid and D-Lactic acid relative to NC, while sodium lactate was more abundant in RA compared to OA (Figure S5C). Microbiome analysis revealed that the families Muribaculaceae, Rikenellaceae, and Rhodocyclaceae were more prevalent in RA compared to NC, whereas Caulobacteraceae and Beijerinckiaceae were less abundant in RA compared to NC. Additionally, Bifidobacteriaceae and Moraxellaceae were found to be more abundant in RA than in OA (Figure S5D).

Pathway and functional analysis of RA synovium

To explore the biological functions of RA synovium, we performed Gene Ontology (GO)/Kyoto Encyclopedia of Genes and Genomes (KEGG) enrichment analysis of the significant differential genes from each omics and select the top three entries with the smallest FDR values for each omics. The results revealed enrichment of the "activation of immune response" pathway across eight omics, the "B cell receptor signaling pathway" across nine layers, "lysosomal lumen" across 13 omics, "extracellular matrix structural constituent" across 11 omics, and the "complement and coagulation cascades" across eight omics (Figure 4A, Supplementary materials 4). In contrast, differential

gene enrichment analysis between RA and OA revealed that the "collagen-containing extracellular matrix" pathway was enriched in seven omics, the "extracellular matrix structural constituent conferring compression resistance" in five layers, and both "vacuolar lumen" and "lysosomal lumen" in four omics (Figure S6A). These findings are in alignment with previous research, highlighting the prominent enrichment of immune and cytoskeletal pathways in RA(Li et al., 2019; Xu et al., 2023). Further analysis indicated that differential proteins with succinylation were particularly enriched in the tryptophan (Trp) metabolism pathway (Figure 4B). In contrast, the pathways most significantly enriched in the proteomics and phosphorylatomics were thermogenesis and proteoglycans in cancer, respectively (Figure S6B). Recent studies have reported significant changes in Trp metabolites in RA patients, which correlate closely with inflammation, disease activity, and quality of life, and which influence the proliferation and metabolism of fibroblast-like synoviocytes(Moulin et al., 2024). In our analysis of genes involved in the "activation of immune response" and "rheumatoid arthritis" pathways, we found significant activation of complement and immune pathways in RA, along with high expression of HLA-DRB1 and other human leukocyte antigen (HLA)-specific markers. Elevated mRNA expression of CCL1, CCL2, CCL3, CCL5, CCL3L3, CXCL2, CXCL3, CXCL6, and CXCL12, as well as transcription factors such as IRF1, JUN, MYD88, and TLR1, was observed in RA compared to OA and NC (Figure 4C). Metabolomic analysis highlighted significant enrichment in amino acid metabolism and pathways such as choline metabolism in cancer and central carbon metabolism in RA (Figure S6C).

By comparing the differential gene expression levels between RA and NC, as well as between RA and OA, we predicted that inflammation-related transcription factors such as RELA, NFKB, and JUN are highly active in RA (Figure 4D, Figure S6D). Upon examining the levels of these predicted transcription factors across various omics, we found that, in RA, JUN exhibited higher protein and phosphorylation levels compared to both NC and OA. Additionally, STAT1 showed elevated transcriptional, protein, and acetylation ompared to NC, while STAT3 displayed lower succinylation level in RA relative to NC. RUNX1 also exhibited higher protein and phosphorylation levels in RA compared to NC (Figure 4E). PTM-SEA analysis indicated that several inflammation-related kinases, including PKACA, ULK3, and MAP2K7, were activated in RA compared to NC and OA (Figure 4F, Figure S6E, Figure S7A), while KSEA analysis revealed the activation of kinases such as CSNK2A2,

PRKG1, CSNK2A1, and MAPKAPK2 in RA (Figure 4G, Figure S7B). These kinases' phosphorylation profiles showed distinctive patterns, including decreased phosphorylation of RPS6KA1 and PRKG1, and increased phosphorylation of PAK1 in RA compared to NC (Figure S7C). Joint analysis of kinases and their substrates revealed that in the RA and NC comparison groups, the phosphorylation levels of certain substrates were positively correlated with changes in the modification or expression levels of their corresponding kinases. For example, the phosphorylation level of BAD at serine 118 was highly positively correlated with the phosphorylation level of its kinase PAK1 at threonine 103 ($R = 0.777$, $P < 0.05$). Similarly, the phosphorylation level of LCP1 at serine 5 was positively correlated with the mRNA level of its kinase RPS6KA1 ($R = 0.674$, $P < 0.05$) (Figure S7D). Finally, we plotted the pathways and genes with the most significant changes in RA across all omics into a signaling pathway network diagram, including the activation of immune response, fatty acid metabolic processes, rheumatoid arthritis, extracellular matrix structural constituents, and the PPAR signaling pathway (Figure S7E).

PCAS analysis of super-omics data from RA

The PCAS score integrates various protein-protein and protein-metabolite regulatory relationships to evaluate the significance and reliability of regulated proteins. This score incorporates changes in four dimensions: self-regulation, upstream regulation, downstream regulation, and molecular interactions, with four levels RNA, WCP, PTM, and metabolite data considered. The PCAS score follows three core principles: (1) Balance between the different omic layers' ability to reflect protein activity, sequencing depth, and differential analysis algorithm; (2) Enrichment to mitigate errors due to proteins with multiple modification sites, calculating the proportion of differential molecules involved in the same regulatory pathway; and (3) Fuzziness, where the direction of modification is less important than the overall regulatory relationship (Figure 5A).

Upon ranking differential proteins by PCAS score, we found that key RA-related genes, such as PTPN22(Ding et al., 2023), SUCLG2, and SYK were among the top 25% of differential proteins calculated by RA vs NC. Besides, compared with other comparisons, the comparison between RA and NC found more known RA-associated genes (Figure 5B, Figure S8A, Supplementary materials 5). Further analysis of factors influencing the PCAS score revealed that different omics levels and regulatory layers all have an

impact on the final PCAS score, indicating that our scoring method indeed integrates multidimensional information (Figure 5C, Figure 5D). The fold change (FC) values in WCP and PTM gradually decreased across the PCAS score quartiles (from 0-25% to 75%-100%), emphasizing the importance of WCP and PTM on PCAS score (Figure 5E). High-intensity proteins were more abundant in the last 25% of PCAS score, indicating greater stability in housekeeping genes (Figure 5F). Notably, the PCAS score of differential proteins from RA and NC showed a weak correlation with FC in tyrosine nitration, but a strong positive correlation with FC in O-GlcNAc glycosylation, and a negative correlation with FC in most omics. In contrast, the PCAS score of differential proteins from RA and OA, as well as OA and NC, exhibited a positive correlation with FC in the majority of omics (Figure 5G). Differential analysis of various omics also showed that differential entries from WCP and PTMs, particularly in phosphorylation, acetylation, and succinylation, were more strongly associated with higher PCAS score, while transcriptomic showed the opposite trend (Figure 5H). The top 25% of differential genes by PCAS score between the RA and NC groups exhibited significantly more percent of differential entries compared to differential genes in the other quartiles (Figure 5I). Except for transcriptomics and malonylation, the differential entries in all other omics are primarily distributed among genes with high PCAS scores (Figure S8B). In summary, the PCAS score was derived from an integrative analysis of multiple omics and multiple interaction type.

We further selected the top 20 genes by PCAS score from the differential genes from RA vs NC group, RA vs OA group, and OA vs NC group (Figure 5J, Figure S8C). Taking the RA vs NC group as an example, these genes did not overlap with the top 10 genes identified in single-omics differential analysis between the RA and NC group. Among these genes, we observed that PRKAR2B, PNPLA2, and LIPE exhibited downregulation across transcription, protein, and phosphorylation. PLIN1 showed consistent downregulation in transcription, protein, phosphorylation, and succinylation levels. LDB3 demonstrated downregulation in transcription, protein, and arginine monomethylation, whereas MZB1 and JCHAIN showed upregulation in transcription, protein, and succinylation. CRIP2 exhibited downregulation across protein, lysine trimethylation and acetylation. Remarkably, the directional changes in the transcriptional, protein, and PTMs of these genes were consistent. Additionally, ITIH3 showed downregulation in transcription and upregulation in both protein and succinylation levels, while STK17B

displayed no changes in transcription or protein levels, but exhibited increased phosphorylation at S10 and S12 (Figure 5J).

We selected 5 genes with the highest absolute values of FC in each omics from top 25% differential genes based on PCAS score (Figure 5K, Figure S8D). we found genes from RA vs NC group that the intensity of several PTMs such as lactylation, succinylation, malonylation, and lysine trimethylation were generally lower in RA than NC and OA. In contrast, O-GlcNAc glycosylation exhibited the opposite trend. These differential genes may serve as potential biomarkers for RA (Figure 5K).

The calculation of the PCAS score takes into account changes in four key dimensions: self-regulation, upstream regulation, downstream regulation, and molecular interactions. Additionally, it incorporates alterations across four levels of biological data: RNA, WCP, PTM, and metabolism. We present diagrams illustrating the upstream and downstream relationships of top genes based PCAS score of RA vs NC, such as STK17B, PLIN1, LDB3, ITIH3, RGCC, and ADH1C (Figure 5L, Figure S9). For instance, changes in the phosphorylation of STK17B lead to downstream alterations in RPS6KB1 phosphorylation, while also interacting with multiple molecules, including TPM2, IGHM, and ATXN2L, all of which undergo various changes of PTMs. Clearly, STK17B undergoes multiple regulatory changes at the molecular, downstream, and interaction levels, which contributes to its high PCAS score. This analysis highlights the ability of the PCAS analysis method to identify genes with significant regulatory impact (Figure 5L).

RA synovium exhibits tumor-like characteristic

We grouped the top 25% genes based on PCAS score from RA vs NC into several modules according to the interactions among these genes. Modules 1 and 2 were predominantly composed of genes involved in PTM interactions, while Modules 3, 4, 5, 6, and 7 were enriched in genes associated with transcription factor (TF) interactions (Figure 6A, Figure S10A). We then conducted GO/KEGG pathway analyses for the quartile genes based on PCAS score from differential comparison (Figure 6B, Figure S10B). RA synovium was enriched in immune-related and adhesion-related pathways, in line with the results of the previous individual enrichment analyses of each omics. Notably, RA also displayed enrichment in pathways such as integrin-mediated signaling, SH2 domain binding, and pyruvate metabolism, which were not typically observed in conventional enrichment analyses (Figure

6B, Figure 4A). Gene Set Enrichment Analysis (GSEA) further confirmed RA enrichment in previously identified pathways, such as kinase activity, focal adhesion, and fatty acid metabolism(Wu et al., 2020). In addition, novel pathways, including epithelial-mesenchymal transition (EMT), VEGFA-VEGFR2 signaling, RAS signaling, and MYC targets v1, were enriched in RA, indicating new areas of relevance for the disease (Figure 6C). Moreover, compared to OA, RA displayed significant enrichment in the “PD-L1 expression and PD-1 checkpoint pathway in cancer" pathway (Figure S10B).

Interestingly, we found that most genes in the epithelial-mesenchymal transition, RAS signaling, VEGFA-VEGFR2 signaling, fatty acid metabolism, MYC targets v1, integrin-mediated signaling, and pyruvate metabolism pathways were enriched among the top 25% of genes based on PCAS score in RA vs NC (Figure 6D, Figure S11A). The integrin signaling pathway, which plays a critical role in signal transduction, angiogenesis, inflammation, and tumorigenesis(Cooper and Giancotti, 2019), and MYC, which can modulate the tumor microenvironment, immune checkpoints, and cytokine secretion to promote tumorigenesis(Jung et al., 2017), are both highly relevant to RA. Given that RA is an immune-driven disease with invasive characteristics and that synovial angiogenesis is active, the enrichment of cancer-related pathways in RA synovium suggests that RA shares tumor-like features.

Finally, by integrating the genes from the seven identified modules with the enriched pathways, we found that the genes in module 2 had the highest proportion belonging to important pathways such as immune response activation, cell-substrate junctions, and RAS signaling, suggesting that module 2 plays a relatively more important role in RA (Figure 6E). Several top genes based on PCAS score, including STK17B and PTPN22, are also in Module 2, and their molecular interactions primarily involve PTMs and protein-protein interactions (Figure 6F). Modules 5 and 6, in contrast, are predominantly involved in epithelial-mesenchymal transition and SH2 domain binding (Figure S11B).

Clinical and applied investigations of PCAS analysis outcomes

We conducted an analysis of the top 20 genes based on PCAS score in RA vs NC, and explored their correlations with clinical indicators (Figure 7A). Our findings revealed that the phosphorylation level of STK17B at S12 was positively correlated with erythrocyte sedimentation rate (ESR) and C-reactive protein (CRP) (Figure 7B). Additionally, we performed the same analysis on

the most functionally important genes in Figure 6F and found relationships between these genes and clinical indicators, as well. For example, the phosphorylation level of MATR3 at S157 showed a positive correlation with rheumatoid factor and ESR (Figure 7C, Figure 7D). We searched the DGIdb database for FDA-approved drugs and found that the number of FDA-approved drugs targeting the differential genes of RA vs NC decreased progressively across quartiles (from 0-25% to 75%-100%) of the PCAS score (Figure 7E). Besides, we examined the top 20 genes based on PCAS score of RA vs NC, along with genes in Figure 6F, for FDA-approved drugs across the DrugBank, DGIdb, and DSigDB databases (Supplemental Table 2). Notably, several genes within the top 10, including CRIP2, LIPE, PLIN1, PRKG1, and STK17B, had existing targeted drugs.

We also assessed the correlation between differential PTMs of these top 20 genes based PCAS score of RA vs NC and their known associations with diseases across OncoKB (Supplemental Table 3). PLIN1 showed high expression in various malignancies. PLIN1 phosphorylation was found to be associated with melanoma and lung adenocarcinoma. Similarly, RGCC phosphorylation was linked to colorectal cancer, while PNPLA2 phosphorylation was associated with neutral lipid storage myopathy. Next, we analyzed the differential PTMs of the top 20 genes based PCAS score of RA vs NC, as well as those in Figure 6F, and examined their effects on protein functional activity (Supplementary Materials 6). A total of 129 differential PTM sites were identified, 14 of which were associated with known alterations in protein activity. These were categorized into 14 functional processes, 9 biological processes, and 8 protein interactions (Figure 7F).

To further explore the connection between RA and cancer, we analyzed the expression of cancer-related genes within the top 30 genes based PCAS score of each comparison. Notably, we found that the transcription and phosphorylation levels of the oncogene AR were lower in RA compared to NC, whereas RA showed higher phosphorylation of the oncogenes CNBP and FES. Additionally, ETV6 and MSH6, both tumor suppressor genes, exhibited increased phosphorylation in RA compared to NC. The acetylation levels of NBN and NSD3 were also higher in RA than in OA. On the other hand, the phosphorylation levels of PRKCB and TEC, both cancer-related genes, were lower in RA compared to NC, while SKI exhibited higher phosphorylation levels than in the other two groups (Figure 7G).

Through PCAS analysis, we constructed a super-omics landscape,

representing the primary genes and crucial pathways involved in the pathogenesis of RA. This landscape not only elucidates the interrelationships between genes, pathways, and their upstream and downstream interactions, but also highlights the potential targeted drugs for each molecular entity, providing a molecular blueprint for future RA research (Figure 8).

DISCUSSION

Rheumatoid arthritis (RA) is a systemic autoimmune disorder primarily affecting the synovial joints(Radu and Bungau, 2021) It is also classified as an immune-mediated inflammatory disease. The immunopathogenesis of RA spans several decades, beginning with the production of autoantibodies against post-translationally modified proteins. Over the years, this leads to asymptomatic autoimmunity and progressive immune system remodeling, eventually resulting in the transformation of fibroblast-like synoviocytes (FLS) from benign mesenchymal cells to aggressive, tumor-like cells capable of tissue destruction and invasion(Weyand and Goronzy, 2021). Despite extensive research, the mechanisms by which these cells acquire their pathogenic state remain incompletely understood. Current therapeutic targets for RA include biologic and targeted synthetic DMARDs (b/tsDMARDs), which act on signaling molecules and adaptive immune system components (e.g., TNF-α, IL-6 inhibitors)(Brown et al., 2024). Although early inflammation control improves patient outcomes, a significant proportion of patients do not achieve adequate therapeutic goals despite initiating csDMARDs or b/tsDMARDs. Furthermore, some patients, although in remission, face difficulties when tapering their medications. As personalized cancer therapies continue to evolve, RA precision medicine has lagged behind, and no reliable biomarkers have been established for clinical use(Brown et al., 2024). Given the limited understanding of RA's molecular mechanisms and the paucity of effective treatments, more in-depth research into its underlying pathogenesis is crucial.

In recent years, various omics techniques, particularly the emergence of various post-translational modification (PTM) omics, have provided powerful methods for generating comprehensive molecular profiles of cells and tissues. These approaches offer significant potential for investigating disease mechanisms. However, in RA, systematic multi-omics studies remain scarce, with existing studies often lacking diversity, particularly in the range of PTMs explored. To address this gap, we introduced the concept of super-omics and developed the PCAS method for processing super-omics data. Using these approaches, we conducted a thorough analysis of RA synovial tissue and

discovered that RA shares characteristics with tumor-like diseases. We have identified certain genes, such as STK17B, that may play a significant role in the occurrence and development of RA.

Multi-omics refers to the integration of two or more omics, such as genomics, transcriptomics, and proteomics, to conduct comprehensive investigations. The primary goal is to identify composite biomarkers by correlating and deeply integrating data across multiple omic layers. Super-omics, however, extends this approach by integrating over ten different omics, with protein serving as the focal point. In contrast to traditional multi-omics studies, super-omics incorporates at least three omic layers, making it a more robust approach for understanding disease biology.

Traditional multi-omics analyses typically rely on differential analysis at the single omic level, followed by statistical correlation and pathway analysis. However, these methods often integrate only 2-3 omic datasets at a time, which limits their ability to capture the full complexity of disease mechanisms. In contrast, PCAS enables the simultaneous integration a dozen of omic data types, consolidating the findings across different omic layers, identifying key molecular alterations, and providing the regulatory relationships between key molecules. By assigning a PCAS score to each differential protein, we can efficiently prioritize the most significant molecules for further investigation.

Our PCAS analysis revealed several novel findings, particularly regarding cancer-associated pathways that had not been previously highlighted in conventional immune-related analyses. These included the integrin-mediated signaling pathway, VEGFA-VEGFR2 signaling, RAS signaling, MYC targets v1, and SH2 domain binding. These pathways were largely enriched in the top quartile of genes based PCAS score, suggesting their critical importance in RA pathogenesis. Moreover, multiple cancer-related genes within the top 30 genes based PCAS score showed significant changes in phosphorylation and acetylation levels in RA, further supporting the hypothesis that RA may resemble a tumor-like disease.

Our findings underscore the invasive characteristics of RA synovial tissue, which exhibits elevated angiogenesis and infiltration, forming pannus that eventually invades joint cartilage and bone(Paleolog, 2002). Chronic inflammation is a hallmark of RA and is also considered a risk factor for malignancies. A recent large-scale real-world study(Wang et al., 2023) confirmed that RA patients have a higher risk of lymphoma and lung cancer,

further suggesting the tumor-like nature of RA.

In conclusion, we have developed and introduced the super-omics approach, which provides a comprehensive molecular blueprint of RA pathogenesis, paving the way for identifying the key genes and pathways involved. While the methodology is still in its infancy, it holds great promise as a robust framework for more integrated and impactful studies of life sciences research. As the saying goes, 'Don’t miss the big picture while chasing the details'—in the intricate web of molecular mechanisms, focusing on key molecules and their interactions rather than haphazardly dissecting individual functions is vital for advancing RA research. The super-omics landscape presented here plants the seeds for future breakthroughs, offering fertile ground for innovative studies and therapeutic interventions targeting RA.

ACKNOWLEDGMENTS

We are thankful for the State Key Laboratory for Diagnosis and Treatment of Infectious Diseases. We appreciate the assistance provided by the First Affiliated Hospital of Zhejiang University School of Medicine and the Sir Run Run Shaw Hospital to this study. This study has received support from the National Natural Science Foundation of China (grant numbers 82203610), the National Key R&D Program of China (grant numbers 2022YFC3602003), the Natural Science Foundation of Zhejiang Province (grant numbers LR22H160011), the opening foundation of the State Key Laboratory for Diagnosis and Treatment of Infectious Diseases (grant number SKLID2023KF06), and the National Key Research and Development Program (grant number 2022YFA1303801).

AUTHOR CONTRIBUTIONS

Conceptualization, X.O., L.W., F.J.; methodology, S.J., Q.M., M.Z., Z.S., F.J.; validation, L.X., S.J., Q.H.; formal analysis, N.A., D.C., J.Z., L.S., D.Z., J.Y., F.J.; data curation, L.X., N.A., F.Z., F.J.; investigation, W.C., J.X., D.Z., Y.L., J.W., J.Z., D.X., J.L., Y.C., Y.H.; writing – original draft, L.X., N.A., S.J., X.O.; writing – review & editing, all authors; supervision, Z.S., L.W., J.L., F.J.; project administration, L.X., N.A., X.O., J.L., F.J.; funding acquisition, J.Z., Z.S., J.L., F.J.;

DECLARATION OF INTERESTS

The authors declare no competing interests.

651 **KEY RESOURCES TABLE**

REAGENT or RESOURCE	SOURCE	IDENTIFIER
Biological samples		
Tissue samples	This paper	N/A
Chemicals		
Urea	Sigma	U5378
sodium chloride	Aladdin	C111535
protease inhibitor	Sangon	C600387
0.5M EDTA	Beyotime	ST063
Phosphatase inhibitor	Beyotime	P1081
Deacetylase inhibitor	Beyotime	P1113
PR-619	MCE	HY-13814
PUGNAc	Aladdin	P275897
DTT	Sigma	43816
CAA	Aladdin	C106072
Tris-HCl (pH 8.0)	Beyotime	ST780
Tris-HCl (pH 10.0)	Sangon	B548129
Tyrisin	Beierli	BELT001
TFA	Thermo	85183
ACN	Sigma	34851
Water	Aladdin	W433894
Triethylammonium acetate	Aladdin	T345383
Ethanolamine	Sigma	398136
DMP	Sigma	D8388
Hydroxylamine	Sigma	467804
TEAB	Aladdin	T331003
ammonium hydroxide	Sigma	5438300100
ammonium bicarbonate	Sigma	A6141
Formic acid	Thermo	28905
Critical commercial assays		
TMTpro 18-plex	Thermo	A52047
Fe-NTA Phosphopeptide Enrichment Kit	Thermo	A32992

PTMScan Acetyl-Lysine Motif [Ac-K] Kit	CST	13416
PTMScan O-GlcNAc [GlcNAc-S/T] Motif Kit	CST	95220
PTMScan Mono-Methyl Arginine Motif [mme-RG] Kit	CST	12235
PTMScan Pan-Methyl Lysine Kit	CST	14809
PTMScan Glutaryl-Lysine [Glut-K] Kit	CST	26101
PTMScan Malonyl-Lysine [Mal-K] Kit	CST	93872
PTMScan Succinyl-Lysine Motif [Succ-K] Kit	CST	13764
PTMScan Nitro-Tyrosine Motif [Nitro-Y] Kit	CST	44462
Anti-L-lactyllysine kit	Micron Bio	WM102
Deposited data		
DrugBank	(Knox et al., 2011)	https://go.drugbank.com/
DGIdb	(Cannon et al., 2024)	https://dgidb.org/
DSigDB	(Yoo et al., 2015)	https://dsigdb.tanlab.org
PTMD	(Xu et al., 2018)	https://ptmd.biocuckoo.cn/
hTFtarget	(Zhang et al., 2020)	https://guolab.wchscu.cn
iPTMnet	(Huang et al., 2018)	https://research.bioinformatics.udel.edu/iptmnet/
UbiBrowser	(Wang et al., 2022)	http://ubibrowser.bio-it.cn/ubibrowser_v3/

DEPOD	(Damle and Köhn, 2019)	https://depod.bioss.uni-freiburg.de/
UbiNet	(Li et al., 2021)	https://awi.cuhk.edu.cn/~ubinet
Phospho.ELM	(Diella et al., 2008)	http://phospho.elm.eu.org/
PhosphoSitePlus	(Hornbeck et al., 2015)	https://www.phosphosite.org/
KEGG	(Kanehisa et al., 2021)	https://www.genome.jp/kegg/
BioGRID	(Oughtred et al., 2021)	https://thebiogrid.org/
UniprotKB	(Consortium, 2025)	https://www.uniprot.org/
Enzyme and substrate dataset	This paper	N/A
Software and algorithms		
R v4.3.0	R Development Core Team	https://www.r-project.org/
MaxQuant v2.6.2.0	(Cox and Mann, 2008)	http://maxquant.org/
PCAS algorithms	This paper	N/A
Other		
Sep-Pak C18 1 cc Vac Cartridge	waters	WAT023590
Empore C18 diaphragm	3M	98060402181

RESOURCE AVAILABILITY

Lead contact

Requests for additional information, resources, and reagents should be addressed to the lead contact, Feiyang Ji (feiyangji@zju.edu.cn).

Materials availability

This study did not generate new unique reagents.

Data and code availability

Raw proteomic data files and processed proteomic datasets have been deposited in the ProteomeXchange Consortium (https://proteomecentral.proteomexchange.org) via the iProX partner repository (dataset identifier: PXD059446)(Chen et al., 2022; Ma et al., 2019). The raw and processed transcriptomic data have been submitted to the GEO database (dataset identifier: GSE285865)(Clough and Barrett, 2016). Raw and processed metabolomic data are available in the MetaboLights database (dataset identifier: MTBLS11642)(Kale et al., 2016). All other data can be obtained upon request from the lead contact.

EXPERIMENTAL MODEL AND SUBJECT DETAILS

Human Subjects

6 RA patients, 6 OA patients and 6 patients with meniscus injuries (NC patients) were included in this study. RA were diagnosed according to the 1987 American College of Rheumatology criteria for and knee OA were diagnosed according to American College of Rheumatology criteria, respectively. The detailed clinical information of all Subjects is presented in supplemental Table S1. Ethical approval was obtained from the Ethics Committee of the First Affiliated Hospital, Zhejiang University School of Medicine, and informed consent was obtained from all participants included in this prospective study.

METHOD DETAILS

Specimen Acquisition

All synovial tissues were obtained from the knee joints of 18 patients who underwent knee replacement surgery and arthroscopic surgery at the First Affiliated Hospital of Zhejiang University School of Medicine. To avoid RNA and protein degradation, all synovial tissues were obtained within 30 minutes after surgery. After washed twice with cold PBS, synovial tissue was immediately freeze in liquid nitrogen after then stored at -80 °C until use.

16S Sequencing

DNA Extraction and Amplification

Synovial tissue samples were promptly snap-frozen and stored at −80°C following collection. DNA was extracted from the tissues using the MagPure Soil DNA LQ Kit (Qiagen, Guangzhou, China) according to the manufacturer's instructions. DNA concentration was determined with a NanoDrop 2000 spectrophotometer (Thermo Fisher Scientific, Waltham, MA, USA), and DNA

integrity was assessed via agarose gel electrophoresis. The V3-V4 regions of the bacterial 16S rRNA gene were amplified in a 25 μL reaction mixture using universal primers (343F: 5′-TACGGRAGGCAGCAG-3′ and 798R: 5′-AGGGTATCTAATCCT-3′). The reverse primer contained a sample barcode, and both primers were tagged with Illumina sequencing adapters.

Library Construction and Sequencing

Amplified products were analyzed by gel electrophoresis to confirm successful amplification. PCR products were then purified using Agencourt AMPure XP beads (Beckman Coulter, USA) and quantified with the Qubit dsDNA Assay Kit (Thermo Fisher Scientific, Waltham, MA, USA). Concentrations were normalized for sequencing. Sequencing was performed on an Illumina NovaSeq 6000 platform, employing paired-end sequencing with 250-base cycles (Illumina Inc., San Diego, CA; OE Biotech Co., Shanghai, China).

Bioinformatics Analysis

The raw sequencing data were obtained in FASTQ format. Adapter sequences were trimmed from paired-end reads using Cutadapt software. Following trimming, reads underwent quality filtering, denoising, merging, and chimera removal using DADA2(Callahan et al., 2016), with default parameters in QIIME2(Bolyen et al., 2019). This process generated representative reads and an Amplicon Sequence Variant (ASV) abundance table. Representative reads for each ASV were selected in QIIME2 and annotated by aligning to the Silva database (Version 138) using the q2-feature-classifier, with default settings. For ITS data, the UNITE database was used for annotation. All 16S rRNA gene amplicon sequencing and subsequent data analysis were carried out by OE Biotech Co., Ltd. (Shanghai, China).

RNA Sequencing

RNA Isolation and Library Preparation

Total RNA was extracted from tissue samples using the RNeasy Lipid Tissue Mini Kit (Qiagen, Hilden, Germany) following the manufacturer’s protocol. RNA purity and concentration were assessed with a NanoDrop 2000 spectrophotometer (Thermo Fisher Scientific, USA), while RNA integrity was evaluated using the Agilent 2100 Bioanalyzer (Agilent Technologies, Santa Clara, CA, USA). RNA-seq library construction was performed using the VAHTS Universal V6 RNA-seq Library Prep Kit as per the manufacturer's instructions. RNA sequencing and analysis were conducted by OE Biotech Co.,

Ltd. (Shanghai, China).

RNA Sequencing, Quantification, and Normalization

Libraries were sequenced on an Illumina NovaSeq 6000 platform, generating paired-end reads of 150 bp. Approximately 47 million raw reads were generated per sample. Raw reads in FASTQ format were processed using Fastp(Chen et al., 2018) to remove low-quality reads, resulting in approximately 46 million clean reads per sample. Clean reads were then aligned to the reference genome using HISAT2(Kim et al., 2015). Gene expression was quantified in fragments per kilobase of transcript per million mapped reads (FPKM)(Roberts et al., 2011), and read counts for each gene were determined using HTSeq-count(Anders et al., 2015).

Non-targeted metabolomics

Sample Preparation

Thirty milligrams of the sample were accurately weighed and transferred into a 1.5 mL Eppendorf tube. To this, two small steel beads were added, followed by 400 μL of a methanol-water solution (4:1, v/v) containing a mixed internal standard at a concentration of 4 μg/mL. The mixture was pre-chilled at -40°C for 2 minutes, then homogenized using a bead mill at 60 Hz for 2 minutes. Ultrasonic extraction was performed in an ice-water bath for 10 minutes, after which the sample was incubated at -40°C for 2 hours. The sample was then centrifuged at 13,000 rpm for 20 minutes at 4°C. A 150 μL aliquot of the supernatant was carefully transferred into an LC vial using a syringe and stored at -80°C until analysis by LC-MS. Quality control (QC) samples were prepared by pooling equal volumes of extract from all samples. All reagents were pre-chilled at -20°C before use.

LC-MS/MS Analysis

Metabolomic analysis was carried out by Shanghai Luming Biological Technology Co., Ltd. (Shanghai, China) using an ACQUITY UPLC I-Class Plus system (Waters Corporation, Milford, USA) coupled with a Q-Exactive mass spectrometer (Thermo Fisher Scientific, Waltham, MA, USA), equipped with a heated electrospray ionization (ESI) source. Both ESI positive and negative ion modes were employed for metabolic profiling. Chromatographic separation was achieved using an ACQUITY UPLC HSS T3 column (1.8 μm, 2.1 × 100 mm) in both modes. The mobile phase consisted of (A) water with 0.1% formic acid (v/v) and (B) acetonitrile with 0.1% formic acid (v/v). The gradient elution

program was as follows: 0 min, 5% B; 2 min, 5% B; 4 min, 30% B; 8 min, 50% B; 10 min, 80% B; 14 min, 100% B; 15 min, 100% B; 15.1 min, 5% B; 16 min, 5% B. The flow rate was 0.35 mL/min, and the column temperature was maintained at 45°C. The injection volume was 3 µL. Mass spectrometric detection was performed over a range of m/z 70 to 1,050 with a resolution of 70,000 for full MS scans and 17,500 for HCD MS/MS scans. Collision energies were set at 10, 20, and 40 eV. The mass spectrometer parameters were as follows: spray voltage, 3800 V (+) and 3000 V (−); sheath gas flow rate, 35 arbitrary units; auxiliary gas flow rate, 8 arbitrary units; capillary temperature, 320°C; aux gas heater temperature, 350°C; S-lens RF level, 50.

Data Preprocessing and Statistical Analysis

LC-MS data were processed using Progenesis QI V2.3 software (Nonlinear Dynamics, Newcastle, UK) for baseline correction, peak detection, integration, retention time alignment, and normalization. Parameters included a 5 ppm precursor mass tolerance, 10 ppm product mass tolerance, and a 5% product ion threshold. Compound identification was based on accurate mass-to-charge ratios (m/z), fragmentation patterns, and isotopic distributions, referencing databases such as the Human Metabolome Database (HMDB), Lipidmaps (V2.3), Metlin, and in-house databases. Missing values (>50% of data points missing per group) were imputed by replacing them with half of the minimum detected value. Inaccurate compound identifications (scores <36 out of 60) were excluded. The resulting data matrix was constructed from both positive and negative ion mode data.

Orthogonal Partial Least-Squares Discriminant Analysis (OPLS-DA) was applied to identify metabolites distinguishing the groups. To assess model reliability, 7-fold cross-validation and 200 permutations (Response Permutation Testing, RPT) were performed. Variable Importance in Projection (VIP) scores from the OPLS-DA model were used to prioritize metabolites contributing to group separation. Statistical significance of differences between groups was evaluated using a two-tailed Student's t-test. Differential metabolites were selected with VIP scores >1.0 and p-values <0.05.

Liquid chromatography tandem mass spectrometry (LC-MS/MS) proteomics

Sample Preparation

Twenty milligrams of joint synovial tissue was homogenized in liquid nitrogen

and resuspended in 200 µL of 4°C lysis buffer (8 M urea, 50 mM Tris-HCl pH 8.0, 75 mM NaCl, 2.5 mM DTT, 1 mM EDTA, 1× protease inhibitor cocktail, 1× phosphatase inhibitor cocktail, 1× acetylation inhibitor cocktail, 20 µM PUGNAc). The sample was sonicated in an ice-water bath for 4 min, followed by a 2 min resting period, repeating the cycle three times. The lysate was then centrifuged at 15,000 × g for 20 min at 4°C, and the supernatant was collected. Protein concentration was determined using the BCA assay. DTT was added to the supernatant to a final concentration of 5 mM and incubated at 30°C for 30 min. After cooling to room temperature, CAA was added to a final concentration of 15 mM, and the sample was incubated at 25°C for 30 min in the dark. Based on the protein concentration, 1 mg of protein from each sample was mixed with 3 volumes of 50 mM Tris-HCl (pH 8.0). Porcine trypsin was added at a 1:50 (w/w) protein-to-enzyme ratio, and the digestion was performed at 25°C for 12 hours with agitation at 200 rpm. TFA was added to the digestion mixture to a final concentration of 0.5%, and the sample was incubated on ice for 10 min. The mixture was then centrifuged at 1500 × g for 10 min at 4°C, and the supernatant was collected. Peptides were desalted using a C18 column, which was washed sequentially with two volumes of acetonitrile (ACN) and three volumes of 0.1% TFA. After acidification, the peptides were passed through the column and wash three times with 0.1% TFA. Finally, peptides were eluted with 50% ACN containing 0.1% TFA and dried under vacuum.

Tandem mass tag (TMT) labeling of peptides

The dried peptides were dissolved in 100 µL of 50 mM TEAB (triethylammonium bicarbonate buffer). To prepare the TMT labeling reagent, 40 µL of acetonitrile (ACN) was added to 0.5 mg of the TMT reagent, followed by vortexing and incubation. The dissolved peptides were then transferred to TMT labeling tubes and incubated at room temperature for 1.5 hours. After incubation, 10 µL of 5% hydroxylamine was added to quench the reaction, and the mixture was incubated at room temperature for an additional 15 min. The labeled samples were pooled and dried by vacuum centrifugation. The dried peptides were reconstituted in 2 mL of 0.1% TFA and desalted using a C18 column. After desalting, the peptides were dried again by vacuum centrifugation.

Offline bRP fractionation

TMT-labeled peptides were fractionated using an Agilent 1260

chromatography system with solvent A consisting of pure water containing 0.1% triethylamine and solvent B containing acetonitrile with 0.1% triethylamine. The flow rate was set to 0.5 mL/min. Prior to loading the sample, the column was equilibrated for 30 min with the following gradient: 90% solvent B for 10 min, 50% solvent B for 5 min, and 2% solvent B for 15 min. The sample was dissolved in solvent A to a final peptide concentration of 20 mg/mL, followed by centrifugation at 15,000 × g for 5 min at room temperature, and the supernatant was collected for analysis. Fractions were collected every minute, yielding a total of 70 fractions. The liquid chromatography gradient was as follows: 0 min at 2% solvent B, 5 min at 12% solvent B, 54 min at 30% solvent B, 57 min at 36% solvent B, 60 min at 51% solvent B, 65 min at 90% solvent B, and 75 min at 90% solvent B. After collection, the fractions were dried and combined into 10 intervals. One percent of the total peptide was set aside for standard proteomics analysis, while the remaining fractions were used for proteomics analysis focused on post-translational modifications.

Phosphopeptide enrichment

The peptides were dissolved in 200 µL of Binding/Wash Buffer (80% acetonitrile with 0.1% TFA) and centrifuged at 15,000 × g for 10 min at room temperature to collect the supernatant. The inner tube of the kit was trimmed at the bottom and placed in a 1.5 mL EP tube, followed by centrifugation at 1000 × g for 30 s at room temperature to discard the filtrate. Next, 300 µL of Binding/Wash Buffer was added to the inner tube, and the centrifugation was repeated at 1000 × g for 30 s to discard the filtrate. This step was repeated once. Afterward, a rubber filter was inserted into the bottom of the inner tube, and the peptide supernatant was added. The top cap was placed on the tube, and the mixture was incubated at room temperature for 30 min, with gentle tapping every 10 min. After removing the rubber filter, the top cap was loosened, and the inner tube was centrifuged at 1000 × g for 30 s at room temperature to collect the filtrate. Binding/Wash Buffer (300 µL) was added to the inner tube, and centrifugation was performed again at 1000 × g for 30 s to discard the filtrate, repeating the step twice. Next, 300 µL of mass spectrometry-grade water was added to the inner tube, followed by centrifugation at 1000 × g for 30 s to discard the filtrate. Finally, the inner tube was transferred to a new 1.5 mL EP tube, and 100 µL of Elution Buffer (5% ammonia solution) was added. The tube was centrifuged at 1000 × g for 30 s to collect the eluate. The elution step was repeated, and both eluates were combined and dried under vacuum.

Antibody-based PTM peptide enrichment

To prepare antibody-conjugated beads for the enrichment of post-translationally modified peptides, protein A/G beads were covalently coupled with antibodies. First, the antibody-bound protein A/G beads were centrifuged at 2000 × g for 30 s at 4°C, and the supernatant was discarded. The beads were then washed three times with 1 mL of pre-chilled antibody cross-linking wash buffer (100 mM sodium borate, pH 9.0). Afterward, 1 mL of antibody cross-linking buffer (20 mM DMP in antibody cross-linking wash buffer) was added, and the mixture was incubated on a 3D shaker at room temperature for 30 min. The beads were then centrifuged to remove the supernatant. The beads were blocked by washing twice with 1 mL of pre-chilled antibody blocking buffer (200 mM ethanolamine, pH 8.0), followed by resuspension in 1 mL of antibody blocking buffer and incubation on a 3D shaker at 4°C for 2 hours. The supernatant was discarded after centrifugation. The beads were then washed three times with 1 mL of pre-chilled IAP buffer (50 mM MOPS/NaOH, pH 7.2, 10 mM Na2HPO4, 50 mM NaCl) and stored at 4°C for short-term use. For peptide loading, dried peptides were dissolved in pre-chilled IAP buffer, vortexed, and sonicated. After centrifugation at 15,000 × g for 5 min at 4°C, the supernatant was collected and added to the antibody-conjugated beads. The mixture was incubated on a 3D shaker at 4°C for 2 hours. After centrifugation at 2000 × g for 30 s at 4°C, the supernatant was retained, and the beads were washed five times by adding 0.5 mL of pre-chilled IAP buffer, mixing by inversion, and centrifuging at 2000 × g for 30 s at 4°C. The beads were washed once more with 0.5 mL of pre-chilled mass spectrometry-grade water, following the same centrifugation steps. The beads were then incubated with 50 µL of 0.15% TFA at room temperature on a 3D shaker for 10 min, followed by centrifugation at 2000 × g for 30 s at room temperature to collect the supernatant. This step was repeated, and the supernatants were pooled into a single 1.5 mL EP tube. The collected supernatant was desalted using homemade C18 cartridges and then vacuum-dried.

Glycosylated peptide enrichment

The peptides were dissolved in a solution of 95% acetonitrile (ACN) and 1% trifluoroacetic acid (TFA), and centrifuged at 15,000 × g for 5 min at room temperature to collect the supernatant. The MAX column was equilibrated by washing sequentially with 1 mL of ACN (three times), 1 mL of 100 mM triethylammonium acetate buffer (three times), 1 mL of mass

spectrometry-grade water (three times), and 1 mL of 95% ACN + 1% TFA solution (three times). The peptide solution was then loaded onto the equilibrated column, and the process was repeated once. After loading the peptides, the column was washed with 0.5 mL of 95% ACN + 1% TFA once, followed by five washes with 1 mL of 95% ACN + 1% TFA. Finally, the glycosylated peptides were eluted with 500 µL of 50% ACN + 0.1% TFA, and the eluate was vacuum-dried.

LC-MS/MS analysis

For general proteomics, TMT-labeled peptide samples, prepared after offline bRP fractionation, were desalted, subjected to vacuum evaporation, and then resuspended in 2% ACN and 0.1% formic acid (FA). LC-MS/MS analysis was performed using a Thermo Fisher Scientific Orbitrap Exploris 480 mass spectrometer coupled with an UltiMate NCS-3500RSC system. Gradient elution was carried out at a flow rate of 450 nL/min over 120 minutes. The solvent gradient composition was as follows: 3%-8% solvent B from 0 to 3 minutes, 8%-26% solvent B from 4 to 90 minutes, 26%-38% solvent B from 91 to 110 minutes, 38%-80% solvent B from 111 to 115 minutes, and 80% solvent B from 116 to 120 minutes. MS spectra were acquired at a resolution of 60,000 over a mass range of 400–1200 m/z, with a normalized automatic gain control (AGC) target of 300%. MS2 spectra were collected at a resolution of 15,000, using Turbo TMT and higher-energy collision-induced dissociation (HCD) with a collision energy of 35%. The isolation window was set to 1.6 m/z, and the dynamic exclusion time was 30 seconds.

For phosphoproteomics, the solvent gradient was as follows: 2%-5% solvent B from 0 to 5 minutes, 5%-22% solvent B from 6 to 90 minutes, 22%-35% solvent B from 91 to 110 minutes, 35%-80% solvent B from 111 to 116 minutes, and 80% solvent B from 117 to 120 minutes. The MS spectra were acquired with a resolution of 60,000 over a mass range of 350–1400 m/z, using the same AGC target (300%). MS2 spectra were obtained with a resolution of 15,000, Turbo TMT, and HCD at 35% collision energy, with an isolation window of 1.6 m/z and a dynamic exclusion time of 20 seconds.

For other post-translational modifications (PTMs), the solvent gradient was: 6%-11% solvent B from 0 to 3 minutes, 11%-26% solvent B from 4 to 40 minutes, 26%-40% solvent B from 41 to 52 minutes, 40%-80% solvent B from 53 to 56 minutes, and 80% solvent B from 57 to 60 minutes. MS spectra were recorded at a resolution of 60,000 in the mass range of 350–1400 m/z with a

300% AGC target. MS2 spectra were obtained at a resolution of 15,000, using Turbo TMT and HCD at 35%, with a 1.6 m/z isolation window and a dynamic exclusion time of 20 seconds.

Raw data processing

Protein identification and quantification were performed using MaxQuant, except for complex glycosylation analysis. TMT18plex quantification was used for the whole-cell proteome, acetylome, and phosphoproteome. The human UniProtKB database was employed for searching, with automatic reverse database and known contaminants as decoys. Carbamidomethylation of cysteine was set as a fixed modification, while N-terminal acetylation and methionine oxidation were considered variable modifications. For phosphoproteomics, acetylomics, and other post-translational modification analyses, additional variable modifications were included: phosphorylation (79.966331), acetyl-Lysine (42.010565), O-GlcNAc (203.079373), mono-methyl arginine (14.015650), pan-methyl lysine (14.015650; 28.031300; 42.046950), glutaryl-Lysine (114.031694), malonyl-Lysine (86.000394), succinyl-Lysine (100.016044), nitro-Tyrosine (44.985078), and lactyl-Lysine (72.021129). A maximum of five modifications per peptide was allowed, and trypsin was used as the enzyme with up to two missed cleavages. Default MaxQuant settings were used for all other parameters.

For complex glycosylation analysis (including N- and O-glycosylation), raw data were processed using pGlyco and pQuant(Zeng et al., 2021) for qualitative and quantitative analysis, respectively. pGlyco-N-Human and Multi-Site-O-Glycan were used as glycan databases for N- and O-glycosylation, with TMT18 quantification applied. Max missed cleavages were 2, maximum variable modifications on peptides were 3, and precursor tolerance was 4 ppm. Other settings were kept at the software defaults.

STATISTICAL ANALYSIS

Normalization and differential analysis

Transcriptomic data: Sequencing data were quality-controlled, and genes expressed in at least 80% of the samples were retained. Differential expression analysis was performed on the filtered count matrix using the DESeq2 package(Love et al., 2014). Genes with an absolute fold change ≥ 2 and an FDR < 0.05 were considered differentially expressed. p-values were adjusted using the Benjamini-Hochberg method.

Proteomic and PTM data: Raw data obtained from MaxQuant were cleaned by removing reverse hits and data with localization probability < 0.75. Quantitative data were log2-transformed and median-normalized before performing differential analysis using the limma package(Ritchie et al., 2015). A absolute fold change ≥ 1.5 and an FDR < 0.05 were applied to identify significantly differentially expressed proteins.

Enrichment analysis

Gene Ontology (GO) and Kyoto Encyclopedia of Genes and Genomes (KEGG) Enrichment Analysis: Differentially expressed genes were subjected to GO and KEGG functional enrichment analysis using the clusterProfiler package(Wu et al., 2021). This analysis assessed biological processes (BP), molecular functions (MF), cellular components (CC), and signaling pathways related to the genes. A p-value < 0.05 was considered statistically significant.

Gene Set Enrichment Analysis (GSEA): Gene sets from the MSigDB database(Liberzon, 2014), including Hallmark, GO, KEGG, Reactome, and WikiPathways, were used for GSEA. ClusterProfiler was utilized to perform GSEA based on gene fold change values or PCAS scores. A p-value < 0.05 was considered statistically significant.

PTM-SEA enrichment analysis

For phosphorylation modification data, PTM-Signature Enrichment Analysis (PTM-SEA) was performed based on the PTMsigDB v2.0.0 database(Krug et al., 2019). Using the ssGSEA 2.0 package(Barbie et al., 2009) , enrichment analysis was conducted to obtain NES scores and p-values from 1000 permutation tests. The analysis identified phosphorylation modification-related features, such as stress disturbances, kinase activities, signaling pathways, and diseases. Differential analysis was used to filter features with a p-value < 0.05 as significantly enriched.

KSEA kinase activity analysis

Kinase-substrate enrichment analysis (KSEA) was performed on phosphorylation data using the KSEAapp package(Wiredja et al., 2017) to evaluate kinase activities associated with the identified phosphorylation sites. Kinase-substrate relationships were obtained from the PhosphoSitePlus and NetworKIN databases(Linding et al., 2007) .

Transcription factor activity analysis

Transcription factor-regulon interactions were retrieved from the CollecTRI database(Müller-Dott et al., 2023). Transcription factors with at least five target genes were selected. Transcription factor activity was evaluated using a univariate linear model (ULM) based on the fold changes of the target genes.

Correlation analysis

Pearson correlation analysis was applied to assess the relationships between samples, genes, or genes and clinical indicators. A p-value < 0.05 was considered statistically significant, and the correlation coefficient (r) was calculated to represent the strength of the association.

PCAS analysis

Integration of prior knowledge

Prior knowledge was integrated by compiling relationships from various databases (hTFtarget, iPTMnet, UbiBrowser, DEPOD, UbiNet, Phospho.ELM, PhosphoSitePlus, KEGG, BioGRID, and summarized from the published literature (Supplementary materials 7)), including transcription factor-target gene interactions (TF), enzyme-substrate interactions (ES), enzyme-metabolite interactions (EM), and protein-protein interactions (INTACT), to construct a prior knowledge table. Quantitative and differential gene expression data from transcriptomics, proteomics, PTM, and metabolomic were obtained. The deduplicated quantitative genes from transcriptomics, proteomics, and PTM data were compiled into "GENE". The deduplicated quantitative genes from transcriptomics and proteomics were compiled into "EXP", while the deduplicated quantitative genes from proteomics and PTM were compiled into "FUN". The genes with significant changes were categorized as "GENE_R", "EXP_R", and "FUN_R", respectively, forming the PCAS_ID table.

Using the PCAS_ID table and the integrated prior knowledge table, a PCAS_knowledge table was generated, which was divided into the following sub-tables:

TF Sub-table: Genes in the "GENE" category of PCAS_ID that are transcription factors, and genes in the "EXP" category that are transcription factor target genes.

ES Sub-table: Genes in the "GENE" category of PCAS_ID that are post-translational modification enzymes, and genes in the "FUN" category that

are enzyme substrates.

EM Sub-table: Genes in the "GENE" category of PCAS_ID that correspond to enzymes catalyzing metabolites.

INTACT Sub-table: Genes in the "GENE" category of PCAS_ID that are part of protein-protein interactions.

Each sub-table contains a "regulated" column with values of "YES" or "NO", indicating whether the corresponding gene is regulated (based on "GENE_R", "EXP_R", or "FUN_R"). These sub-tables were merged into a comprehensive PCAS_knowledge_use table, which includes columns for the upstream "gene", downstream "target", "direction" (values of "YES" or "NO"), "type" (values of TF, ES, EM, or INTACT), and "regulated" status (values of "YES" or "NO"). Duplicate values were removed, and the entries with overlapping relationships between ES and INTACT were excluded.

Parameter settings

The following parameters were set based on balance principles:

Omics-level Balancing (BL):

$BL_{RNA} = 1$, $BL_{WCP} = 2$, $BL_{PTM} = 2$, $BL_{META} = 2$

Sequencing Depth (BD):

$BD_{RNA} = 1$, $BD_{WCP} = 1$, $BD_{PTM} = 1$, $BD_{META} = 1$

Differential Analysis Method (BA):

$BA_{RNA} = \sqrt{(All_{RNA} / Regulated_{RNA})}$, $BA_{WCP} = \sqrt{(All_{WCP} / Regulated_{WCP})}$, $BA_{PTM} = \sqrt{(All_{PTM} / Regulated_{PTM})}$, $BA_{META} = \sqrt{(All_{META} / Regulated_{META})}$

The following enrichment principles were applied:

Protein Site Enrichment (ES):

$ES_{RNA} = 1$, $ES_{WCP} = 1$, $ES_{META} = 1$, ES_{PTM} = (number of differential sites in the protein / total detected sites in the protein) × (total differential proteins / sum of differential sites in proteins)

Regulatory Mode (ER):

The number of differential molecules for a specific regulation type and direction divided by the total detected molecules of that regulation type and direction.

PCAS score calculation

The PCAS score was calculated in three tiers:

1. Omics-Level Score (Scoreomic):

$Score_{RNA} = BL_{RNA} \times BD_{RNA} \times BA_{RNA} \times ES_{RNA}$

$Score_{WCP} = BL_{WCP} \times BD_{WCP} \times BA_{WCP} \times ES_{WCP}$

$Score_{PTM} = BL_{PTM} \times BD_{PTM} \times BA_{PTM} \times ES_{PTM}$

$Score_{META} = BL_{META} \times BD_{META} \times BA_{META} \times ES_{META}$

2. Regulation type Score (Scoreregulation):

$Score_{TF}$, $Score_{ES}$, $Score_{EM}$, and $Score_{INTACT}$ were calculated for each regulatory type.

3. Directionality Score (Scoredirection):

$Score_{up}$, $Score_{down}$, $Score_{self}$, and $Score_{intact}$ were calculated.

The individual scores were computed as follows:

$PACS\ score = Score_{self} + Score_{up} + Score_{down} + Score_{intact}$

$Score_{self} = Score_{RNA} + Score_{WCP} + Score_{PTM}$

$Score_{up} = ER_{TF} \times Score_{self} + ER_{ES} \times Score_{self}$

$Score_{down} = ER_{TF} \times Score_{TF} + ER_{ES} \times Score_{ES} + ER_{EM} \times Score_{EM}$

$Score_{intact} = ER_{INTACT} \times Score_{INTACT}$

For cases where the upstream and downstream genes are the same, an additional coefficient of r = 0.5 was applied. The resulting PCAS scores were sorted in descending order to generate the PCAS score table. The top 25% of proteins based on PCAS score were selected, and clustering was performed using the igraph package. The clustering results were added to the PCAS score table in the "Cluster" column.

FIGURE LEGENDS

Figure 1. Super-omics and PCAS analytical model

In this analogy, omics can be compared to a fishing rod, and the changes occurring during a biological process are akin to the fish in a pool. The central principle is that changes at different biological levels are represented by fish residing in different layers of the pool. Conventional multi-omics research involves fewer fishing rods and fewer water layers, while super-omics research involves a greater number of rods and more water layers. The PCAS analysis is likened to inferring the number of fish in a pool by examining the parent-child relationships across various fish colors.

Figure 2. Super-omics analysis of RA synovial tissues

(A) Study workflow and the number of identifications across various omics platforms. RA, rheumatoid arthritis. OA, Osteoarthritis; NC, normal control; TMT, Tandem Mass Tag; LC-MS, Liquid Chromatograph Mass Spectrometer; mRNA, transcriptomics; WCP, proteomics; Meta, metabolomics; ASV, microbiomics; P, phosphorylation, Ac, acetylation; Lac, lactylation; Oglc, O-GlcNAc glycosylation; Rmme, arginine monomethylation; Pmm, lysine monomethylation; Pmd, lysine dimethylation; Pmt, lysine trimethylation; Succ, succinylation; Mal, malonylation; Glut, glutarylation; Ynit, tyrosine nitration; Ng, N-glycosylation; Og, O-glycosylation.

(B) UpSet plot showing the cross-distribution of different post-translational modification (PTM) quantification data of proteins.

(C) Scatter plot of the number of modifications on the same protein across PTM quantification data, with a pie chart representing the proportion of each

PTM type.

(D) Box plot displaying the correlation coefficients between proteomic data and other omics.

(E) Subcellular localization of proteins across various PTM and proteomic datasets.

(F) Scatter-bar plot showing the ratio of median intensity of each PTM to median intensity of protein for total detected proteins across various groups (* p value < 0.05)

Figure 3. Differential analysis of super-omics data

(A) Volcano plot depicting differential analysis between RA and NC groups across transcriptomics, proteomics, metabolomics, and phosphorylation modifications.

(B) Manhattan plot showing omics-based differential analysis between RA and NC groups.

(C) Circos plot illustrating differential entries across all omics comparisons.

(D) Heatmap showing omics-based changes in genes such as HLA-DRB1, PTPN22, ETS1, SUCLG2, HIF1A, SYK, and BTK between RA and NC groups.

(E) Scatter plot of intensity vs fold change (FC) correlation for different omics in RA vs NC groups.

(F) First, the top five genes with the largest absolute fold change (FC) values were selected from each comparison group for each PTMs omics. Subsequently, the top ten genes with the highest intensity values were chosen from this subset. Finally, a heatmap was generated to display the log (total intensity), log (FC) and z-score intensity for these selected genes.

(G) Upset plot showing the overlap of differential genes between RA vs NC groups across different omics. The table lists genes that exhibit multiple types of PTMs simultaneously.

(H) Circos plot showing differential entries for genes with a large number of modification sites or higher proportions of differential modification sites in RA vs NC.

Figure 4. Direct enrichment analysis of differential results from super-omics data

(A) Heatmap showing Gene Ontology (GO) /Kyoto Encyclopedia of Genes and Genomes (KEGG) enrichment analysis between RA and NC groups across various omics.

(B) Bubble plot displaying GO/KEGG enrichment analysis for succinylation between RA and NC groups.

(C) Heatmap of differential entries in the "Rheumatoid Arthritis" and "Activation of Immune Response" pathways.

(D) Bar plot illustrating the predicted transcription factors with the most significant changes in activity between the RA and NC groups.

(E) Circos plot showing the intensity of gene in figure 4D across transcriptome, proteome and differential PTMs between the RA and NC groups.

(F) Bar plot illustrating the top 15 kinases from the PTM-sea analysis between the RA and NC groups.

(G) Bar plot illustrating the top 15 kinases identified from KSEA kinase analysis between the RA and NC groups.

Figure 5. Principles, influencing factors, and analysis results of PCAS

(A) PCAS analytical model diagram. transcription factor-target gene interactions (TF), enzyme-substrate interactions (ES), enzyme-metabolite interactions (EM), and protein-protein interactions (INTACT) represent four primary molecular regulatory mechanisms; transcriptome (RNA), proteome (WCP), and Post-translational modification omics (PTM) are the three primary omics levels. The enrichment ratio is defined as the proportion of differential molecules in a specific dimension and regulatory mechanism, calculated using enrichment analysis, or the proportion of differential modification sites in a PTM dimension relative to all detected modification sites.

(B) Scatter plot showing the differential genes between RA and NC groups, ranked in descending order by PCAS score. The red dots indicate RA-related genes that have been previously reported.

(C) Box plot showing RNA, WCP and PTM scores for PCAS score quartile differential genes between RA and NC groups.

(D) Box plot displaying self/up/down/intact scores for PCAS score quartile differential genes between RA and NC groups.

(E) Violin plot displaying fold change (FC) distribution of PCAS score quartile differential genes across omics between RA and NC groups.

(F) Violin plot showing intensity distribution of quartile differential genes in various omics between RA and NC groups.

(G) Heatmap showing the correlation between PCAS score and fold change across omics.

(H) Box plots showing the PCAS score and the distribution of differential and non-differential genes across various omics between RA and NC group.

(I) Box plot showing the number of differential and non-differential entries for PCAS score quartile differential genes between RA and NC groups.

(J) Circos plot showing z-score intensity of top 20 genes based on PCAS score across transcriptome, proteome and differential PTMs between the RA and NC groups.

(K) Circos plot illustrating the z-score intensity of the top 5 differential entries with the largest absolute fold change across various omics datasets for the top 25% of genes based on PCAS score between the RA and NC groups.

(L) Upstream and downstream interaction diagram for Serine/Threonine Kinase 17b (STK17B), which shows the changes of various omics in STK17B as well as its upstream and downstream genes.

Figure 6. Pathway enrichment analysis and network analysis of PCAS results

(A) Network diagram for Module 4. The Network diagram showing three interactions between genes such as INTACT, PTM and TF, as well as the value of the gene's PCAS score.

(B) Integrated heatmap showing GO/KEGG enrichment analysis for quartile genes based on PCAS score between RA and NC groups.

(C) Integrated heatmap showing Gene Set Enrichment Analysis (GSEA) analysis for differential genes based on PCAS score between RA, OA , and NC groups.

(D) Scatter plot showing the genes related with "Activation of Immune Response," "Epithelial-Mesenchymal Transition," "RAS Signaling," and "VEGFA-VEGFR2 Signaling" pathways among quartile genes based on PCAS score between RA and NC groups.

(E) Sankey diagram showing the relationships between interaction modules and pathways of RA and NC groups.

(F) Network diagram for module 2 and important pathways. The network diagram showing INTACT and TF interaction types between genes. Meanwhile, it also showing the value of the gene PCAS score, and the signaling pathway.

Figure 7. Application research of PCAS results in clinical

(A) The correlation between differential omics values of the top 20 PCAS score genes and clinical parameters. CRP, C-reactive protein; ESR, erythrocyte sedimentation Rate; RF, rheumatoid factor; DAS28, Disease Activity Score-28; Anti-cyclic citrullinated peptide (CCP)

(B) Scatter plot of the correlation between differential omics results of STK17B and MZB1 and clinical parameters.

(C) The correlation between differential omics values of genes from Figure 6F excluding "other" genes and clinical parameters.

(D) Scatter plot of the correlation between differential omics results of MART3 and clinical parameters.

(E) The proportion of quartile genes based on PCAS score with targeted drugs in the RA and NC groups. T, true, have targetd drug; F, false, do not have targetd drug.

(F) Statistical plot of the impact of differential modification sites on protein function for the top 20 genes based on PCAS score in the RA and NC groups, and genes from Figure 6F excluding 'other' genes.

(G) The cancer-associated genes among the top 30 genes based on PCAS score with differential omics values across comparison groups.

Figure 8. Super-omics landscape of RA.

The landscape showing the changes of each gene in the three dimensions:

RNA, WCP, and PTM; Meanwhile, it also showing the relationship between genes, the PCAS score of gene, and the signaling pathway. Finally, the blueprint also provides targeted drugs for the genes (displayed with red borders and text) and differential post-translational modification sites that affect protein function (with underlines added to the corresponding sites).

SUPPLEMENTARY FIGURE LEGENDS

Figure S1. Correlation between different samples in each omics

(A) Heatmap showing correlation coefficients between samples in different omics. RA, rheumatoid arthritis. OA, Osteoarthritis; NC, normal control; mRNA, transcriptomics; WCP, proteomics; Meta, metabolomics; ASV, microbiomics; P, phosphorylation, Ac, acetylation; Lac,lactylation; Oglc, O-GlcNAc glycosylation; Rmme, arginine monomethylation; Pmm, lysine monomethylation; Pmd, lysine dimethylation; Pmt, lysine trimethylation; Succ, succinylation; Mal, malonylation; Glut, glutarylation; Ynit, tyrosine nitration; Ng, N-glycosylation; Og, O-glycosylation (Og).

(B) Pie chart depicting the distribution of different PTMs across proteins with different number of modification types (1, 2, 3, 4, or more than 4).

Figure S2. Statistical analysis of qualitative and quantitative identification results of super-omics data

(A) PCA plot of samples across different groups.

(B) Bar plot showing the number of quantifications across various omics.

(C) Box plot of total intensity values for different PTM omics across all samples.

(D) Identification of metabolites in all samples.

(E) Relative abundance of microbial families in different groups.

Figure S3. Differential analysis of quantitative results in super-omics

Volcano plots of differential analysis between different groups across various

omics.

Figure S4. Screening of candidate clinical diagnostic biomarkers for RA

(A) Manhattan plot showing differential analysis across various omics between RA and OA groups, as well as OA and NC groups.

(B) Scatter plot of intensity vs fold change (FC) correlation for different omics between RA vs OA and OA vs NC.

(C) Upset plot showing the overlap of differential genes between RA and NC groups, as well as OA and NC groups, across different omics.

(D) Bar plot depicting the top 10 genes with the highest number of regulated PTM sites between the RA and OA groups, as well as between the OA and NC groups.

(E) Bar plot depicting the top 10 genes (at least 10 quantified PTM sites) with the highest percent of regulated PTM sites between RA vs OA and OA vs NC.

Figure S5. Integrated analysis between different omics

(A) Scatter plot showing the combined analysis of transcriptomics and proteomics for RA vs NC, RA vs OA, and OA vs NC.

(B) Scatter plot of proteomic and PTM combined analysis for RA vs NC, RA vs OA, and OA vs NC.

(C) Heatmap of differential metabolites across comparison groups.

(D) Differential microbial abundance at the family level across comparison groups.

Figure S6. Enrichment analysis and kinase analysis of multi-omics data from different groups

(A) Heatmap displaying Gene Ontology (GO) /Kyoto Encyclopedia of Genes and Genomes (KEGG) enrichment analysis heatmap between RA vs OA, and OA vs NC groups.

(B) Bubble plot displaying GO/KEGG enrichment analysis for proteomics and

phosphorylation modification in RA vs NC groups.

(C) Bar plot displaying the pathway enrichment analysis of differential metabolic between RA and NC groups.

(D) Bar plot illustrating the predicted transcription factors with the most significant changes in activity in RA vs OA, and OA vs NC.

(E) Bar plot illustrating the top 15 kinases from the PTM-sea analysis between RA vs OA, and OA vs NC.

Figure S7. Kinase analysis of phosphorylation modifications

(A) Heatmap showing the signature set scores of molecular signaling pathways and kinase-substrate using regulated PTMs across different groups by the PTM-sea method.

(B) Bar plot displaying the top 15 kinases from KSEA kinase analysis between RA vs OA, and OA vs NC groups.

(C) Heatmap of transcriptome and proteome results (with differences marked by *) and differential post-translational modification results for genes identified in Figures 4F and 4G.

(D) Scatter plot showing the changes in substrate phosphorylation modification sites and their correlation with changes in kinase expression or modification between RA and NC groups.

(E) Network diagram showing differential proteins and pathways in RA vs NC groups.

Figure S8. Identification of important genes in RA using PCAS analysis.

(A) Scatter plot showing the differential genes in RA vs OA, and OA vs NC, ranked in descending order by PCAS score. The red dots indicate RA-related genes that have been previously reported.

(B) PCAS score distribution of genes associated with differential entries in different omics (0-25%, 25%-50%, 50%-75%, 75%-100%).

(C) Circos plot showing z-score intensity of top 20 genes based on PCAS score across transcriptome, proteome and differential PTMs in RA vs OA, and

OA vs NC. Differential transcriptome and proteome results are marked with *.

(D) Circos plot illustrating the z-score intensity of the top 5 differential entries with the largest absolute fold change across various omics datasets for the top 25% of genes based on PCAS score between RA vs OA, and OA vs NC.

Figure S9. Upstream and downstream regulatory genes of high PCAS score genes and their changes

Upstream and downstream interaction diagram for PLIN1, LDB3, ITIH3, RGCC, and ADH1C. The interaction diagram showing the changes of various omics in PLIN1, LDB3, ITIH3, RGCC, and ADH1C as well as their upstream and downstream genes.

Figure S10. Network analysis and enrichment analysis of PCAS results

(A) Network diagrams for Modules 1, 2, 3, 5, 6, and 7 from regulated genes with top 25% PACS score. The Network diagram showing three interactions between genes such as INTACT, PTM and TF, as well as the value of the gene's PCAS score.

(B) Integrated heatmap showing GO/KEGG enrichment analysis for quartile genes based on PCAS score in RA vs OA, and OA vs NC.

Figure S11. The network and pathway joint analysis of the PCAS results

(A) Scatter plot showing the regulated genes related with "Cell-Substrate Junction," "Integrin-Mediated Signaling Pathway," "Fatty Acid Metabolism," "Pyruvate Metabolism," and "MYC Targets v1" pathway, based on PCAS score between RA and NC groups.

(B) Network diagram showing the relationship for module 5 and module 6 with important pathways. The Network diagram showing three interactions between genes such as INTACT, PTM, and TF. Meanwhile, it also showing the value of the gene PCAS score, and the signaling pathway.

REFERENCES

Anders, S., Pyl, P.T., and Huber, W. (2015). HTSeq--a Python framework to work with high-throughput sequencing data. Bioinformatics (Oxford, England) *31*, 166-169.

Barbie, D.A., Tamayo, P., Boehm, J.S., Kim, S.Y., Moody, S.E., Dunn, I.F., Schinzel, A.C., Sandy, P., Meylan, E., Scholl, C.*, et al.* (2009). Systematic RNA interference reveals that oncogenic KRAS-driven cancers require TBK1. Nature *462*, 108-112.

Bolyen, E., Rideout, J.R., Dillon, M.R., Bokulich, N.A., Abnet, C.C., Al-Ghalith, G.A., Alexander, H., Alm, E.J., Arumugam, M., Asnicar, F.*, et al.* (2019). Reproducible, interactive, scalable and extensible microbiome data science using QIIME 2. Nature biotechnology *37*, 852-857.

Brown, P., Pratt, A.G., and Hyrich, K.L. (2024). Therapeutic advances in rheumatoid arthritis. BMJ (Clinical research ed) *384*, e070856.

Callahan, B.J., McMurdie, P.J., Rosen, M.J., Han, A.W., Johnson, A.J., and Holmes, S.P. (2016). DADA2: High-resolution sample inference from Illumina amplicon data. Nature methods *13*, 581-583.

1414 Cannon, M., Stevenson, J., Stahl, K., Basu, R., Coffman, A., Kiwala, S., McMichael,
1415 J.F., Kuzma, K., Morrissey, D., Cotto, K.*, et al.* (2024). DGIdb 5.0: rebuilding the
1416 drug-gene interaction database for precision medicine and drug discovery platforms.
1417 Nucleic acids research *52*, D1227-d1235.
1418 Chambers, R.E., MacFarlane, D.G., Whicher, J.T., and Dieppe, P.A. (1983). Serum
1419 amyloid-A protein concentration in rheumatoid arthritis and its role in monitoring
1420 disease activity. Annals of the rheumatic diseases *42*, 665-667.
1421 Chen, L., Yang, T., Sun, X., Wong, C.C.L., and Yang, D. (2024). Protein Tyrosine
1422 Amination: Detection, Imaging, and Chemoproteomic Profiling with Synthetic Probes.
1423 Journal of the American Chemical Society *146*, 11944-11954.
1424 Chen, S., Zhou, Y., Chen, Y., and Gu, J. (2018). fastp: an ultra-fast all-in-one FASTQ
1425 preprocessor. Bioinformatics (Oxford, England) *34*, i884-i890.
1426 Chen, T., Ma, J., Liu, Y., Chen, Z., Xiao, N., Lu, Y., Fu, Y., Yang, C., Li, M., Wu, S.*, et*
1427 *al.* (2022). iProX in 2021: connecting proteomics data sharing with big data. Nucleic
1428 acids research *50*, D1522-d1527.
1429 Cheng, M., Zhao, Y., Cui, Y., Zhong, C., Zha, Y., Li, S., Cao, G., Li, M., Zhang, L.,
1430 Ning, K.*, et al.* (2022). Stage-specific roles of microbial dysbiosis and metabolic
1431 disorders in rheumatoid arthritis. Annals of the rheumatic diseases *81*, 1669-1677.
1432 Clough, E., and Barrett, T. (2016). The Gene Expression Omnibus Database.
1433 Methods in molecular biology (Clifton, NJ) *1418*, 93-110.
1434 Consortium, U. (2025). UniProt: the Universal Protein Knowledgebase in 2025.
1435 Nucleic acids research *53*, D609-d617.

1436 Consortium, W.T.C.C. (2007). Genome-wide association study of 14,000 cases of
1437 seven common diseases and 3,000 shared controls. Nature *447*, 661-678.
1438 Cooper, J., and Giancotti, F.G. (2019). Integrin Signaling in Cancer:
1439 Mechanotransduction, Stemness, Epithelial Plasticity, and Therapeutic Resistance.
1440 Cancer cell *35*, 347-367.
1441 Cox, J., and Mann, M. (2008). MaxQuant enables high peptide identification rates,
1442 individualized p.p.b.-range mass accuracies and proteome-wide protein quantification.
1443 Nature biotechnology *26*, 1367-1372.
1444 Damle, N.P., and Köhn, M. (2019). The human DEPhOsphorylation Database
1445 DEPOD: 2019 update. Database : the journal of biological databases and curation
1446 *2019*.
1447 Demicco, M., Liu, X.Z., Leithner, K., and Fendt, S.M. (2024). Metabolic heterogeneity
1448 in cancer. Nature metabolism *6*, 18-38.
1449 Diella, F., Gould, C.M., Chica, C., Via, A., and Gibson, T.J. (2008). Phospho.ELM: a
1450 database of phosphorylation sites--update 2008. Nucleic acids research *36*,
1451 D240-244.
1452 Ding, Q., Hu, W., Wang, R., Yang, Q., Zhu, M., Li, M., Cai, J., Rose, P., Mao, J., and
1453 Zhu, Y.Z. (2023). Signaling pathways in rheumatoid arthritis: implications for targeted
1454 therapy. Signal transduction and targeted therapy *8*, 68.
1455 Floudas, A., Smith, C.M., Tynan, O., Neto, N., Krishna, V., Wade, S.M., Hanlon, M.,
1456 Cunningham, C., Marzaioli, V., Canavan, M.*, et al.* (2022). Distinct stromal and
1457 immune cell interactions shape the pathogenesis of rheumatoid and psoriatic arthritis.

1458 Annals of the rheumatic diseases *81*, 1224-1242.

1459 Fu, Y., Yu, J., Li, F., and Ge, S. (2022). Oncometabolites drive tumorigenesis by
1460 enhancing protein acylation: from chromosomal remodelling to nonhistone
1461 modification. Journal of experimental & clinical cancer research : CR *41*, 144.

1462 Hornbeck, P.V., Zhang, B., Murray, B., Kornhauser, J.M., Latham, V., and Skrzypek,
1463 E. (2015). PhosphoSitePlus, 2014: mutations, PTMs and recalibrations. Nucleic acids
1464 research *43*, D512-520.

1465 Huang, H., Arighi, C.N., Ross, K.E., Ren, J., Li, G., Chen, S.C., Wang, Q., Cowart, J.,
1466 Vijay-Shanker, K., and Wu, C.H. (2018). iPTMnet: an integrated resource for protein
1467 post-translational modification network discovery. Nucleic acids research *46*,
1468 D542-d550.

1469 Jung, M., Russell, A.J., Liu, B., George, J., Liu, P.Y., Liu, T., DeFazio, A., Bowtell,
1470 D.D., Oberthuer, A., London, W.B.*, et al.* (2017). A Myc Activity Signature Predicts
1471 Poor Clinical Outcomes in Myc-Associated Cancers. Cancer research *77*, 971-981.

1472 Kale, N.S., Haug, K., Conesa, P., Jayseelan, K., Moreno, P., Rocca-Serra, P., Nainala,
1473 V.C., Spicer, R.A., Williams, M., Li, X.*, et al.* (2016). MetaboLights: An Open-Access
1474 Database Repository for Metabolomics Data. Current protocols in bioinformatics *53*,
1475 14.13.11-14.13.18.

1476 Kanehisa, M., Furumichi, M., Sato, Y., Ishiguro-Watanabe, M., and Tanabe, M. (2021).
1477 KEGG: integrating viruses and cellular organisms. Nucleic acids research *49*,
1478 D545-d551.

1479 Kim, D., Langmead, B., and Salzberg, S.L. (2015). HISAT: a fast spliced aligner with

1480 low memory requirements. Nature methods *12*, 357-360.

1481 Knox, C., Law, V., Jewison, T., Liu, P., Ly, S., Frolkis, A., Pon, A., Banco, K., Mak, C.,
1482 Neveu, V.*, et al.* (2011). DrugBank 3.0: a comprehensive resource for 'omics'
1483 research on drugs. Nucleic acids research *39*, D1035-1041.

1484 Krug, K., Mertins, P., Zhang, B., Hornbeck, P., Raju, R., Ahmad, R., Szucs, M., Mundt,
1485 F., Forestier, D., Jane-Valbuena, J.*, et al.* (2019). A Curated Resource for
1486 Phosphosite-specific Signature Analysis. Molecular & cellular proteomics : MCP *18*,
1487 576-593.

1488 Li, J.M., Deng, H.S., Yao, Y.D., Wang, W.T., Hu, J.Q., Dong, Y., Wang, P.X., Liu, L.,
1489 Liu, Z.Q., Xie, Y.*, et al.* (2023). Sinomenine ameliorates collagen-induced arthritis in
1490 mice by targeting GBP5 and regulating the P2X7 receptor to suppress NLRP3-related
1491 signaling pathways. Acta pharmacologica Sinica *44*, 2504-2524.

1492 Li, W.C., Bai, L., Xu, Y., Chen, H., Ma, R., Hou, W.B., and Xu, R.J. (2019).
1493 Identification of differentially expressed genes in synovial tissue of rheumatoid arthritis
1494 and osteoarthritis in patients. Journal of cellular biochemistry *120*, 4533-4544.

1495 Li, Z., Chen, S., Jhong, J.H., Pang, Y., Huang, K.Y., Li, S., and Lee, T.Y. (2021).
1496 UbiNet 2.0: a verified, classified, annotated and updated database of E3 ubiquitin
1497 ligase-substrate interactions. Database : the journal of biological databases and
1498 curation *2021*.

1499 Liberzon, A. (2014). A description of the Molecular Signatures Database (MSigDB)
1500 Web site. Methods in molecular biology (Clifton, NJ) *1150*, 153-160.

1501 Linding, R., Jensen, L.J., Ostheimer, G.J., van Vugt, M.A., Jørgensen, C., Miron, I.M.,

1502 Diella, F., Colwill, K., Taylor, L., Elder, K.*, et al.* (2007). Systematic discovery of in vivo
1503 phosphorylation networks. Cell *129*, 1415-1426.
1504 Love, M.I., Huber, W., and Anders, S. (2014). Moderated estimation of fold change
1505 and dispersion for RNA-seq data with DESeq2. Genome biology *15*, 550.
1506 Ma, J., Chen, T., Wu, S., Yang, C., Bai, M., Shu, K., Li, K., Zhang, G., Jin, Z., He, F.*,*
1507 *et al.* (2019). iProX: an integrated proteome resource. Nucleic acids research *47*,
1508 D1211-d1217.
1509 McInnes, I.B., and Schett, G. (2011). The pathogenesis of rheumatoid arthritis. The
1510 New England journal of medicine *365*, 2205-2219.
1511 Moulin, D., Millard, M., Taïeb, M., Michaudel, C., Aucouturier, A., Lefèvre, A.,
1512 Bermúdez-Humarán, L.G., Langella, P., Sereme, Y., Wanherdrick, K.*, et al.* (2024).
1513 Counteracting tryptophan metabolism alterations as a new therapeutic strategy for
1514 rheumatoid arthritis. Annals of the rheumatic diseases *83*, 312-323.
1515 Müller-Dott, S., Tsirvouli, E., Vazquez, M., Ramirez Flores, R.O., Badia, I.M.P.,
1516 Fallegger, R., Türei, D., Lægreid, A., and Saez-Rodriguez, J. (2023). Expanding the
1517 coverage of regulons from high-confidence prior knowledge for accurate estimation of
1518 transcription factor activities. Nucleic acids research *51*, 10934-10949.
1519 Oughtred, R., Rust, J., Chang, C., Breitkreutz, B.J., Stark, C., Willems, A., Boucher, L.,
1520 Leung, G., Kolas, N., Zhang, F.*, et al.* (2021). The BioGRID database: A
1521 comprehensive biomedical resource of curated protein, genetic, and chemical
1522 interactions. Protein science : a publication of the Protein Society *30*, 187-200.
1523 Paleolog, E.M. (2002). Angiogenesis in rheumatoid arthritis. Arthritis research *4 Suppl*

1524 *3*, S81-90.

1525 Radu, A.F., and Bungau, S.G. (2021). Management of Rheumatoid Arthritis: An
1526 Overview. Cells *10*.

1527 Ritchie, M.E., Phipson, B., Wu, D., Hu, Y., Law, C.W., Shi, W., and Smyth, G.K.
1528 (2015). limma powers differential expression analyses for RNA-sequencing and
1529 microarray studies. Nucleic acids research *43*, e47.

1530 Roberts, A., Trapnell, C., Donaghey, J., Rinn, J.L., and Pachter, L. (2011). Improving
1531 RNA-Seq expression estimates by correcting for fragment bias. Genome biology *12*,
1532 R22.

1533 Rudd, P.M., Wormald, M.R., and Dwek, R.A. (1998). Glycosylation and the immune
1534 system. Journal of protein chemistry *17*, 519.

1535 Scherer, H.U., van der Woude, D., and Toes, R.E.M. (2022). From risk to chronicity:
1536 evolution of autoreactive B cell and antibody responses in rheumatoid arthritis. Nature
1537 reviews Rheumatology *18*, 371-383.

1538 Smolen, J.S., Aletaha, D., Barton, A., Burmester, G.R., Emery, P., Firestein, G.S.,
1539 Kavanaugh, A., McInnes, I.B., Solomon, D.H., Strand, V.*, et al.* (2018). Rheumatoid
1540 arthritis. Nature reviews Disease primers *4*, 18001.

1541 Souto-Carneiro, M.M., Klika, K.D., Abreu, M.T., Meyer, A.P., Saffrich, R., Sandhoff, R.,
1542 Jennemann, R., Kraus, F.V., Tykocinski, L., Eckstein, V.*, et al.* (2020). Effect of
1543 Increased Lactate Dehydrogenase A Activity and Aerobic Glycolysis on the
1544 Proinflammatory Profile of Autoimmune CD8+ T Cells in Rheumatoid Arthritis. Arthritis
1545 & rheumatology (Hoboken, NJ) *72*, 2050-2064.

1546 Tobón, G.J., Youinou, P., and Saraux, A. (2010). The environment, geo-epidemiology,
1547 and autoimmune disease: Rheumatoid arthritis. Autoimmunity reviews *9*, A288-292.
1548 Wang, F., Palmer, N., Fox, K., Liao, K.P., Yu, K.H., and Kou, S.C. (2023). Large-scale
1549 real-world data analyses of cancer risks among patients with rheumatoid arthritis.
1550 International journal of cancer *153*, 1139-1150.
1551 Wang, X., Li, Y., He, M., Kong, X., Jiang, P., Liu, X., Diao, L., Zhang, X., Li, H., Ling,
1552 X.*, et al.* (2022). UbiBrowser 2.0: a comprehensive resource for proteome-wide
1553 known and predicted ubiquitin ligase/deubiquitinase-substrate interactions in
1554 eukaryotic species. Nucleic acids research *50*, D719-d728.
1555 Weyand, C.M., and Goronzy, J.J. (2021). The immunology of rheumatoid arthritis.
1556 Nature immunology *22*, 10-18.
1557 Wiredja, D.D., Koyutürk, M., and Chance, M.R. (2017). The KSEA App: a web-based
1558 tool for kinase activity inference from quantitative phosphoproteomics. Bioinformatics
1559 (Oxford, England) *33*, 3489-3491.
1560 Wu, B., Qiu, J., Zhao, T.V., Wang, Y., Maeda, T., Goronzy, I.N., Akiyama, M., Ohtsuki,
1561 S., Jin, K., Tian, L.*, et al.* (2020). Succinyl-CoA Ligase Deficiency in Pro-inflammatory
1562 and Tissue-Invasive T Cells. Cell metabolism *32*, 967-980.e965.
1563 Wu, T., Hu, E., Xu, S., Chen, M., Guo, P., Dai, Z., Feng, T., Zhou, L., Tang, W., Zhan,
1564 L.*, et al.* (2021). clusterProfiler 4.0: A universal enrichment tool for interpreting omics
1565 data. Innovation (Cambridge (Mass)) *2*, 100141.
1566 Wu, T., Su, D., Zhang, L., Liu, T., Wang, Q., Yan, C., Liu, M., Ji, H., Lei, J., Zheng, M.*,*
1567 *et al.* (2024). Mitochondrial Control of Proteasomal Psmb5 Drives the Differentiation

1568 of Tissue-Resident Memory T Cells in Patients with Rheumatoid Arthritis. Arthritis &
1569 rheumatology (Hoboken, NJ) *76*, 1743-1757.
1570 Wu, X., Xu, M., Geng, M., Chen, S., Little, P.J., Xu, S., and Weng, J. (2023). Targeting
1571 protein modifications in metabolic diseases: molecular mechanisms and targeted
1572 therapies. Signal transduction and targeted therapy *8*, 220.
1573 Xu, H., Wang, Y., Lin, S., Deng, W., Peng, D., Cui, Q., and Xue, Y. (2018). PTMD: A
1574 Database of Human Disease-associated Post-translational Modifications. Genomics,
1575 proteomics & bioinformatics *16*, 244-251.
1576 Xu, Z., Liu, Y., He, S., Sun, R., Zhu, C., Li, S., Hai, S., Luo, Y., Zhao, Y., and Dai, L.
1577 (2023). Integrative Proteomics and N-Glycoproteomics Analyses of Rheumatoid
1578 Arthritis Synovium Reveal Immune-Associated Glycopeptides. Molecular & cellular
1579 proteomics : MCP *22*, 100540.
1580 Yan, L., Zheng, M., Fan, M., Yao, R., Zou, K., Feng, S., and Wu, M. (2024). A
1581 Chemoselective Enrichment Strategy for In-Depth Coverage of the Methyllysine
1582 Proteome. Angewandte Chemie (International ed in English) *63*, e202408564.
1583 Yoo, M., Shin, J., Kim, J., Ryall, K.A., Lee, K., Lee, S., Jeon, M., Kang, J., and Tan,
1584 A.C. (2015). DSigDB: drug signatures database for gene set analysis. Bioinformatics
1585 (Oxford, England) *31*, 3069-3071.
1586 Zeng, W.F., Cao, W.Q., Liu, M.Q., He, S.M., and Yang, P.Y. (2021). Precise, fast and
1587 comprehensive analysis of intact glycopeptides and modified glycans with pGlyco3.
1588 Nature methods *18*, 1515-1523.
1589 Zhang, F., Wei, K., Slowikowski, K., Fonseka, C.Y., Rao, D.A., Kelly, S., Goodman,

1590 S.M., Tabechian, D., Hughes, L.B., Salomon-Escoto, K.*, et al.* (2019). Defining
1591 inflammatory cell states in rheumatoid arthritis joint synovial tissues by integrating
1592 single-cell transcriptomics and mass cytometry. Nature immunology *20*, 928-942.
1593 Zhang, Q., Liu, W., Zhang, H.M., Xie, G.Y., Miao, Y.R., Xia, M., and Guo, A.Y. (2020).
1594 hTFtarget: A Comprehensive Database for Regulations of Human Transcription
1595 Factors and Their Targets. Genomics, proteomics & bioinformatics *18*, 120-128.
1596

General approach

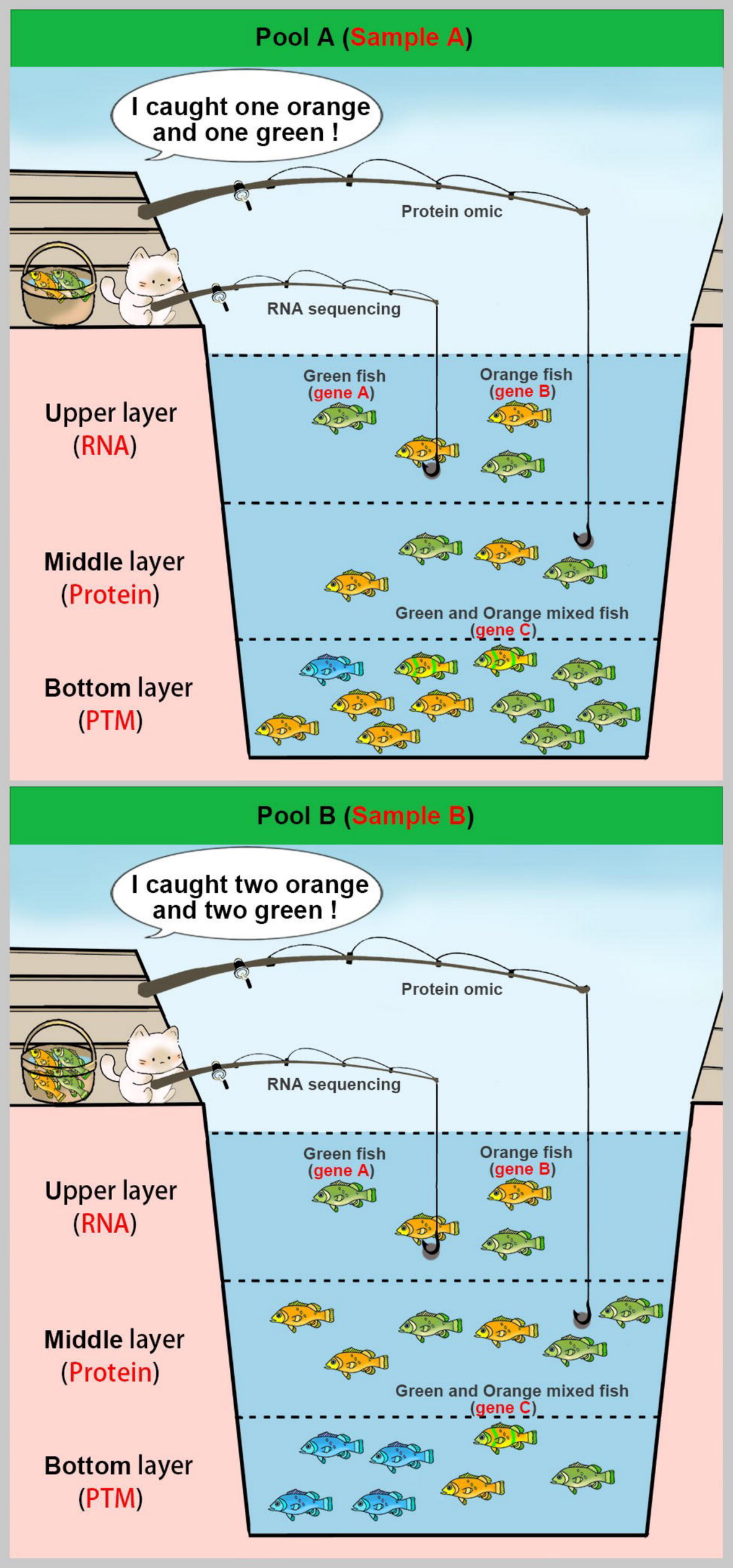

More orange and green fish were caught in pool B !

▼ ▼ ▼

There were more orange and green fish in pool B !

Error ! ! !

V S

Super omic + PCAS

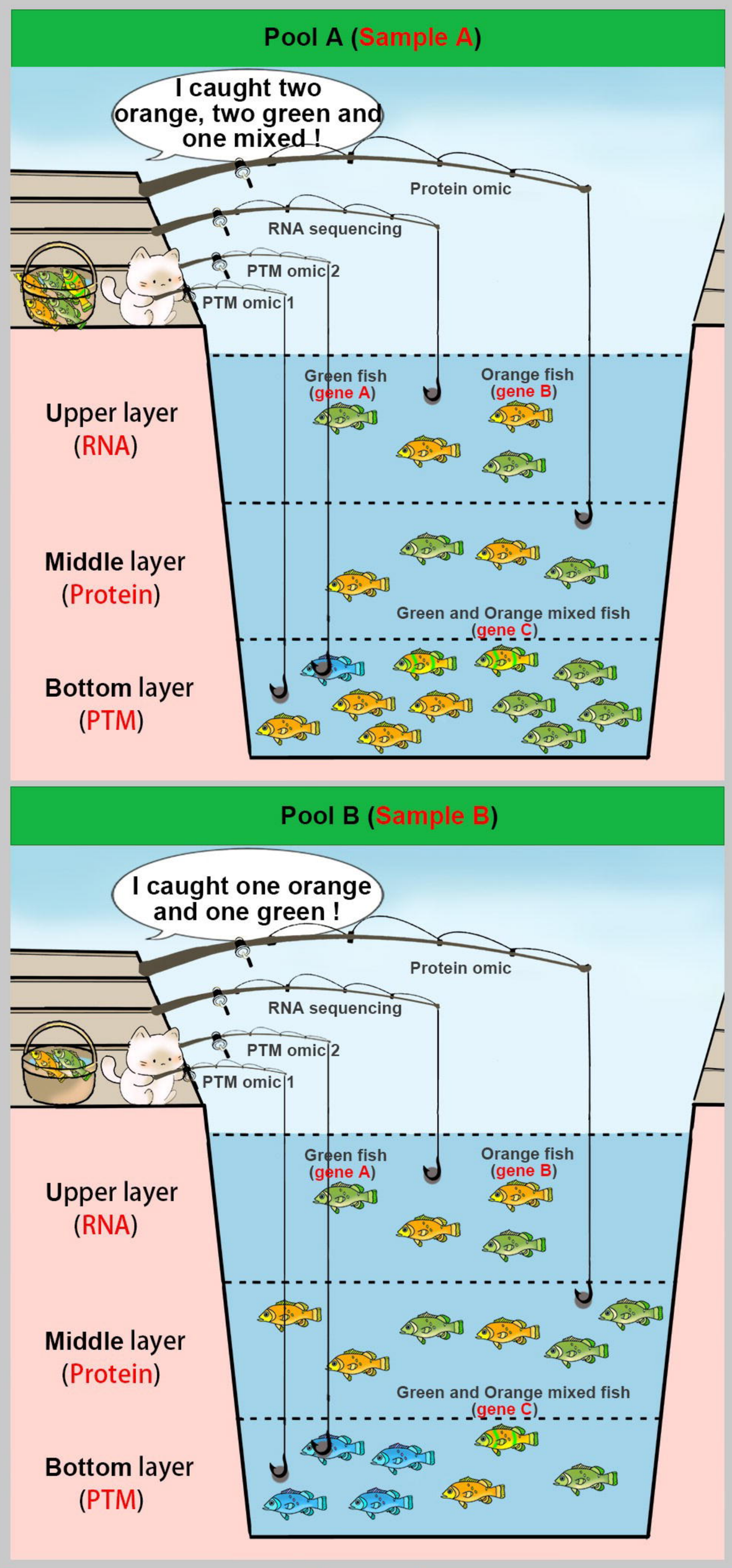

More orange and green fish were caught in pool A !

\+ PCAS

More mixed-color offspring fish were caught in pool A !

▼ ▼ ▼

There were more orange and green fish in pool A !

Correct ! ! !

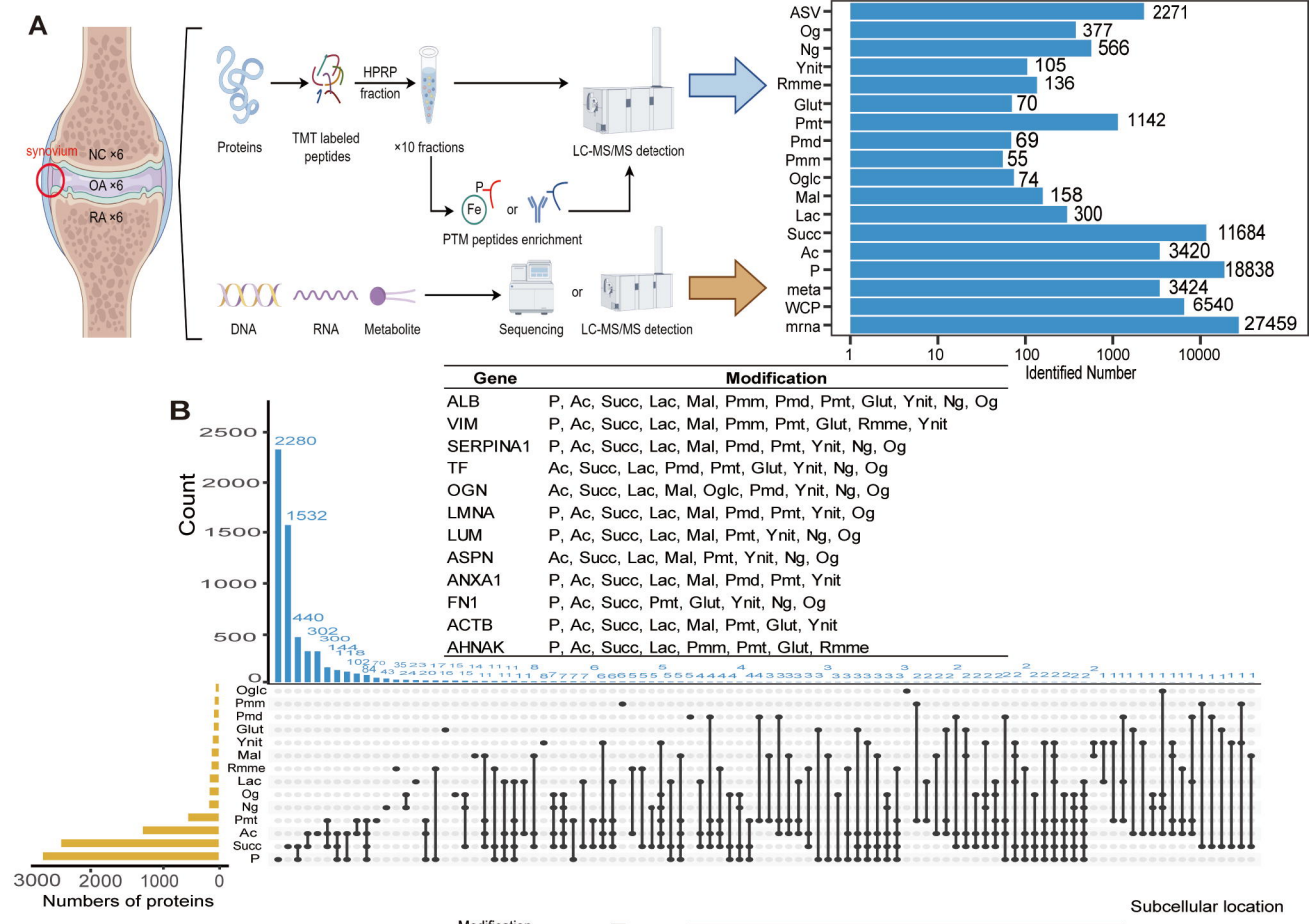

Gene	Modification
ALB	P, Ac, Succ, Lac, Mal, Pmm, Pmd, Pmt, Glut, Ynit, Ng, Og
VIM	P, Ac, Succ, Lac, Mal, Pmm, Pmt, Glut, Rmme, Ynit
SERPINA1	P, Ac, Succ, Lac, Mal, Pmd, Pmt, Ynit, Ng, Og
TF	Ac, Succ, Lac, Pmd, Pmt, Glut, Ynit, Ng, Og
OGN	Ac, Succ, Lac, Mal, Oglc, Pmd, Ynit, Ng, Og
LMNA	P, Ac, Succ, Lac, Mal, Pmd, Pmt, Ynit, Og
LUM	P, Ac, Succ, Lac, Mal, Pmt, Ynit, Ng, Og
ASPN	Ac, Succ, Lac, Mal, Pmt, Ynit, Ng, Og
ANXA1	P, Ac, Succ, Lac, Mal, Pmd, Pmt, Ynit
FN1	P, Ac, Succ, Pmt, Glut, Ynit, Ng, Og
ACTB	P, Ac, Succ, Lac, Mal, Pmt, Glut, Ynit
AHNAK	P, Ac, Succ, Lac, Pmm, Pmt, Glut, Rmme

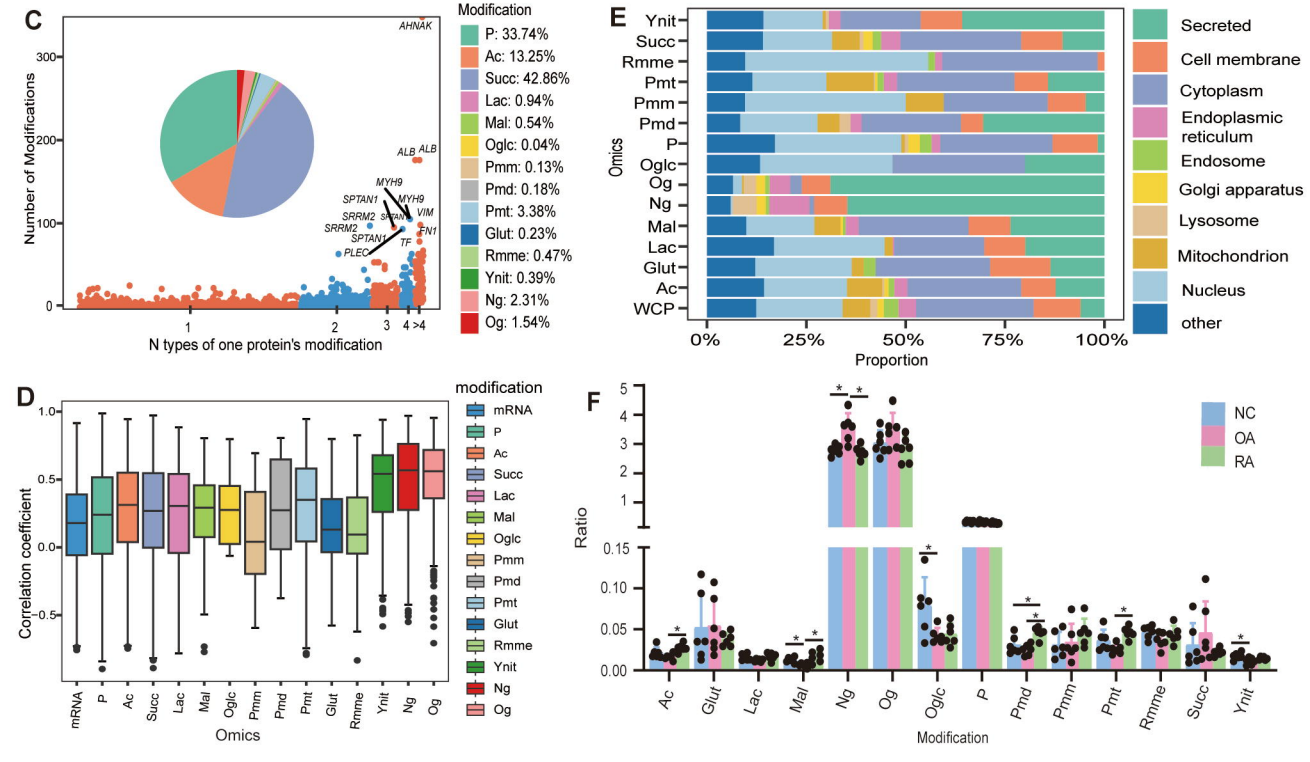

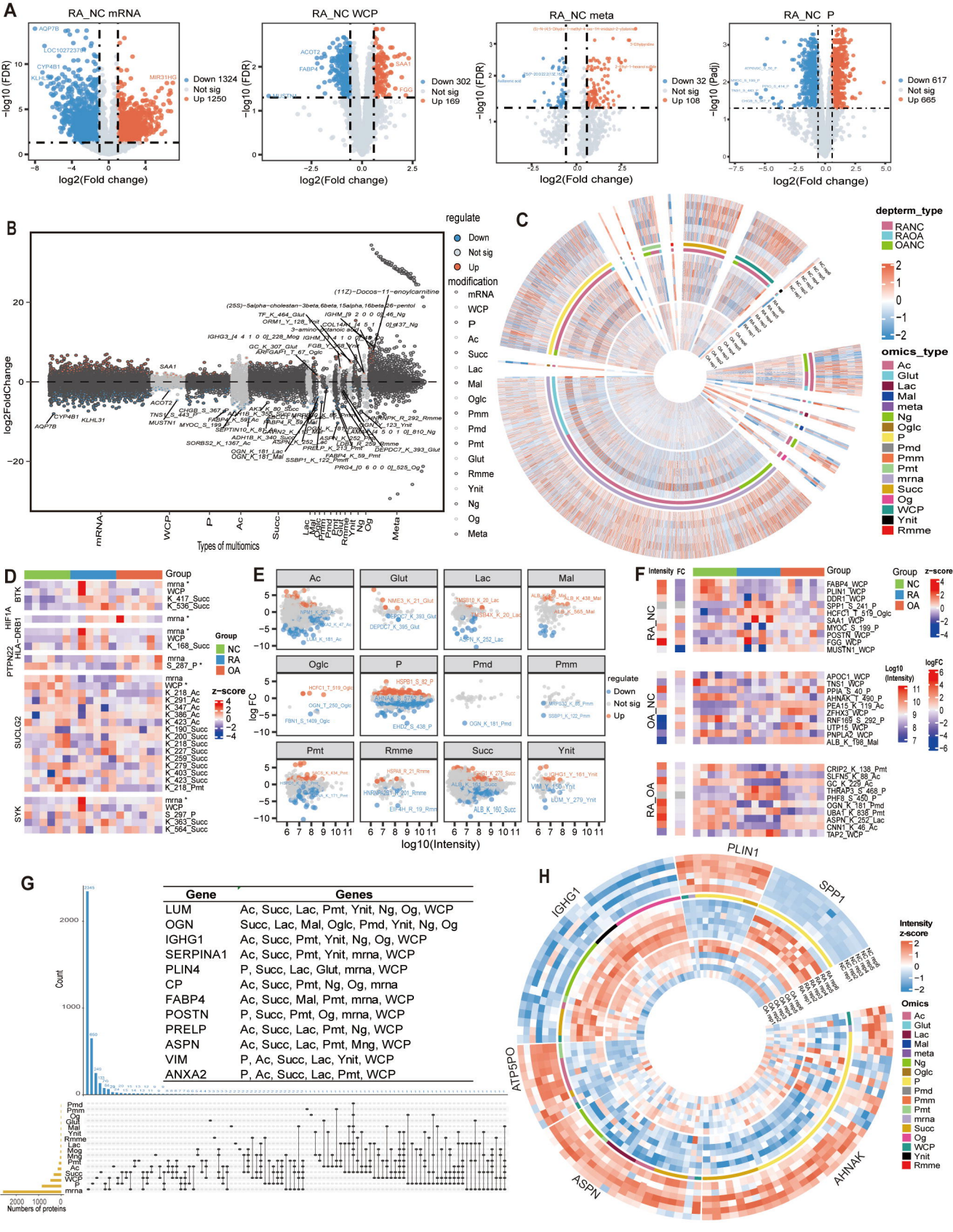

Gene	Genes
LUM	Ac, Succ, Lac, Pmt, Ynit, Ng, Og, WCP
OGN	Succ, Lac, Mal, Oglc, Pmd, Ynit, Ng, Og
IGHG1	Ac, Succ, Pmt, Ynit, Ng, Og, WCP
SERPINA1	Ac, Succ, Pmt, Ynit, mrna, WCP
PLIN4	P, Succ, Lac, Glut, mrna, WCP
CP	Ac, Succ, Pmt, Ng, Og, mrna
FABP4	Ac, Succ, Mal, Pmt, mrna, WCP
POSTN	P, Succ, Pmt, Og, mrna, WCP
PRELP	Ac, Succ, Lac, Pmt, Ng, WCP
ASPN	Ac, Succ, Lac, Pmt, Mng, WCP
VIM	P, Ac, Succ, Lac, Ynit, WCP
ANXA2	P, Ac, Succ, Lac, Pmt, WCP

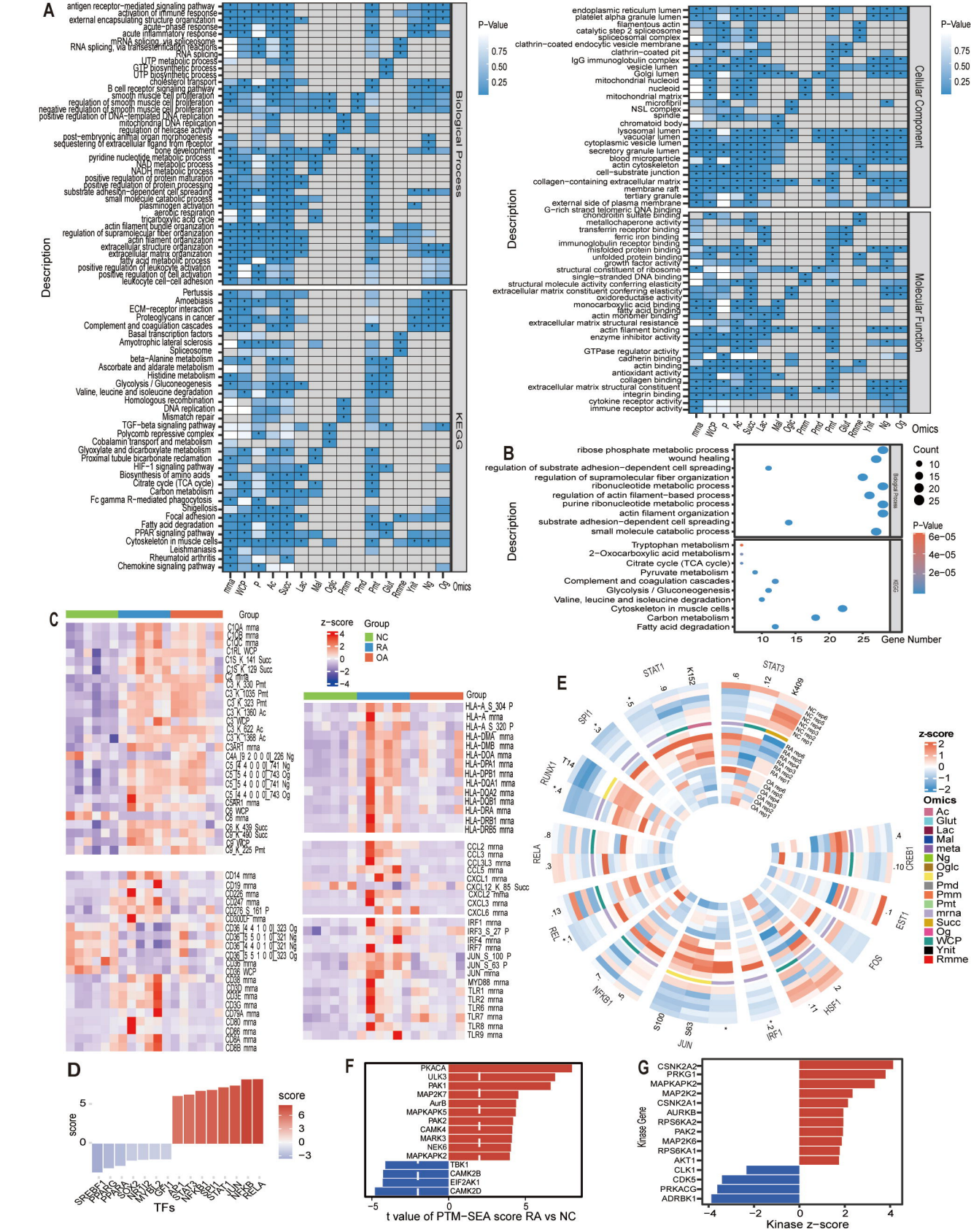
A
Biological Process
Cellular Component
Molecular Function
KEGG
Description
Omics
P-Value
B
Count
Gene Number
C
Group
z-score
NC
RA
OA
D
score
TFs
E
z-score
Omics
F
t value of PTM-SEA score RA vs NC
G
Kinase Gene
Kinase z-score

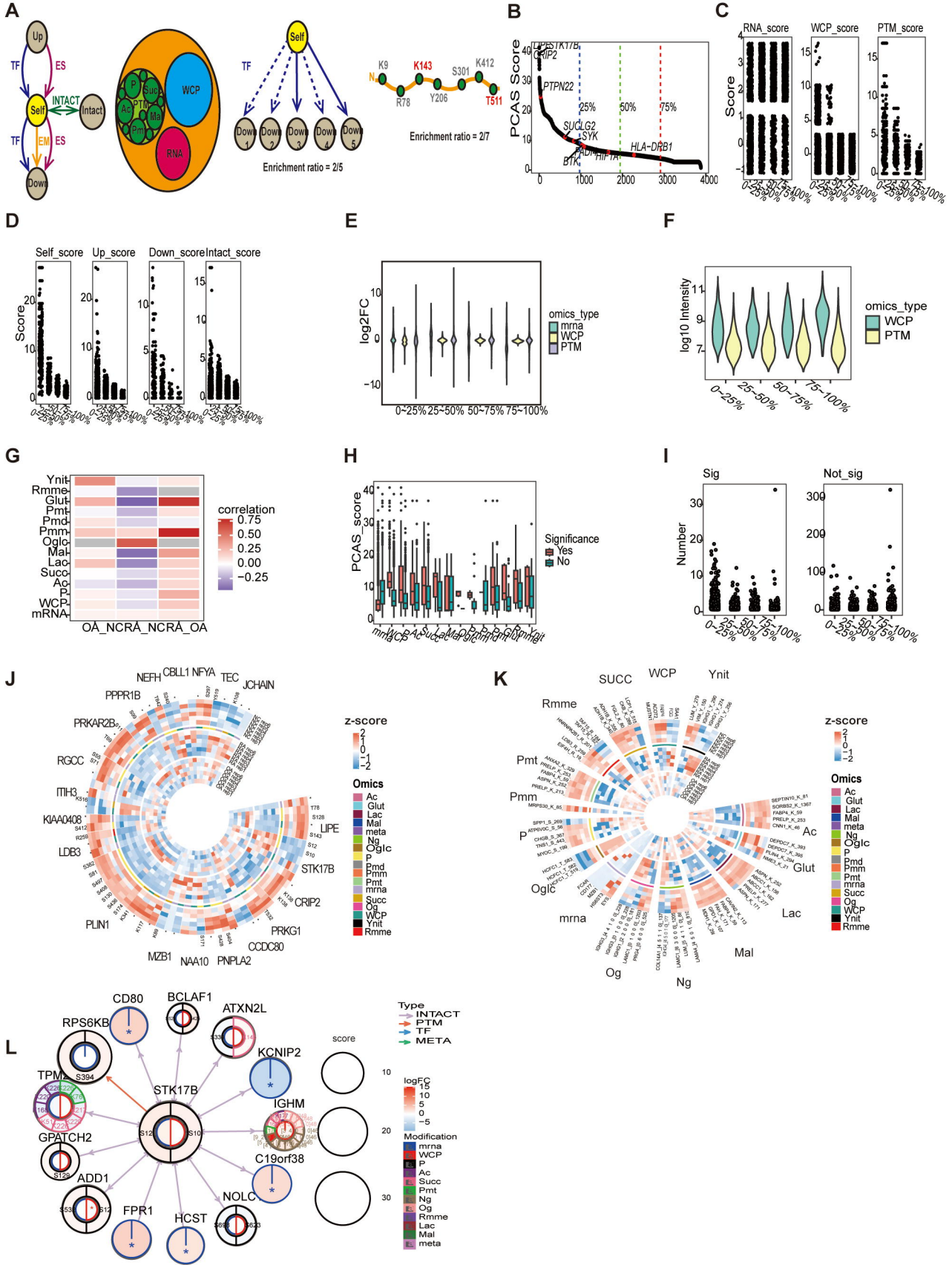
A
Up
TF
ES
Self
INTACT
Intact
TF
EM
ES
Down
WCP
RNA
Self
TF
Down 1
Down 2
Down 3
Down 4
Down 5
Enrichment ratio = 2/5
K9
K143
S301
K412
R78
Y206
T511
Enrichment ratio = 2/7
B
PCAS Score
LPS
STK17B
CRIP2
PTPN22
SUCLG2
SYK
HLA-DRB1
BTK
HIF1A
25%
50%
75%
C
RNA_score
WCP_score
PTM_score
Score
D
Self_score
Up_score
Down_score
Intact_score
Score
E
log2FC
omics_type
mrna
WCP
PTM
0~25%
25~50%
50~75%
75~100%
F
log10 Intensity
omics_type
WCP
PTM
0~25%
25~50%
50~75%
75~100%
G
Ynit
Rmme
Glut
Pmt
Pmd
Pmm
Oglc
Mal
Lac
Succ
Ac
P
WCP
mRNA
OA_NCRA_NCRA_OA
correlation
0.75
0.50
0.25
0.00
−0.25
H
PCAS_score
Significance
Yes
No
I
Sig
Not_sig
Number
J
NEFH
CBLL1
NFYA
TEC
JCHAIN
PPPR1B
PRKAR2B
RGCC
ITIH3
KIAA0408
LDB3
PLIN1
MZB1
NAA10
PNPLA2
CCDC80
PRKG1
CRIP2
STK17B
LIPE
z-score
Omics
Ac
Glut
Lac
Mal
meta
Ng
Oglc
P
Pmd
Pmm
Pmt
mrna
Succ
Og
WCP
Ynit
Rmme
K
SUCC
WCP
Ynit
Rmme
Pmt
Pmm
P
Oglc
mrna
Og
Ng
Mal
Lac
Glut
Ac
z-score
Omics
Ac
Glut
Lac
Mal
meta
Ng
Oglc
P
Pmd
Pmm
Pmt
mrna
Succ
Og
WCP
Ynit
Rmme
L
CD80
BCLAF1
ATXN2L
RPS6KB
KCNIP2
TPM2
STK17B
IGHM
GPATCH2
C19orf38
ADD1
NOLC
FPR1
HCST
Type
INTACT
PTM
TF
META
score
logFC
Modification
mrna
WCP
P
Ac
Succ
Pmt
Ng
Og
Rmme
Lac
Mal
meta

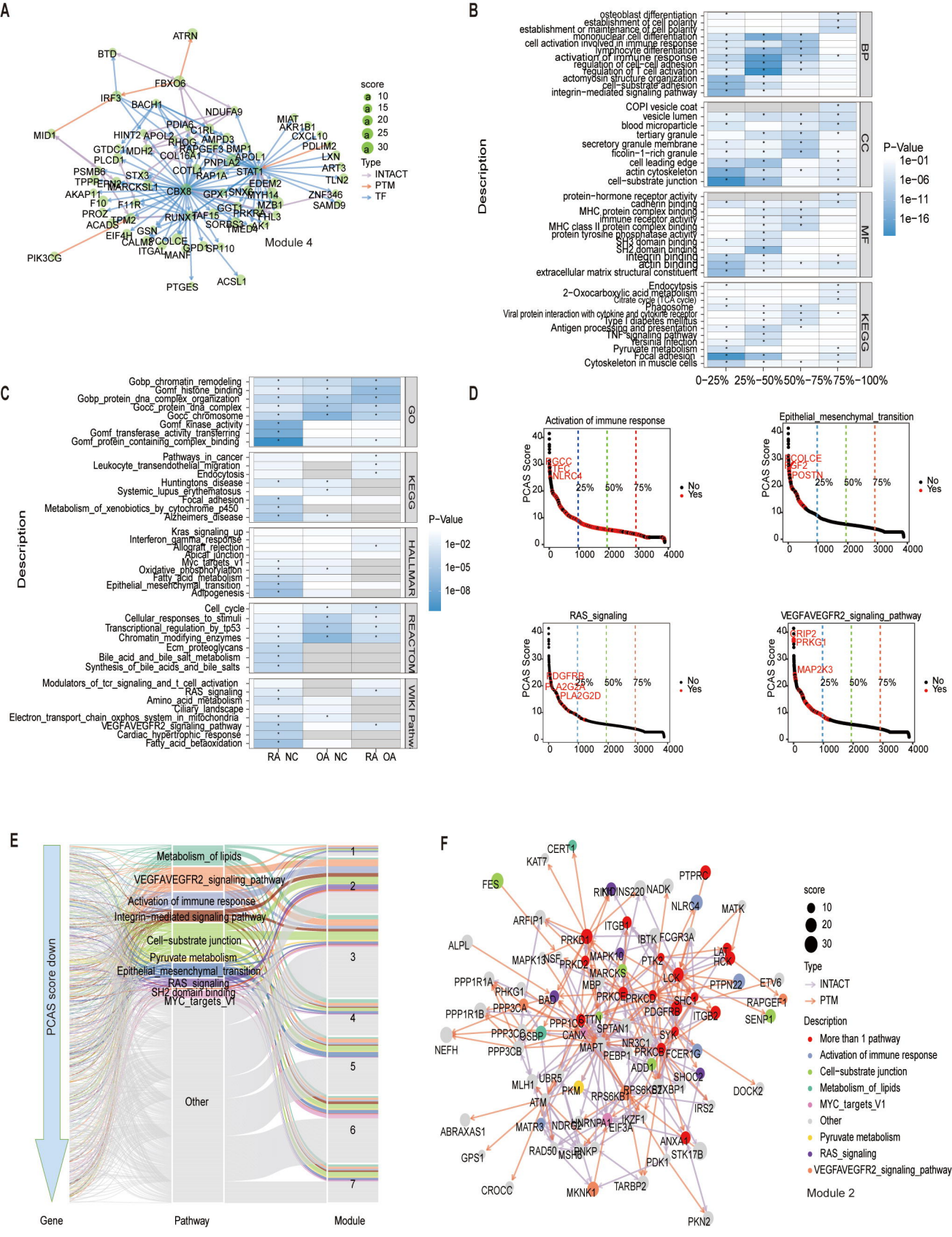
A
Module 4
score
10
15
20
25
30
Type
INTACT
PTM
TF
B
BP
CC
MF
KEGG
Description
P-Value
1e-01
1e-06
1e-11
1e-16
0-25%
25%-50%
50%-75%
75%-100%
C
GO
KEGG
HALLMAR
REACTOM
WIKI Pathw
RA NC
OA NC
RA OA
P-Value
1e-02
1e-05
1e-08
D
Activation of immune response
Epithelial_mesenchymal_transition
RAS_signaling
VEGFAVEGFR2_signaling_pathway
PCAS Score
No
Yes
E
PCAS score down
Metabolism_of_lipids
VEGFAVEGFR2_signaling_pathway
Activation of immune response
Integrin-mediated signaling pathway
Cell-substrate junction
Pyruvate metabolism
Epithelial_mesenchymal_transition
RAS_signaling
SH2 domain binding
MYC_targets_V1
Other
Gene
Pathway
Module
F
score
10
20
30
Type
INTACT
PTM
Description
More than 1 pathway
Activation of immune response
Cell-substrate junction
Metabolism_of_lipids
MYC_targets_V1
Other
Pyruvate metabolism
RAS_signaling
VEGFAVEGFR2_signaling_pathway
Module 2

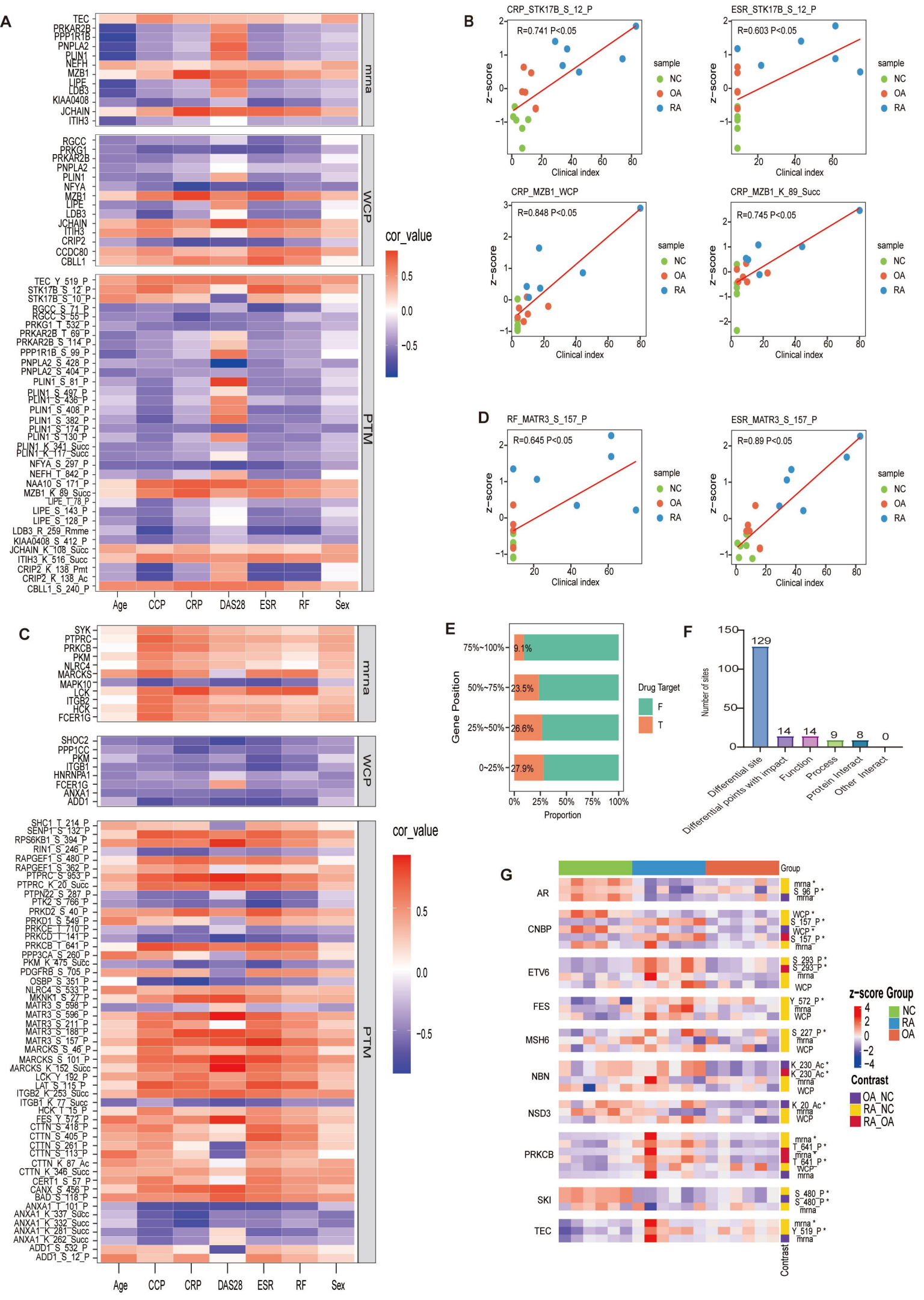
A
TEC
PRKAR2B
PPP1R1B
PNPLA2
PLIN1
NEFH
MZB1
LIPE
LDB3
KIAA0408
JCHAIN
ITIH3
mrna
RGCC
PRKG1
PRKAR2B
PNPLA2
PLIN1
NFYA
MZB1
LIPE
LDB3
JCHAIN
ITIH3
CRIP2
CCDC80
CBLL1
WCP
TEC_Y_519_P
STK17B_S_12_P
STK17B_S_10_P
RGCC_S_71_P
RGCC_S_55_P
PRKG1_T_532_P
PRKAR2B_T_69_P
PRKAR2B_S_114_P
PPP1R1B_S_99_P
PNPLA2_S_428_P
PNPLA2_S_404_P
PLIN1_S_81_P
PLIN1_S_497_P
PLIN1_S_436_P
PLIN1_S_408_P
PLIN1_S_382_P
PLIN1_S_174_P
PLIN1_S_130_P
PLIN1_K_341_Succ
PLIN1_K_117_Succ
NFYA_S_297_P
NEFH_T_842_P
NAA10_S_171_P
MZB1_K_89_Succ
LIPE_T_78_P
LIPE_S_143_P
LIPE_S_128_P
LDB3_R_259_Rmme
KIAA0408_S_412_P
JCHAIN_K_108_Succ
ITIH3_K_516_Succ
CRIP2_K_138_Pmt
CRIP2_K_138_Ac
CBLL1_S_240_P
PTM
Age
CCP
CRP
DAS28
ESR
RF
Sex
cor_value
0.5
0.0
-0.5
B
CRP_STK17B_S_12_P
R=0.741 P<0.05
ESR_STK17B_S_12_P
R=0.603 P<0.05
CRP_MZB1_WCP
R=0.848 P<0.05
CRP_MZB1_K_89_Succ
R=0.745 P<0.05
z-score
Clinical index
sample
NC
OA
RA
D
RF_MATR3_S_157_P
R=0.645 P<0.05
ESR_MATR3_S_157_P
R=0.89 P<0.05
C
SYK
PTPRC
PRKCB
PKM
NLRC4
MARCKS
MAPK10
LCK
ITGB2
HCK
FCER1G
mrna
SHOC2
PPP1CC
PKM
ITGB1
HNRNPA1
FCER1G
ANXA1
ADD1
WCP
SHC1_T_214_P
SENP1_S_132_P
RPS6KB1_S_394_P
RIN1_S_246_P
RAPGEF1_S_480_P
RAPGEF1_S_362_P
PTPRC_S_953_P
PTPRC_K_20_Succ
PTPN22_S_287_P
PTK2_S_766_P
PRKD2_S_40_P
PRKD1_S_549_P
PRKCE_T_710_P
PRKCD_T_141_P
PRKCB_T_641_P
PPP3CA_S_260_P
PKM_K_475_Succ
PDGFRB_S_705_P
OSBP_S_351_P
NLRC4_S_533_P
MKNK1_S_27_P
MATR3_S_598_P
MATR3_S_596_P
MATR3_S_211_P
MATR3_S_188_P
MATR3_S_157_P
MARCKS_S_46_P
MARCKS_S_101_P
MARCKS_K_152_Succ
LCK_Y_192_P
LAT_S_115_P
ITGB2_K_253_Succ
ITGB1_K_77_Succ
HCK_T_15_P
FES_Y_572_P
CTTN_S_418_P
CTTN_S_405_P
CTTN_S_261_P
CTTN_S_113_P
CTTN_K_87_Ac
CTTN_K_346_Succ
CERT1_S_57_P
CANX_S_456_P
BAD_S_118_P
ANXA1_T_101_P
ANXA1_K_337_Succ
ANXA1_K_332_Succ
ANXA1_K_281_Succ
ANXA1_K_262_Succ
ADD1_S_532_P
ADD1_S_12_P
E
75%~100%
9.1%
50%~75%
23.5%
25%~50%
26.6%
0~25%
27.9%
Gene Position
Proportion
Drug Target
F
Number of sites
129
14
14
9
8
0
Differential site
Differential points with impact
Function
Process
Protein Interact
Other Interact
G
Group
AR
CNBP
ETV6
FES
MSH6
NBN
NSD3
PRKCB
SKI
TEC
Contrast
z-score Group
NC
RA
OA
OA_NC
RA_NC
RA_OA

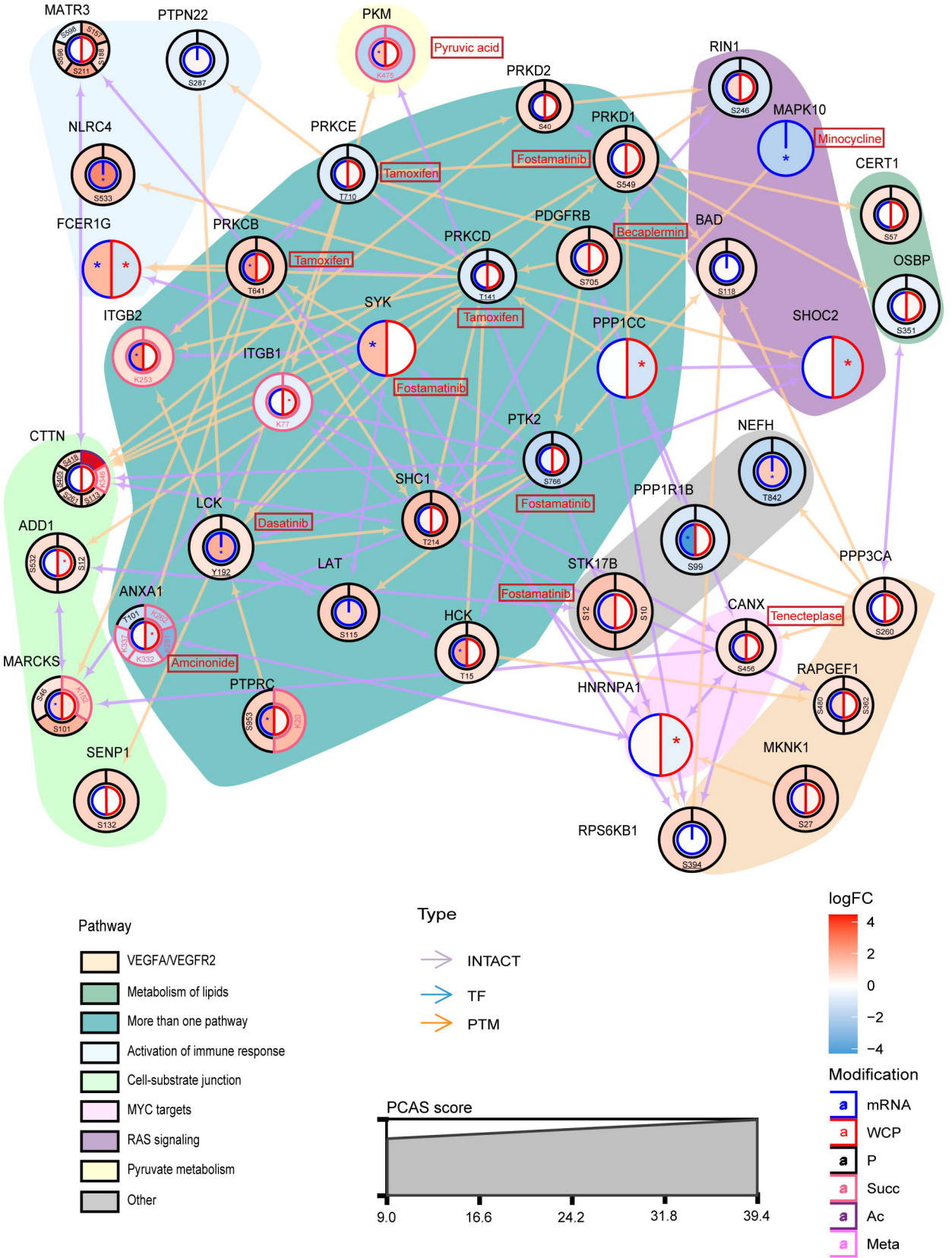
MATR3
PTPN22
PKM
Pyruvic acid
RIN1
PRKD2
MAPK10
Minocycline
NLRC4
PRKCE
Tamoxifen
Fostamatinib
PRKD1
CERT1
FCER1G
PRKCB
Tamoxifen
PRKCD
PDGFRB
Becaplermin
BAD
OSBP
ITGB2
SYK
Tamoxifen
PPP1CC
SHOC2
ITGB1
Fostamatinib
CTTN
PTK2
NEFH
SHC1
Fostamatinib
PPP1R1B
ADD1
LCK
Dasatinib
LAT
STK17B
PPP3CA
ANXA1
Fostamatinib
CANX
Tenecteplase
HCK
MARCKS
Amcinonide
PTPRC
HNRNPA1
RAPGEF1
SENP1
MKNK1
RPS6KB1
Pathway
VEGFA/VEGFR2
Metabolism of lipids
More than one pathway
Activation of immune response
Cell-substrate junction
MYC targets
RAS signaling
Pyruvate metabolism
Other
Type
INTACT
TF
PTM
logFC
4
2
0
−2
−4
Modification
mRNA
WCP
P
Succ
Ac
Meta
PCAS score
9.0
16.6
24.2
31.8
39.4

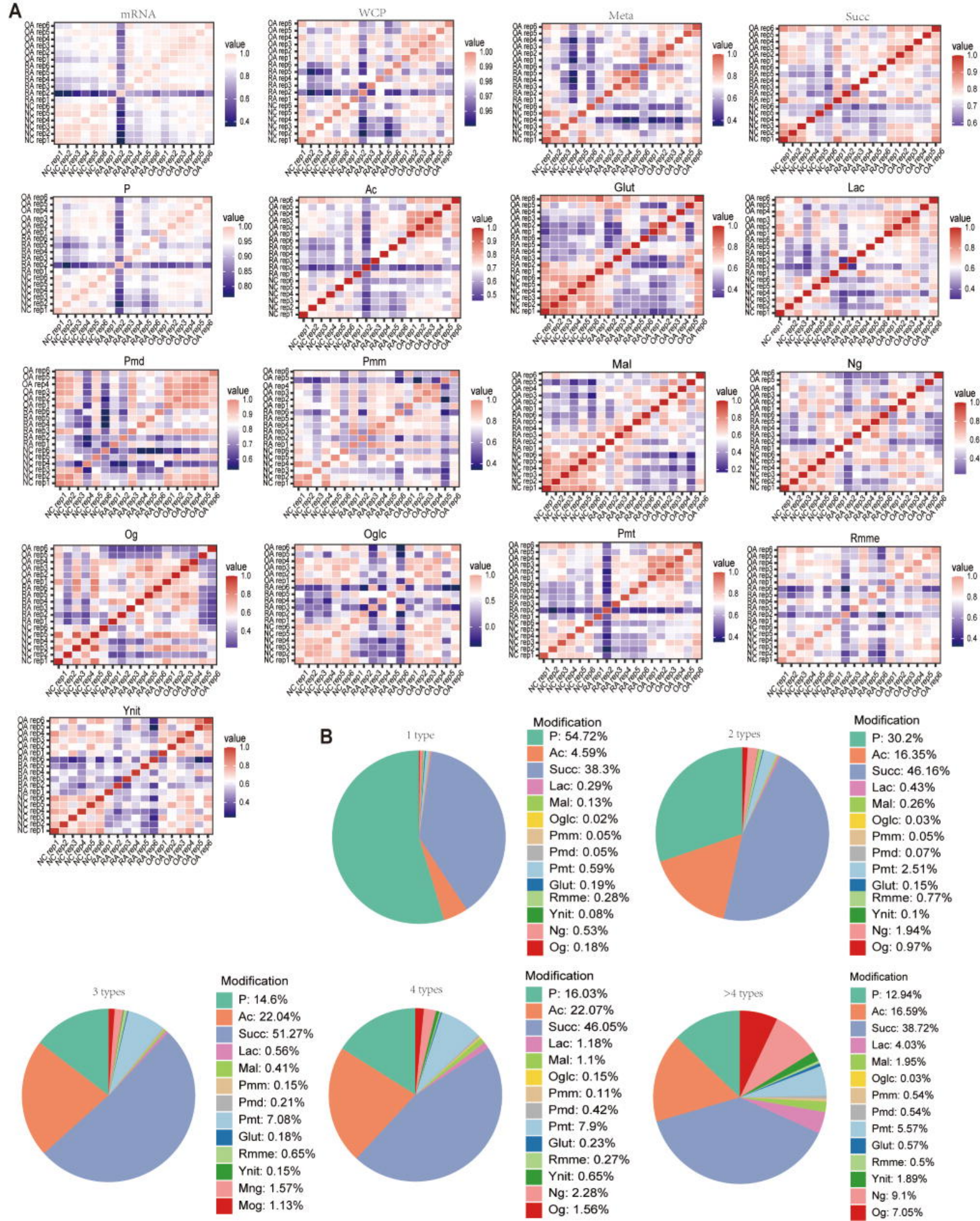
A
mRNA
WCP
Meta
Succ
P
Ac
Glut
Lac
Pmd
Pmm
Mal
Ng
Og
Oglc
Pmt
Rmme
Ynit
value
B
1 type
Modification
P: 54.72%
Ac: 4.59%
Succ: 38.3%
Lac: 0.29%
Mal: 0.13%
Oglc: 0.02%
Pmm: 0.05%
Pmd: 0.05%
Pmt: 0.59%
Glut: 0.19%
Rmme: 0.28%
Ynit: 0.08%
Ng: 0.53%
Og: 0.18%
2 types
Modification
P: 30.2%
Ac: 16.35%
Succ: 46.16%
Lac: 0.43%
Mal: 0.26%
Oglc: 0.03%
Pmm: 0.05%
Pmd: 0.07%
Pmt: 2.51%
Glut: 0.15%
Rmme: 0.77%
Ynit: 0.1%
Ng: 1.94%
Og: 0.97%
3 types
Modification
P: 14.6%
Ac: 22.04%
Succ: 51.27%
Lac: 0.56%
Mal: 0.41%
Pmm: 0.15%
Pmd: 0.21%
Pmt: 7.08%
Glut: 0.18%
Rmme: 0.65%
Ynit: 0.15%
Mng: 1.57%
Mog: 1.13%
4 types
Modification
P: 16.03%
Ac: 22.07%
Succ: 46.05%
Lac: 1.18%
Mal: 1.1%
Oglc: 0.15%
Pmm: 0.11%
Pmd: 0.42%
Pmt: 7.9%
Glut: 0.23%
Rmme: 0.27%
Ynit: 0.65%
Ng: 2.28%
Og: 1.56%
>4 types
Modification
P: 12.94%
Ac: 16.59%
Succ: 38.72%
Lac: 4.03%
Mal: 1.95%
Oglc: 0.03%
Pmm: 0.54%
Pmd: 0.54%
Pmt: 5.57%
Glut: 0.57%
Rmme: 0.5%
Ynit: 1.89%
Ng: 9.1%
Og: 7.05%

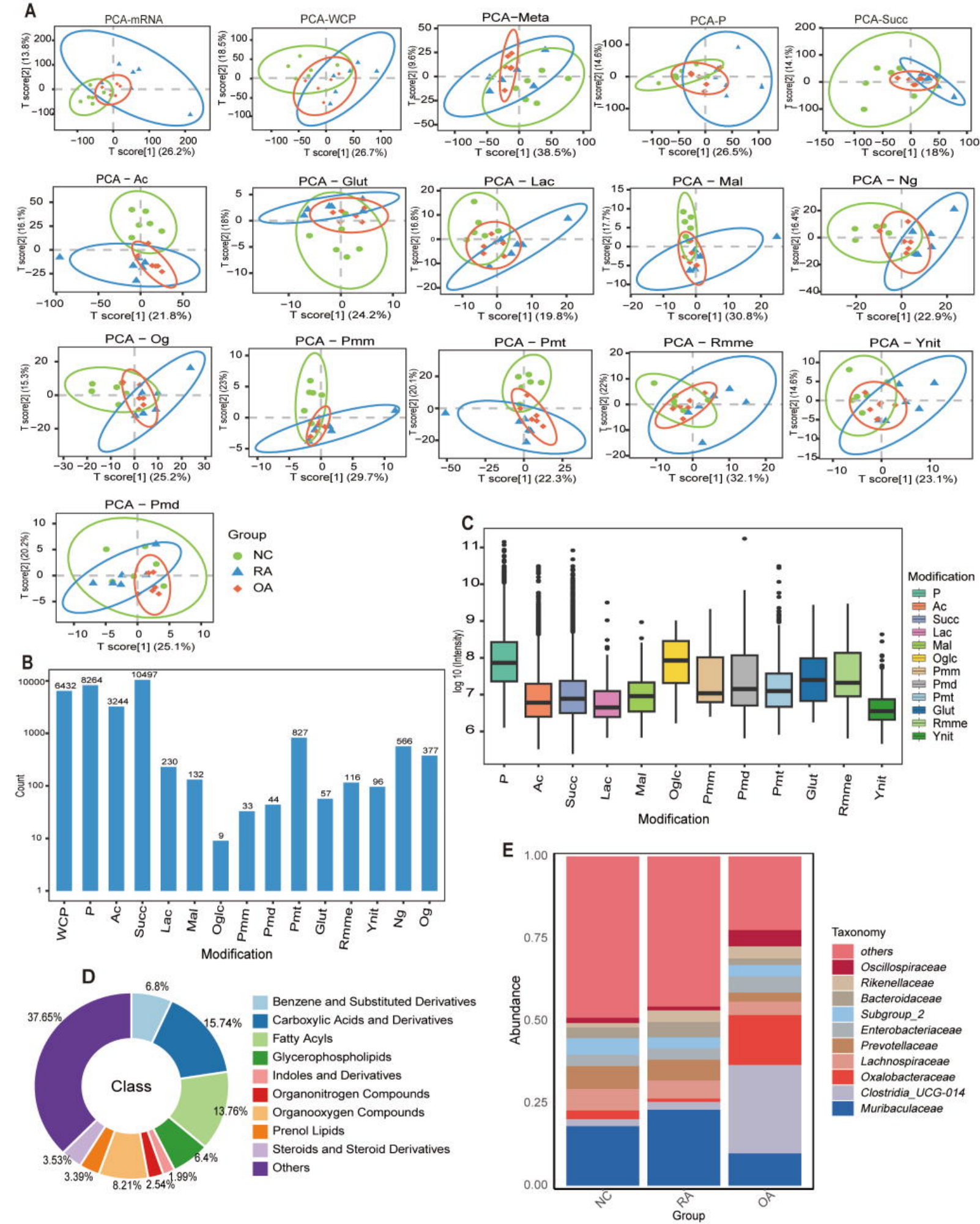
A
PCA-mRNA
T score[1] (26.2%)
T score[2] (13.8%)
PCA-WCP
T score[1] (26.7%)
T score[2] (18.5%)
PCA−Meta
T score[1] (38.5%)
T score[2] (9.6%)
PCA-P
T score[1] (26.5%)
T score[2] (14.6%)
PCA-Succ
T score[1] (18%)
T score[2] (14.1%)
PCA − Ac
T score[1] (21.8%)
T score[2] (16.1%)
PCA − Glut
T score[1] (24.2%)
T score[2] (18%)
PCA − Lac
T score[1] (19.8%)
T score[2] (16.8%)
PCA − Mal
T score[1] (30.8%)
T score[2] (17.7%)
PCA − Ng
T score[1] (22.9%)
T score[2] (16.4%)
PCA − Og
T score[1] (25.2%)
T score[2] (15.3%)
PCA − Pmm
T score[1] (29.7%)
T score[2] (23%)
PCA − Pmt
T score[1] (22.3%)
T score[2] (20.1%)
PCA − Rmme
T score[1] (32.1%)
T score[2] (22%)
PCA − Ynit
T score[1] (23.1%)
T score[2] (14.6%)
PCA − Pmd
T score[1] (25.1%)
T score[2] (20.2%)
Group
NC
RA
OA
B
Count
6432
8264
3244
10497
230
132
9
33
44
827
57
116
96
566
377
WCP
P
Ac
Succ
Lac
Mal
Oglc
Pmm
Pmd
Pmt
Glut
Rmme
Ynit
Ng
Og
Modification
C
log 10 (Intensity)
Modification
P
Ac
Succ
Lac
Mal
Oglc
Pmm
Pmd
Pmt
Glut
Rmme
Ynit
D
Class
6.8%
15.74%
13.76%
6.4%
1.99%
2.54%
8.21%
3.39%
3.53%
37.65%
Benzene and Substituted Derivatives
Carboxylic Acids and Derivatives
Fatty Acyls
Glycerophospholipids
Indoles and Derivatives
Organonitrogen Compounds
Organooxygen Compounds
Prenol Lipids
Steroids and Steroid Derivatives
Others
E
Abundance
NC
RA
OA
Group
Taxonomy
others
Oscillospiraceae
Rikenellaceae
Bacteroidaceae
Subgroup_2
Enterobacteriaceae
Prevotellaceae
Lachnospiraceae
Oxalobacteraceae
Clostridia_UCG-014
Muribaculaceae

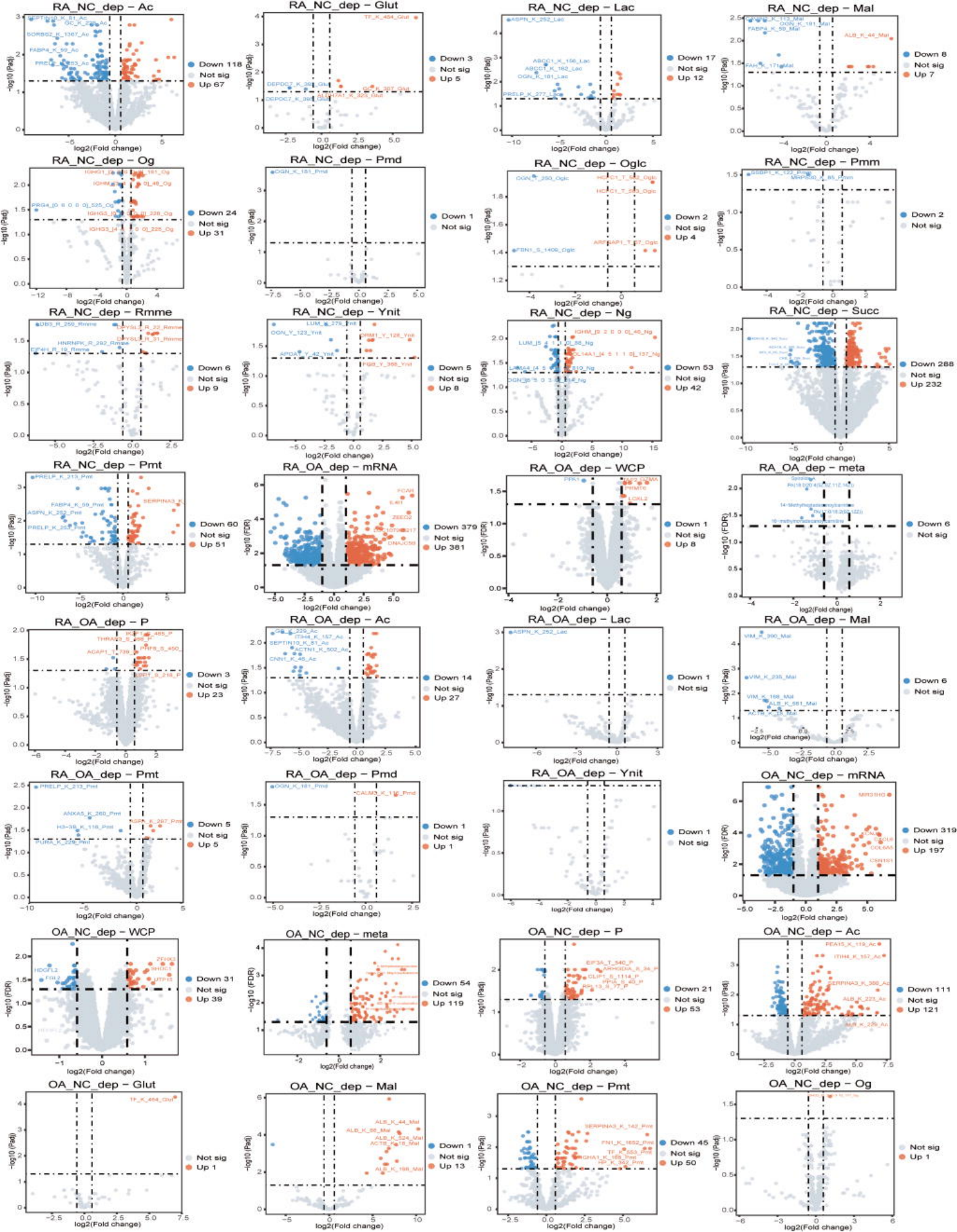
RA_NC_dep – Ac
Down 118
Not sig
Up 67
RA_NC_dep – Glut
Down 3
Not sig
Up 5
RA_NC_dep – Lac
Down 17
Not sig
Up 12
RA_NC_dep – Mal
Down 8
Not sig
Up 7
RA_NC_dep – Og
Down 24
Not sig
Up 31
RA_NC_dep – Pmd
Down 1
Not sig
RA_NC_dep – Oglc
Down 2
Not sig
Up 4
RA_NC_dep – Pmm
Down 2
Not sig
RA_NC_dep – Rmme
Down 6
Not sig
Up 9
RA_NC_dep – Ynit
Down 5
Not sig
Up 8
RA_NC_dep – Ng
Down 53
Not sig
Up 42
RA_NC_dep – Succ
Down 288
Not sig
Up 232
RA_NC_dep – Pmt
Down 60
Not sig
Up 51
RA_OA_dep – mRNA
Down 379
Not sig
Up 381
RA_OA_dep – WCP
Down 1
Not sig
Up 8
RA_OA_dep – meta
Down 6
Not sig
RA_OA_dep – P
Down 3
Not sig
Up 23
RA_OA_dep – Ac
Down 14
Not sig
Up 27
RA_OA_dep – Lac
Down 1
Not sig
RA_OA_dep – Mal
Down 6
Not sig
RA_OA_dep – Pmt
Down 5
Not sig
Up 5
RA_OA_dep – Pmd
Down 1
Not sig
Up 1
RA_OA_dep – Ynit
Down 1
Not sig
OA_NC_dep – mRNA
Down 319
Not sig
Up 197
OA_NC_dep – WCP
Down 31
Not sig
Up 39
OA_NC_dep – meta
Down 54
Not sig
Up 119
OA_NC_dep – P
Down 21
Not sig
Up 53
OA_NC_dep – Ac
Down 111
Not sig
Up 121
OA_NC_dep – Glut
Not sig
Up 1
OA_NC_dep – Mal
Down 1
Not sig
Up 13
OA_NC_dep – Pmt
Down 45
Not sig
Up 50
OA_NC_dep – Og
Not sig
Up 1
log2(Fold change)
-log10 (Padj)
-log10 (FDR)

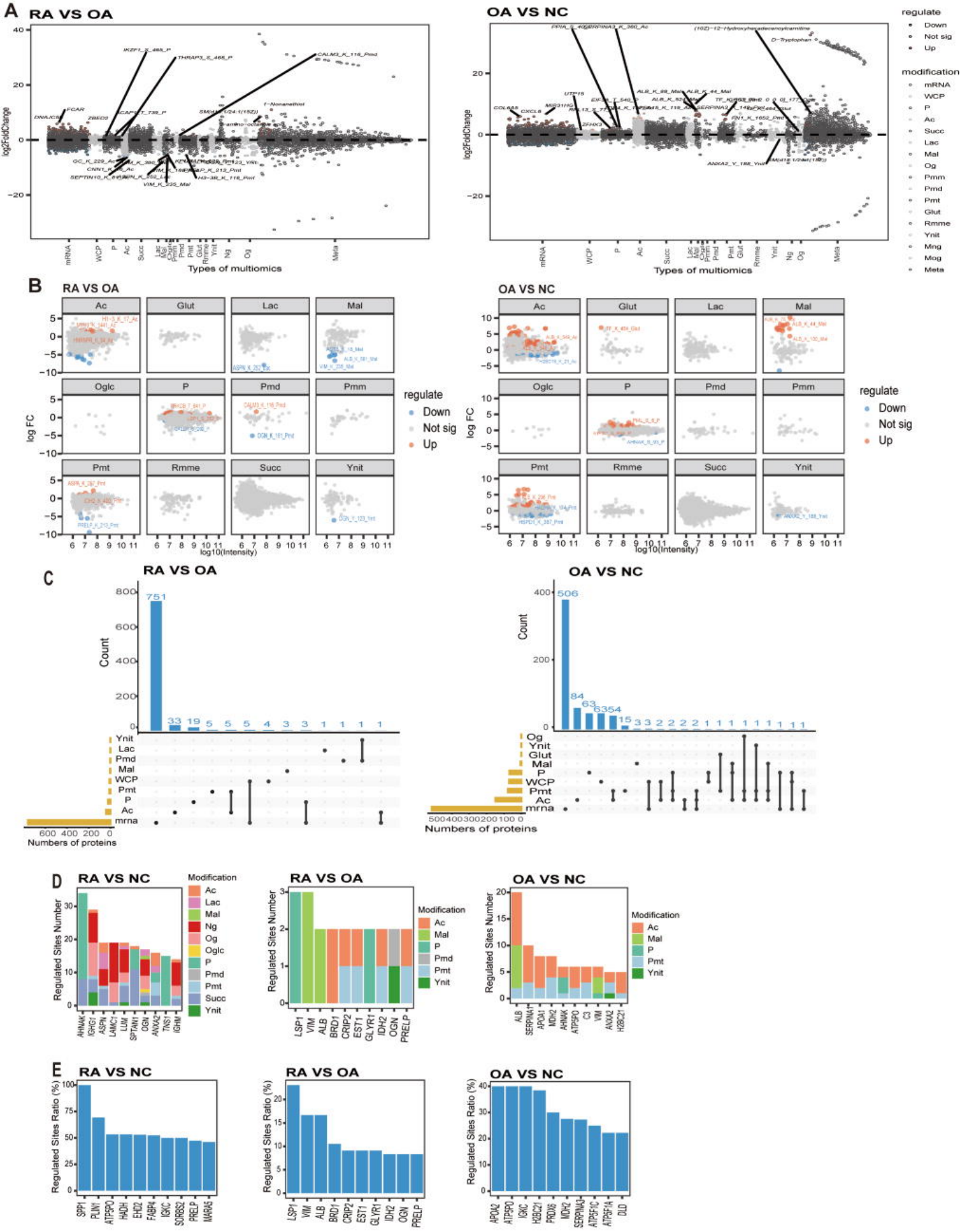
A
RA VS OA
OA VS NC
log2FoldChange
Types of multiomics
regulate
Down
Not sig
Up
modification
mRNA
WCP
P
Ac
Succ
Lac
Mal
Og
Pmm
Pmd
Pmt
Glut
Rmme
Ynit
Mng
Mog
Meta
B
RA VS OA
OA VS NC
Ac
Glut
Lac
Mal
Oglc
P
Pmd
Pmm
Pmt
Rmme
Succ
Ynit
log FC
log10(Intensity)
regulate
Down
Not sig
Up
C
RA VS OA
OA VS NC
Count
Numbers of proteins
D
RA VS NC
RA VS OA
OA VS NC
Regulated Sites Number
Modification
Ac
Lac
Mal
Ng
Og
Oglc
P
Pmd
Pmt
Succ
Ynit
E
RA VS NC
RA VS OA
OA VS NC
Regulated Sites Ratio (%)

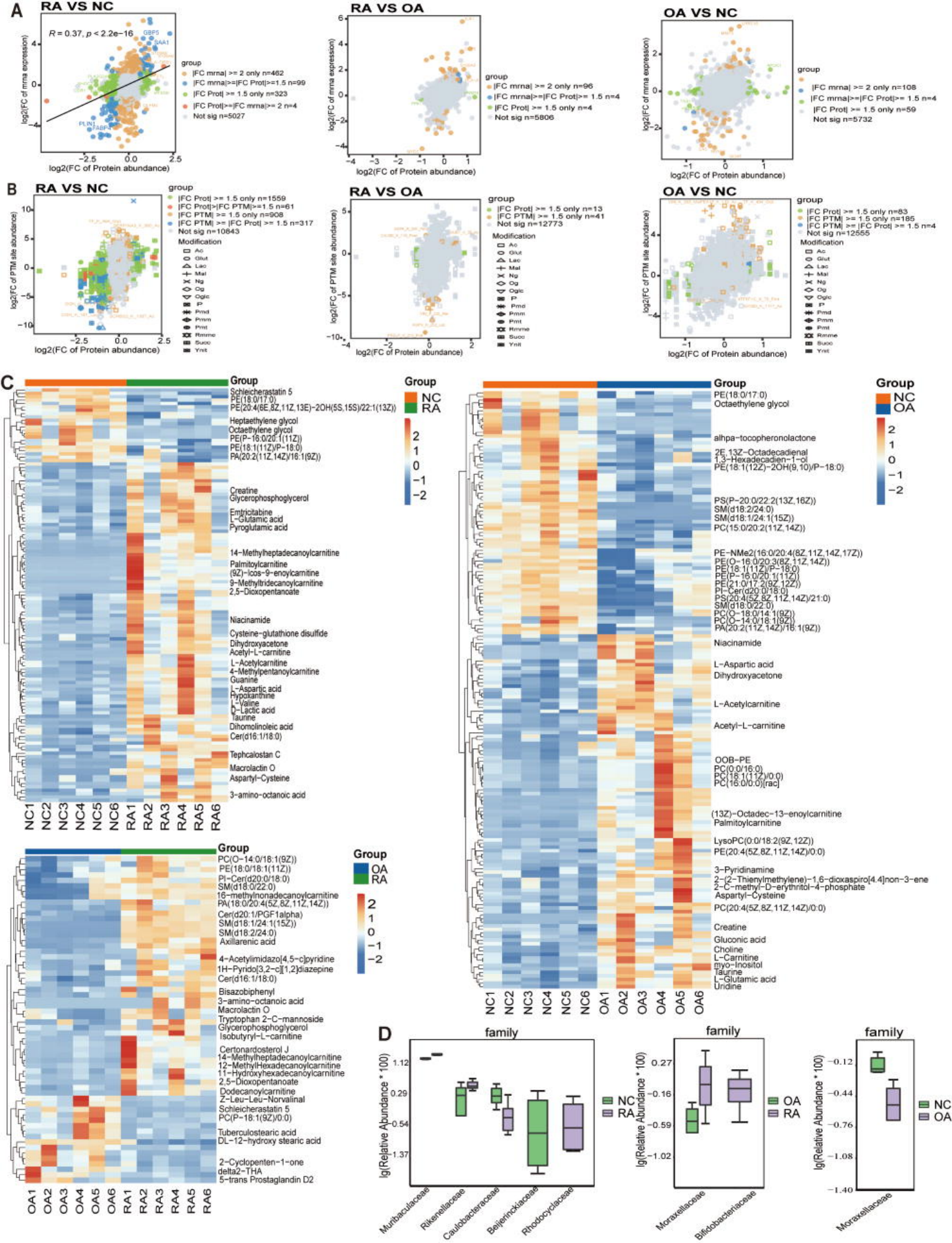
A
RA VS NC
R = 0.37, p < 2.2e−16
GBP5
SAA1
PLIN1
FABP4
log2(FC of mrna expression)
log2(FC of Protein abundance)
group
|FC mrna| >= 2 only n=462
|FC mrna|>=|FC Prot|>=1.5 n=99
|FC Prot| >= 1.5 only n=323
|FC Prot|>=|FC mrna|>= 2 n=4
Not sig n=5027
RA VS OA
group
|FC mrna| >= 2 only n=96
|FC mrna|>=|FC Prot|>= 1.5 n=4
|FC Prot| >= 1.5 only n=4
Not sig n=5806
OA VS NC
group
|FC mrna| >= 2 only n=108
|FC mrna|>=|FC Prot|>= 1.5 n=4
|FC Prot| >= 1.5 only n=59
Not sig n=5732
B
RA VS NC
log2(FC of PTM site abundance)
log2(FC of Protein abundance)
group
|FC Prot| >= 1.5 only n=1559
|FC Prot|>|FC PTM|>=1.5 n=61
|FC PTM| >= 1.5 only n=908
|FC PTM| >= |FC Prot| >= 1.5 n=317
Not sig n=10843
Modification
Ac
Glut
Lac
Mal
Ng
Og
Ogic
P
Pmd
Pmm
Pmt
Rmme
Succ
Ynit
RA VS OA
group
|FC Prot| >= 1.5 only n=13
|FC PTM| >= 1.5 only n=41
Not sig n=12773
OA VS NC
group
|FC Prot| >= 1.5 only n=83
|FC PTM| >= 1.5 only n=185
|FC PTM| >= |FC Prot| >= 1.5 n=4
Not sig n=12555
C
Group
NC
RA
Schleicherastatin 5
PE(18:0/17:0)
PE(20:4(6E,8Z,11Z,13E)−2OH(5S,15S)/22:1(13Z))
Heptaethylene glycol
Octaethylene glycol
PE(P−16:0/20:1(11Z))
PE(18:1(11Z)/P−18:0)
PA(20:2(11Z,14Z)/16:1(9Z))
Creatine
Glycerophosphoglycerol
Emtricitabine
L−Glutamic acid
Pyroglutamic acid
14−Methylheptadecanoylcarnitine
Palmitoylcarnitine
(9Z)−Icos−9−enoylcarnitine
9−Methyltridecanoylcarnitine
2,5−Dioxopentanoate
Niacinamide
Cysteine−glutathione disulfide
Dihydroxyacetone
Acetyl−L−carnitine
L−Acetylcarnitine
4−Methylpentanoylcarnitine
Guanine
L−Aspartic acid
Hypoxanthine
L−Valine
D−Lactic acid
Taurine
Dihomolinoleic acid
Cer(d16:1/18:0)
Tephcalostan C
Macrolactin O
Aspartyl−Cysteine
3−amino−octanoic acid
NC1 NC2 NC3 NC4 NC5 NC6 RA1 RA2 RA3 RA4 RA5 RA6
Group
OA
RA
PC(O−14:0/18:1(9Z))
PE(18:0/18:1(11Z))
PI−Cer(d20:0/18:0)
SM(d18:0/22:0)
16−methylnonadecanoylcarnitine
PA(18:0/20:4(5Z,8Z,11Z,14Z))
Cer(d20:1/PGF1alpha)
SM(d18:1/24:1(15Z))
SM(d18:2/24:0)
Axillarenic acid
4−Acetylimidazo[4,5−c]pyridine
1H−Pyrido[3,2−c][1,2]diazepine
Cer(d16:1/18:0)
Bisazobiphenyl
3−amino−octanoic acid
Macrolactin O
Tryptophan 2−C−mannoside
Glycerophosphoglycerol
Isobutyryl−L−carnitine
Certonardosterol J
14−Methylheptadecanoylcarnitine
12−MethylHexadecanoylcarnitine
11−Hydroxyhexadecanoylcarnitine
2,5−Dioxopentanoate
Dodecanoylcarnitine
Z−Leu−Leu−Norvalinal
Schleicherastatin 5
PC(P−18:1(9Z)/0:0)
Tuberculostearic acid
DL−12−hydroxy stearic acid
2−Cyclopenten−1−one
delta2−THA
5−trans Prostaglandin D2
OA1 OA2 OA3 OA4 OA5 OA6 RA1 RA2 RA3 RA4 RA5 RA6
Group
NC
OA
PE(18:0/17:0)
Octaethylene glycol
alhpa−tocopheronolactone
2E,13Z−Octadecadienal
1,3−Hexadecadien−1−ol
PE(18:1(12Z)−2OH(9,10)/P−18:0)
PS(P−20:0/22:2(13Z,16Z))
SM(d18:2/24:0)
SM(d18:1/24:1(15Z))
PC(15:0/20:2(11Z,14Z))
PE−NMe2(16:0/20:4(8Z,11Z,14Z,17Z))
PE(O−16:0/20:3(8Z,11Z,14Z))
PE(18:1(11Z)/P−18:0)
PE(P−16:0/20:1(11Z))
PE(21:0/17:2(9Z,12Z))
PI−Cer(d20:0/18:0)
PS(20:4(5Z,8Z,11Z,14Z)/21:0)
SM(d18:0/22:0)
PC(O−18:0/14:1(9Z))
PC(O−14:0/18:1(9Z))
PA(20:2(11Z,14Z)/16:1(9Z))
Niacinamide
L−Aspartic acid
Dihydroxyacetone
L−Acetylcarnitine
Acetyl−L−carnitine
OOB−PE
PC(0:0/16:0)
PC(18:1(11Z)/0:0)
PC(16:0/0:0)[rac]
(13Z)−Octadec−13−enoylcarnitine
Palmitoylcarnitine
LysoPC(0:0/18:2(9Z,12Z))
PE(20:4(5Z,8Z,11Z,14Z)/0:0)
3−Pyridinamine
2−(2−Thienylmethylene)−1,6−dioxaspiro[4.4]non−3−ene
2−C−methyl−D−erythritol−4−phosphate
Aspartyl−Cysteine
PC(20:4(5Z,8Z,11Z,14Z)/0:0)
Creatine
Gluconic acid
Choline
L−Carnitine
myo−Inositol
Taurine
L−Glutamic acid
Uridine
NC1 NC2 NC3 NC4 NC5 NC6 OA1 OA2 OA3 OA4 OA5 OA6
D
family
lg(Relative Abundance * 100)
NC
RA
Muribaculaceae
Rikenellaceae
Caulobacteraceae
Beijerinckiaceae
Rhodocyclaceae
OA
Moraxellaceae
Bifidobacteriaceae

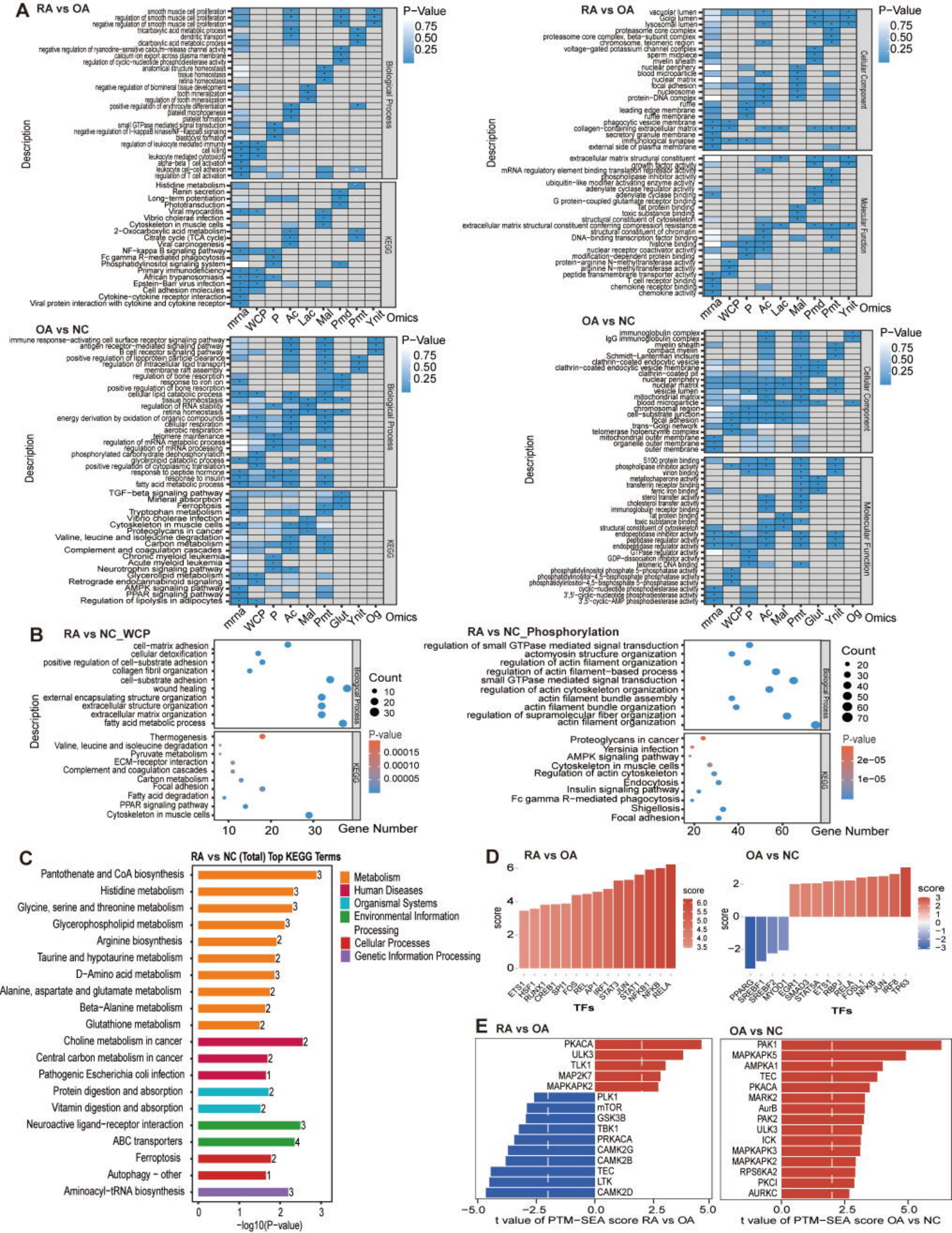
A
RA vs OA
OA vs NC
P-Value
0.75
0.50
0.25
Description
Biological Process
KEGG
Cellular Component
Molecular Function
mrna
WCP
P
Ac
Lac
Mal
Pmd
Pmt
Ynit
Glut
Og
Omics
B
RA vs NC_WCP
RA vs NC_Phosphorylation
Count
P-value
Gene Number
C
RA vs NC (Total) Top KEGG Terms
Metabolism
Human Diseases
Organismal Systems
Environmental Information Processing
Cellular Processes
Genetic Information Processing
-log10(P-value)
D
score
TFs
E
t value of PTM-SEA score RA vs OA
t value of PTM-SEA score OA vs NC

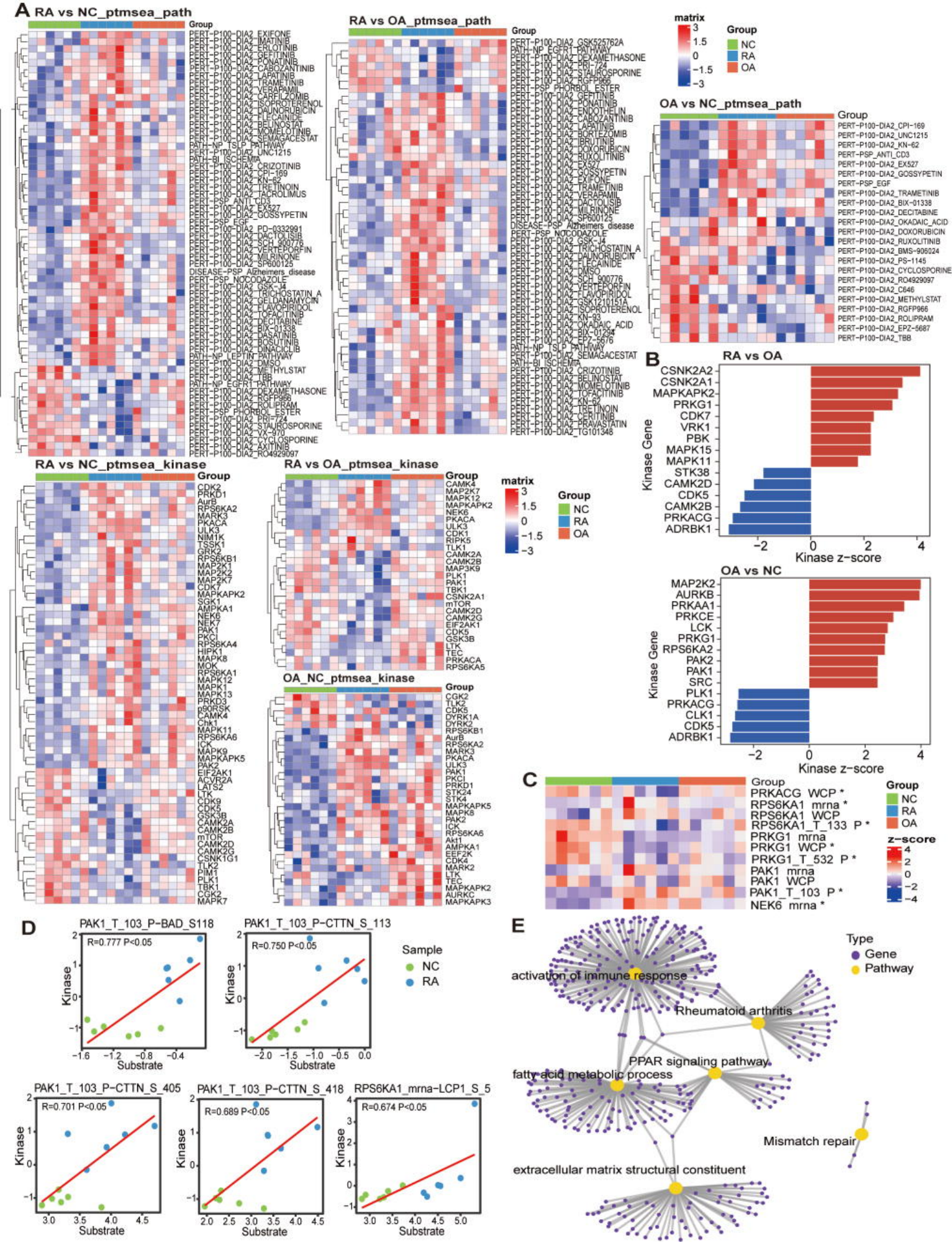
A
RA vs NC_ptmsea_path
RA vs OA_ptmsea_path
OA vs NC_ptmsea_path
Group
matrix
3
1.5
0
−1.5
−3
NC
RA
OA
B
RA vs OA
CSNK2A2
CSNK2A1
MAPKAPK2
PRKG1
CDK7
VRK1
PBK
MAPK15
MAPK11
STK38
CAMK2D
CDK5
CAMK2B
PRKACG
ADRBK1
Kinase Gene
Kinase z−score
OA vs NC
MAP2K2
AURKB
PRKAA1
PRKCE
LCK
PRKG1
RPS6KA2
PAK2
PAK1
SRC
PLK1
PRKACG
CLK1
CDK5
ADRBK1
RA vs NC_ptmsea_kinase
RA vs OA_ptmsea_kinase
OA_NC_ptmsea_kinase
C
PRKACG WCP *
RPS6KA1 mrna *
RPS6KA1 WCP
RPS6KA1_T_133 P *
PRKG1 mrna
PRKG1 WCP *
PRKG1_T_532 P *
PAK1 mrna
PAK1 WCP
PAK1_T_103 P *
NEK6 mrna *
z-score
D
PAK1_T_103_P-BAD_S118
R=0.777 P<0.05
PAK1_T_103_P-CTTN_S_113
R=0.750 P<0.05
PAK1_T_103_P-CTTN_S_405
R=0.701 P<0.05
PAK1_T_103_P-CTTN_S_418
R=0.689 P<0.05
RPS6KA1_mrna-LCP1_S_5
R=0.674 P<0.05
Kinase
Substrate
Sample
NC
RA
E
Type
Gene
Pathway
activation of immune response
Rheumatoid arthritis
PPAR signaling pathway
fatty acid metabolic process
Mismatch repair
extracellular matrix structural constituent

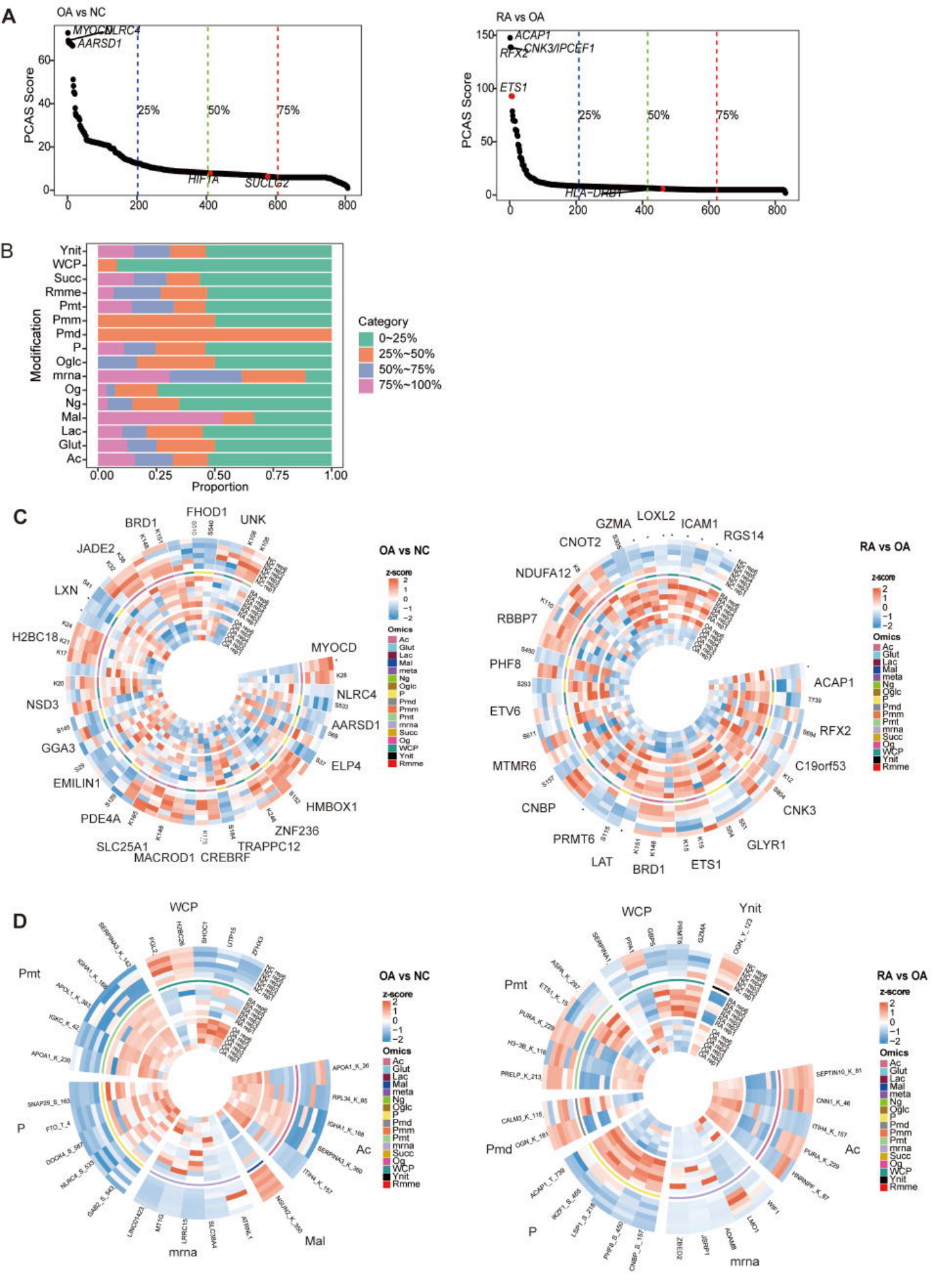
A
OA vs NC
MYOCD
NLRC4
AARSD1
PCAS Score
25%
50%
75%
HIF1A
SUCLG2
RA vs OA
ACAP1
CNK3/IPCEF1
RFX2
ETS1
HLA-DRB1
B
Modification
Ynit
WCP
Succ
Rmme
Pmt
Pmm
Pmd
P
Oglc
mrna
Og
Ng
Mal
Lac
Glut
Ac
Proportion
Category
0~25%
25%~50%
50%~75%
75%~100%
C
OA vs NC
FHOD1
BRD1
UNK
JADE2
LXN
H2BC18
MYOCD
NLRC4
AARSD1
NSD3
GGA3
ELP4
EMILIN1
HMBOX1
PDE4A
ZNF236
SLC25A1
TRAPPC12
MACROD1
CREBRF
RA vs OA
GZMA
LOXL2
ICAM1
RGS14
CNOT2
NDUFA12
RBBP7
PHF8
ACAP1
ETV6
RFX2
MTMR6
C19orf53
CNBP
CNK3
PRMT6
GLYR1
LAT
BRD1
ETS1
z-score
Omics
Ac
Glut
Lac
Mal
meta
Ng
Oglc
P
Pmd
Pmm
Pmt
mrna
Succ
Og
WCP
Ynit
Rmme
D
OA vs NC
WCP
Pmt
P
Ac
Mal
mrna
RA vs OA
WCP
Ynit
Pmt
Pmd
Ac
P
mrna

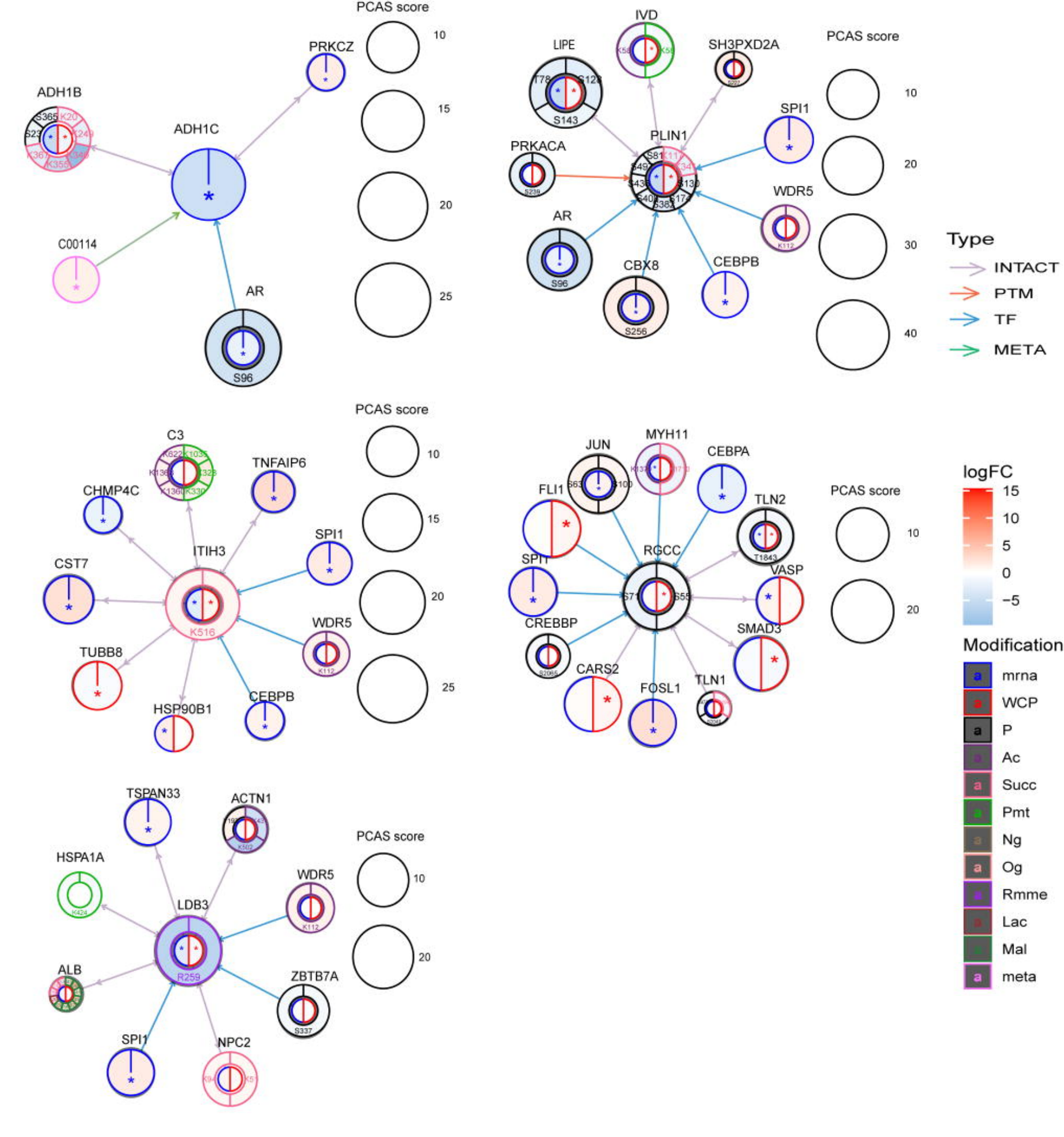
PCAS score
10
15
20
25
PRKCZ
ADH1B
ADH1C
C00114
AR
S96
IVD
LIPE
SH3PXD2A
SPI1
PLIN1
PRKACA
WDR5
AR
CBX8
CEBPB
S143
S256
30
40
Type
INTACT
PTM
TF
META
C3
TNFAIP6
CHMP4C
SPI1
ITIH3
CST7
K516
WDR5
TUBB8
HSP90B1
CEBPB
JUN
MYH11
CEBPA
FLI1
TLN2
RGCC
SPI1
VASP
CREBBP
SMAD3
CARS2
FOSL1
TLN1
logFC
15
10
5
0
−5
Modification
mrna
WCP
P
Ac
Succ
Pmt
Ng
Og
Rmme
Lac
Mal
meta
TSPAN33
ACTN1
HSPA1A
WDR5
LDB3
R259
ALB
ZBTB7A
SPI1
NPC2

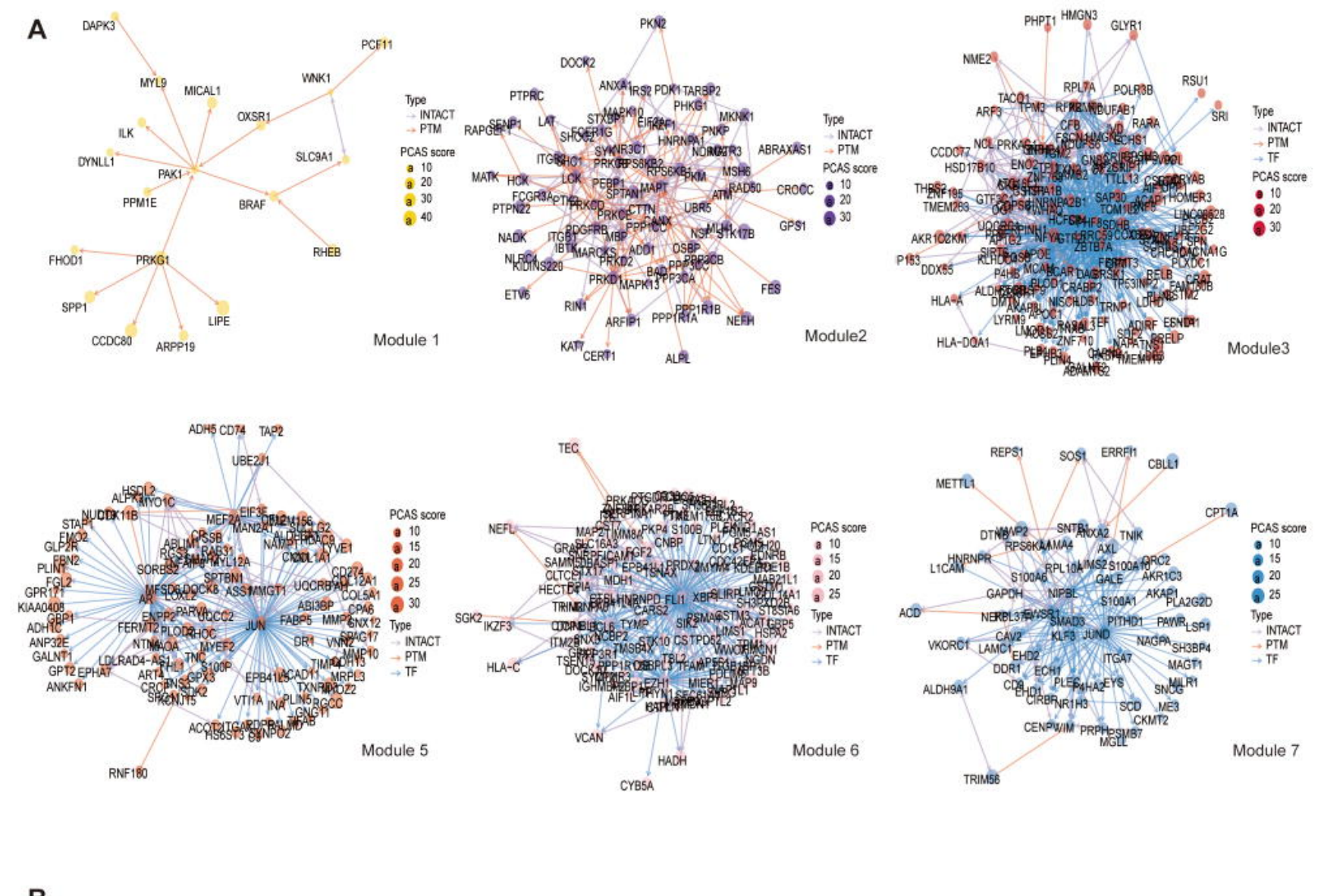
A
Module 1
Module2
Module3
Module 5
Module 6
Module 7
Type
INTACT
PTM
TF
PCAS score

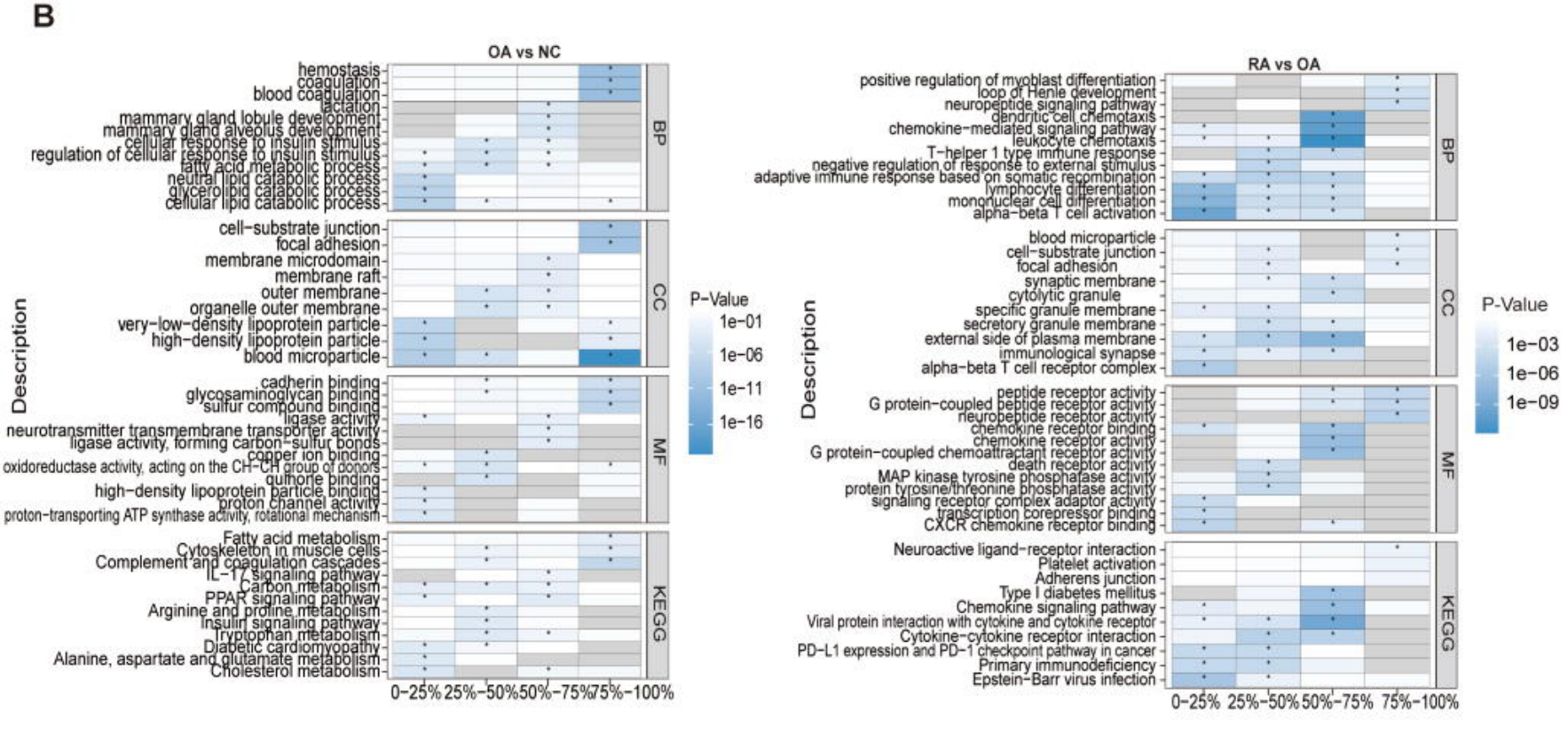
B
OA vs NC
RA vs OA
Description
BP
CC
MF
KEGG
P-Value
0−25%
25%−50%
50%−75%
75%−100%

A

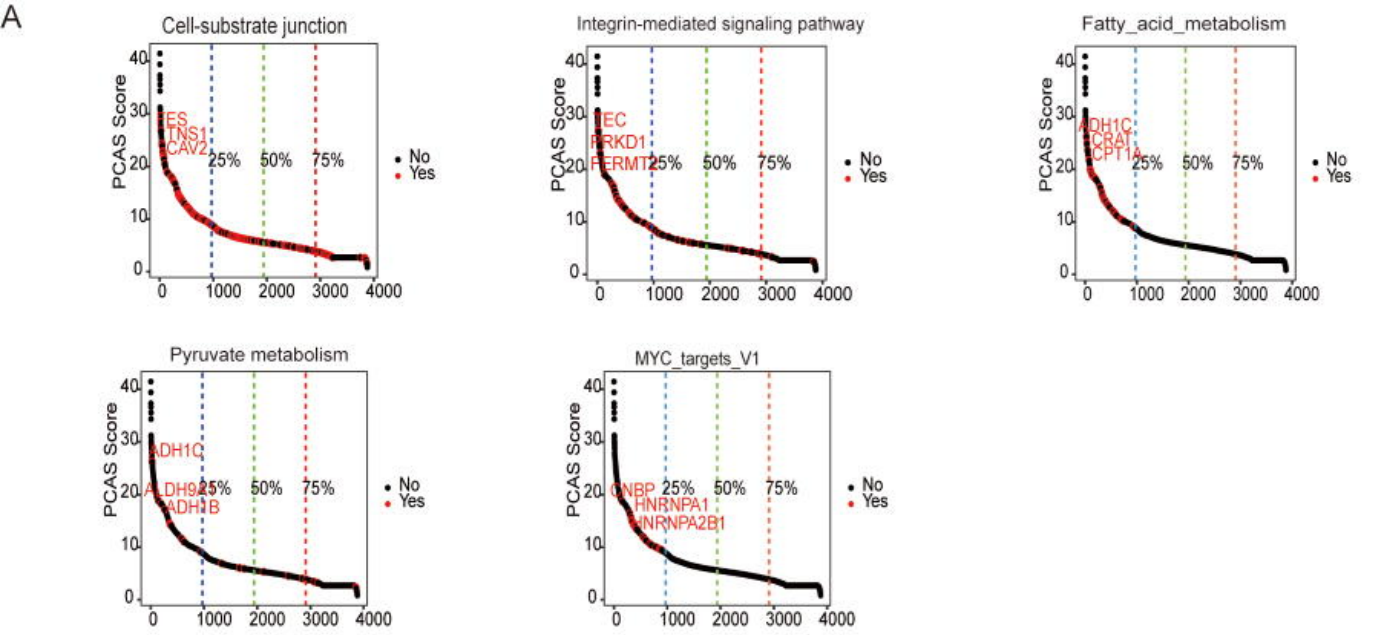
Cell-substrate junction
PCAS Score
ES
TNS1
CAV2
25%
50%
75%
No
Yes
Integrin-mediated signaling pathway
TEC
PRKD1
FERMT2
Fatty_acid_metabolism
ADH1C
CRAT
CPT1A
Pyruvate metabolism
ADH1C
ALDH9A1
ADH1B
MYC_targets_V1
GNBP
HNRNPA1
HNRNPA2B1

B

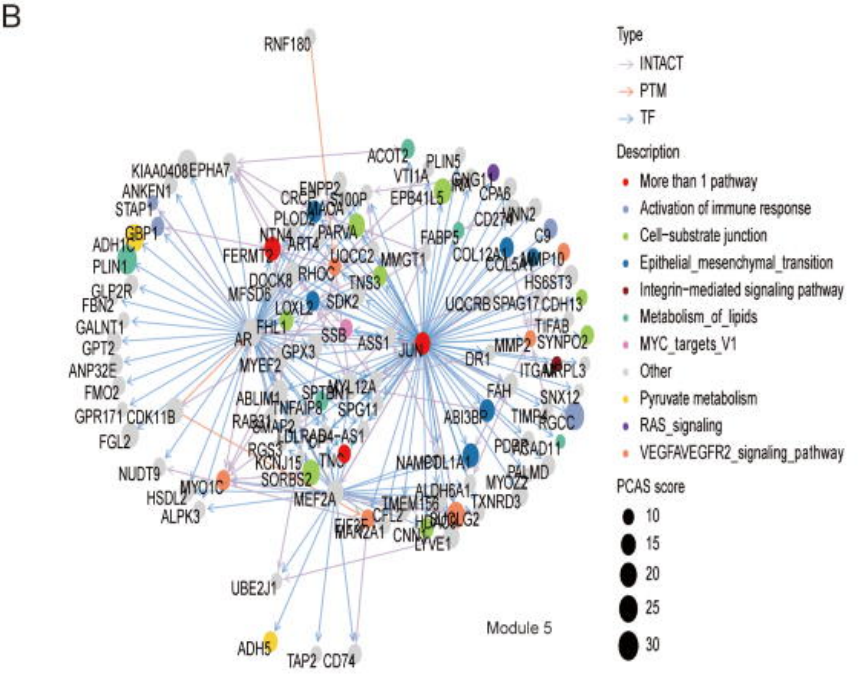
Module 5
Type
INTACT
PTM
TF
Description
More than 1 pathway
Activation of immune response
Cell-substrate junction
Epithelial_mesenchymal_transition
Integrin-mediated signaling pathway
Metabolism_of_lipids
MYC_targets_V1
Other
Pyruvate metabolism
RAS_signaling
VEGFAVEGFR2_signaling_pathway
PCAS score
10
15
20
25
30

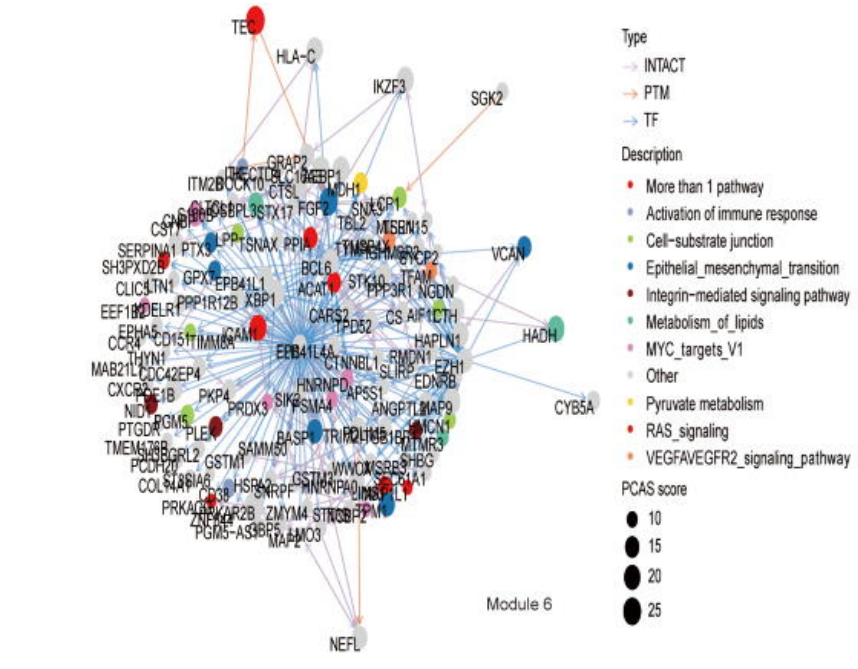
Module 6
Type
INTACT
PTM
TF
Description
More than 1 pathway
Activation of immune response
Cell-substrate junction
Epithelial_mesenchymal_transition
Integrin-mediated signaling pathway
Metabolism_of_lipids
MYC_targets_V1
Other
Pyruvate metabolism
RAS_signaling
VEGFAVEGFR2_signaling_pathway
PCAS score
10
15
20
25